THE HONG KONG
POLYTECHNIC UNIVERSITY
香港理工大學
Pao Yue-kong Library
包玉剛圖書館

Copyright Undertaking

This thesis is protected by copyright, with all rights reserved.

By reading and using the thesis, the reader understands and agrees to the following terms:

1. The reader will abide by the rules and legal ordinances governing copyright regarding the use of the thesis.
2. The reader will use the thesis for the purpose of research or private study only and not for distribution or further reproduction or any other purpose.
3. The reader agrees to indemnify and hold the University harmless from and against any loss, damage, cost, liability or expenses arising from copyright infringement or unauthorized usage.

IMPORTANT

If you have reasons to believe that any materials in this thesis are deemed not suitable to be distributed in this form, or a copyright owner having difficulty with the material being included in our database, please contact lbsys@polyu.edu.hk providing details. The Library will look into your claim and consider taking remedial action upon receipt of the written requests.

Pao Yue-kong Library, The Hong Kong Polytechnic University, Hung Hom, Kowloon, Hong Kong

http://www.lib.polyu.edu.hk

ADDITIVES FOR BUILDING HIGHLY EFFICIENT LEAD-HALIDE PEROVSKITE SOLAR CELLS

CHENG HAIYANG

MPhil

The Hong Kong Polytechnic University

2023

The Hong Kong Polytechnic University
Department of Applied Physics

Additives for Building Highly Efficient Lead-Halide Perovskite Solar Cells

CHENG Haiyang

A thesis submitted in partial fulfillment of the requirements for the degree of Master of Philosophy

June 2023

CERTIFICATE OF ORIGINALITY

I hereby declare that this thesis is my own work and that, to the best of my knowledge and belief, it reproduces no material previously published or written, nor material that has been accepted for the award of any other degree or diploma, except where due acknowledgement has been made in the text.

_____ (Signed)

CHENG HAIYANG (Name of student)

Abstract

Organic-inorganic halide perovskite solar cells (PSCs) have emerged as a promising next-generation photovoltaic technology, thanks to their high power conversion efficiency (PCE), tunable semiconducting properties, relatively easy processing methods, and low-cost raw materials. Various approaches, including compositional engineering, interface engineering, and strain engineering, have been explored to improve the device performance. Among these methods, additive engineering remains the most common approach due to its convenience. Researchers have studied the behavior of perovskite precursor solutions and thoroughly investigated various additives to control crystallization and enhance the device efficiency and stability, resulting in many record efficiencies achieved. This thesis focuses on two new additives for inverted PSCs that demonstrate a significant impact on the device performance. Through sufficient and compelling experiments, we illustrate the mechanism of the improvements. Our research contributes to the ongoing efforts to develop more efficient and stable PSCs, which have great potential for commercialization.

Triple-cation mixed perovskites have gained significant attention recently due to their exceptional optoelectronic properties and stability for perovskite solar cells. However, the introduction of cations with different sizes can cause internal strain in the perovskite lattice, which affects the quality of the resultant films. To address this, we have introduced a small amount of KBF_4 as an additive to improve the quality of triple-cation mixed perovskite thin films. Our study shows that KBF_4 enhances the crystallinity of

the perovskite thin films and reduces internal strain. Additionally, KBF_4 passivates defects in perovskite grains, resulting in longer carrier lifetimes. Consequently, the devices exhibit improved fill factor, enhanced efficiency, and better stability. Under optimum fabrication conditions, triple-cation mixed perovskite solar cells with an inverted structure demonstrate a power conversion efficiency over 23% and excellent stability under different conditions.

Additive engineering has significantly contributed to the remarkable efficiency achieved by perovskite solar cells (PSCs). Numerous additives have been introduced to enhance the device performance, just like the first work, where we use KBF_4 as modulator to release strain. Based on this additive, we further studied the combinational effect of two ammonium salts, PEAI (2-phenylethanamine iodide) and GlyHCl (glycine hydrochloride), to improve the performance of inverted PSCs. Our findings show that the addition of Gly^+ can further enlarges the grain size and reduces defect density after the perovskite was already passivated by PEA^+. This co-additive strategy helped us achieve the highest efficiency of 23.8% on inverted PSCs.

In summary, we employed KBF_4 as an additive to improve the performance of triple-cation mixed perovskite thin films. Our study shows that KBF_4 enhances the crystallinity of the perovskite thin films and reduces internal strain, resulting in improved device efficiency and stability. In the second work, we investigated the combinational effect between PEAI and GlyHCl. These two works demonstrate methods and mechanisms to obtain high-performance inverted PSCs and triple-cation

mixed perovskite thin films. The application of these additives together gave the best efficiency of 23.8%. Overall, our research provides insights into designing and selecting the additives for building efficient and stable PSCs.

List of Publications

1. KBF_4 Additive for Alleviating Microstrain, Improving Crystallinity, and Passivating Defects in Inverted Perovskite Solar Cells. Adv. Funct. Mater., 2022, 32, 2204880, Haiyang Cheng, Chunki Liu, Jing Zhuang, Jiupeng Cao, Tianyue Wang, Wai-Yeung Wong, and Feng Yan*[1]

2. A Convenient Co-Additive Strategy to Boost the Inverted Perovskite Solar Cells. (In progress)
3. Ultrathin Self-Assembly Two-Dimensional Metal–Organic Framework Films as Hole Transport Layers in Ideal-Bandgap Perovskite Solar Cells. ACS Energy Lett., 2022, 7, 10, 3362. Jiupeng Cao, Chun-Ki Liu, Venkatesh Piradi, Hok-Leung Loi, Tianyue Wang, Haiyang Cheng, Xunjin Zhu, Feng Yan*
4. High Open Circuit Voltage Over 1 V Achieved in Tin-Based Perovskite Solar Cells with a 2D/3D Vertical Heterojunction. Adv. Sci., 2022,9, 220024. Tianyue Wang, Hok-Leung Loi, Jiupeng Cao, Zhaotong Qin, Zhiqiang Guan, Yang Xu, Haiyang Cheng, Mitch Guijun Li, Chun-Sing Lee, Xinhui Lu, and Feng Yan*
5. High-Performance Tin–Lead Mixed-Perovskite Solar Cells with Vertical Compositional Gradient. Adv.Mater., 2022, 34, 2107729. Jiupeng Cao, Hok-Leung Loi, Yang Xu, Xuyun Guo, Naixiang Wang, Chun-ki Liu, Tianyue Wang, Haiyang Cheng, Ye Zhu, Mitch Guijun Li, Wai-Yeung Wong, and Feng Yan*

Acknowledgements

Over the course of my researching and writing this paper, I would like to express my thanks to all those who have helped me.

First, I would like to express my gratitude to all those who helped me during the writing of this thesis. A special acknowledgement should be shown to Professor Feng Yan, from whose guides I benefited greatly, I am particularly indebted to Zhuang Jing, Song Jiajun, Liu Hong, Zhao Zeyu and Wang Tianyue, who gave me kind encouragement and useful instruction all through my writing.

Sincere gratitude should also go to all my learned Professors and warm-hearted teachers who have greatly helped me in my study as well as in my life.

And my warm gratitude also goes to my friends and family who gave me much encouragement and financial support respectively. More importantly, I would like to the express my thanks to people who debate and argue with me, who taught me a lesson, and who possess different opinions with me.

I will be very missing to the days I spent in this lab, office and campus.

Table of Contents

List of Figures

List of Tables

Chapter 1 Introduction of Lead Perovskite Solar cells

1.1 Background

Since the onset of the industrial age, the demand for electricity has become a fundamental criterion for assessing a country's development. The global community has been exploiting terrestrial energy resources in a rapacious manner, with conventional sources such as coal, fossil fuels, and natural gas overwhelmingly dominating the energy markets and accounting for the majority of electricity generation. However, two critical issues have arisen. First, the rapid surge in energy demand has exceeded the available energy supply, leading to a significantly diminished availability of conventional energy sources. Second, the potential environmental harm of conventional energy sources has been observed and documented in recent years.

As a result, for decades, the global community has been exploring renewable and green alternatives to conventional energy sources. For instance, solar energy, wind energy, and tidal energy have been practically implemented to provide electricity. Among the various emerging energy sources, solar energy is particularly noteworthy due to its high conversion efficiency. It is noteworthy that many natural energy sources, including coal, fossil fuels, and wind energy, are ultimately derived from the sun. However, these energy sources are not directly converted from solar energy but rather take millions of years to form and accumulate. Therefore, the direct conversion of solar energy into

electricity may be the most efficient and effective approach to resolving the energy crisis.

Solar cells are electronic devices that exploit the photovoltaic phenomenon to convert solar energy into electricity. [2] The type of semiconductor material used as the photo-sensitive layer determines the category of solar cell. Silicon-based solar cells, the first-generation and widely commercialized type, are renowned for their high device efficiency and stability, attributable to the inert chemical nature of silicon[3]. However, the exorbitant cost of silicon purification and fabrication impedes large-scale production. Consequently, researchers are seeking alternative materials to replace silicon. As scientists deepen their comprehension of various semiconductor materials, they have discovered that many inexpensive materials can generate the photovoltaic effect. For instance, GaAs solar cells have achieved efficiency greater than 29% with single-junction cells[4], while CIGS (Copper Indium Gallium Selenide) solar cells have also exhibited efficiencies exceeding 23%[5]. These solar cells, based on thin-film technology, are considered second-generation solar cells.

Over the past decade, third-generation solar cells have experienced rapid and robust growth, with organic solar cells (comprising organic small molecules and polymers) and perovskite solar cells emerging as two prominent advanced materials.[6-7] In addition to leveraging thin-film technology, third-generation solar cells possess unique features, including high tunability. The diversity of organic molecules arises from their highly developed synthesis system, which imparts diverse chemical and physical

properties to the organic materials.[6] Similarly, lead (Pb)-based halide perovskite (ABX_3) is an ideal material for creating light-harvesting devices due to their easily tunable bandgap and exceedingly high power conversion efficiency.[7] To date, the PCE of perovskite solar cells (PSCs) has exceeded 26% in within only one decade.[8-9] The progress made in PSCs has delved into mass production technologies, paving the way for further commercialization.

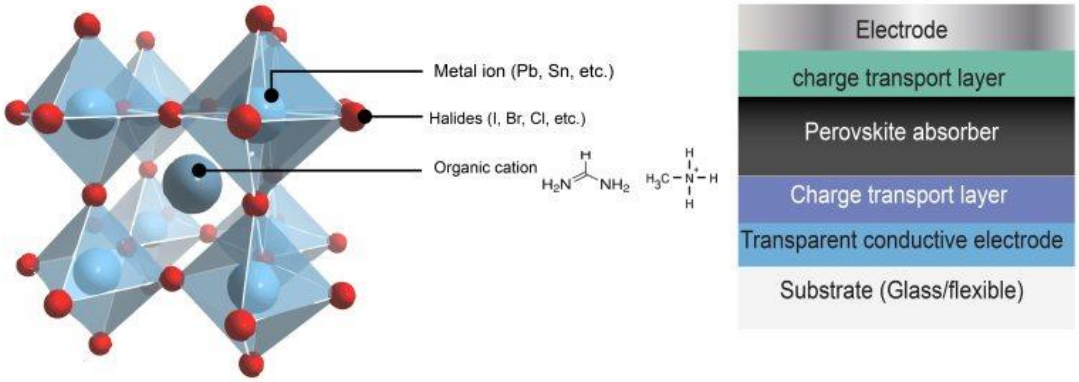

Figure 1.1. The structures and compositions of perovskite solar cells.

The exceptional efficiencies achieved in PSCs primarily rely on the utilization of organic-inorganic halide Pb-based perovskites, which are generally represented by the chemical formula ABX_3 (**Figure 1.1**). In this formula, A cation represents MA^+ (methyl ammonium), FA^+ (formamidinium), or Cs^+ (cesium), B denotes lead/tin, and C signifies halide ions (Br^-, I^-). The bandgap of Pb-based perovskites can be conveniently modulated by altering the type and ratio of A and C sites ions, thereby rendering perovskites a suitable material for constructing tandem solar cells. Furthermore, given their relatively facile fabrication process, methods such as blade coating and roll-to-roll

coating have been extensively developed, enabling the mass production and practical application of PSCs.[2-3, 7]

1.2 Objectives of Research

Although the efficiency of PSCs has approached that of silicon-based solar cells, several challenges still impede their real-world commercialization. For instance, while silicon is chemically and physically inert, exhibiting exceptional stability under high-temperature and intense illumination conditions, perovskites are highly sensitive to air, particularly the water content in air. Exposure to high humidity can cause rapid degradation and loss of light-harvesting ability.[10] Moreover, the intrinsic ionic nature of perovskites makes them vulnerable to light in working conditions. The halide ions can migrate under the built-in electric field, resulting in irreversible aggregation and segregation of halide ions.[11] Consequently, the nonuniform composition of perovskites can significantly decrease conversion efficiency and long-term stability. Apart from device stability issues, the fabrication process for mass production is another critical challenge.[12] For instance, the conventional laboratory-based fabrication method, spin coating, is widely used for thin-film material production. However, spin coating presents challenges for large-area thin-film deposition and results in significant waste of perovskite solution, which is unfavorable for mass production. Therefore, researchers are actively exploring multiple strategies to overcome these challenges.

With the swift development of perovskite theory, numerous engineering approaches have been proposed to address the aforementioned challenges. Composition

engineering involves tuning the type and ratio of A and C site ions.[13] MA-based perovskites were initially a hot topic due to their easily controlled crystallization. However, researchers discovered that FA-based perovskites possess a smaller bandgap, resulting in a higher theoretical efficiency limit. Consequently, all current record efficiencies are achieved using FA-based perovskites. Another successful and widely adopted strategy is additive engineering.[14] Researchers have found that additives can have a significant impact on all aspects of PSCs. For instance, the most common function for additives is defect passivation. Numerous organic molecules, such as Lewis bases, have been demonstrated to reduce defect density. To control crystallization, researchers have utilized ligands to coordinate with Pb^{2+} ions, slowing down the crystallization process and increasing grain size. Moreover, reports have demonstrated that additives can tune perovskite energy levels and facilitate the transport of holes and electrons.

This thesis introduces two additional additives to enhance the performance of PSCs, with a particular focus on improving the power conversion efficiency (PCE) and stability of inverted PSCs, which have lagged behind their normal counterparts. Considering that the inverted structure is crucial in numerous applications, such as flexible electronics and large-area fabrication, studies investigating their performance improvements and mechanisms are still inadequate. The objectives of this work are to provide further insights for designing new and effective additives to enhance the performance of PSCs and to facilitate the commercialization of PSCs.

1.3 Structure of Thesis

The chapter of this thesis are listed as follows:

Chapter 1: Introduction. In this part, the background and the significance of developing high performance perovskite solar cells are introduced.

Chapter 2: Literature review relating to the working mechanisms, basic structures and progress in perovskite solar cells are presented in this chapter.

Chapter 3: KBF_4 Additive for Alleviating Microstrain, Improving Crystallinity and Passivating Defects in Inverted Perovskite Solar Cells. In this part, efficiency over 23% is achieved on PSCs with inverted structures with the help of KBF_4. The mechanism is also thoroughly investigated with various characterization.

Chapter 4: A Binary Ammonium Salts System to Boost the Efficiency of Inverted Perovskite Solar Cells over 23.8%. In this section, a co-additive strategy is put forward and the combinational effect between two additives are studied.

Chapter 5: Conclusion and Prospects. In this chapter, the results and conclusions are refined to give clear picture of our study. Besides, potential studying filed and problems that remain unresolved are put forward to further help improve the performance of PSCs.

Chapter 2 Review of Basic Information of Perovskite Solar Cells and Progress in Additive Engineering

2.1 Introduction

In recent years, perovskites have emerged as highly promising materials with versatile applications across various fields. Notably, their remarkable potential in solar cells has garnered significant attention, primarily due to their exceptional power conversion efficiency, which has seen rapid development over the past decade. Perovskite solar cells have accomplished in almost two decades what took other solar cells hundreds of years to achieve.[7] While silicon-based solar cells remain the commercially dominant first-generation solar cells due to their high efficiency and exceptional chemical stability, the production of ultrahigh-purity metallic silicon (>99.9999%) requires temperatures exceeding 1400 ℃.[15] In comparison, the fabrication of perovskite solar cells is significantly more convenient and relatively inexpensive. This advantage is shared by other third-generation solar cells, including organic photovoltaic cells (OPVs), dye-sensitized solar cells (DSSCs), and quantum dot (QD) solar cells. However, only perovskite solar cells have thus far achieved efficiencies approaching those of silicon-based solar cells.[8-9] These exciting findings have prompted further research efforts to explore the immense potential of perovskite solar cells.

The term perovskite initially referred to calcium titanate ($CaTiO_3$). Subsequently, all metal oxides sharing a similar lattice structure (ABX_3), including $BaTiO_3$, $LiNbO_3$, $PbTiO_3$, $SrTiO_3$, $BiFeO_3$, among others, were also classified as perovskites. However, these metal oxides possess a bandgap greater than 2.5 eV, rendering them unsuitable as light-harvesting materials. In the context of modern perovskite solar cells, perovskites generally refer to organic-inorganic metal halide perovskites, where A typically represents organic small molecules, such as amines or alkali metal cations (MA^+, FA^+, and Cs^+), B represents metal cations that can adopt a sixfold coordination configuration

(Pb, Sn, etc.), and X represents halide atoms, such as I^- and Br^-. In contrast to oxide perovskites, halide perovskites exhibit higher crystallinity due to the strong ionicity of halide anions. In halide perovskites, charge neutralization is established in the lattice structure through the coordination of a large number of cations and anions. Consequently, slight structural strain can result in changes to the lattice structure. The inherently ionic nature of perovskites confers both advantages and disadvantages. As previously mentioned, these include high crystallinity, easily tunable composition, and adjustable bandgap. However, perovskites also suffer from poor stability.[16]

Perovskite structures are highly diverse, and currently achieved record efficiencies are exclusively based on traditional three-dimensional (3D) perovskites, which possess a standard cubic lattice structure and are thus suitable for constructing highly efficient perovskite solar cells owing to their narrow bandgap and high carrier transporting ability. However, the drawback of 3D perovskites is their susceptibility to lattice structure disruption, which can cause rapid decomposition under certain conditions. Consequently, low-dimensional perovskites have garnered increasing attention due to their superior stability. The abundance of low-dimensional perovskite variants, attributable to the diverse range of organic spacers and tunable bandgap, has yielded high-performance perovskite solar cells. For instance, for low-dimensional perovskites with n = 5, the highest efficiency achieved thus far exceeds 22%.[17-19] In any scenario, perovskites have generated significant interest due to their tremendous potential.

2.2 Device Structures of Perovskite Solar Cells

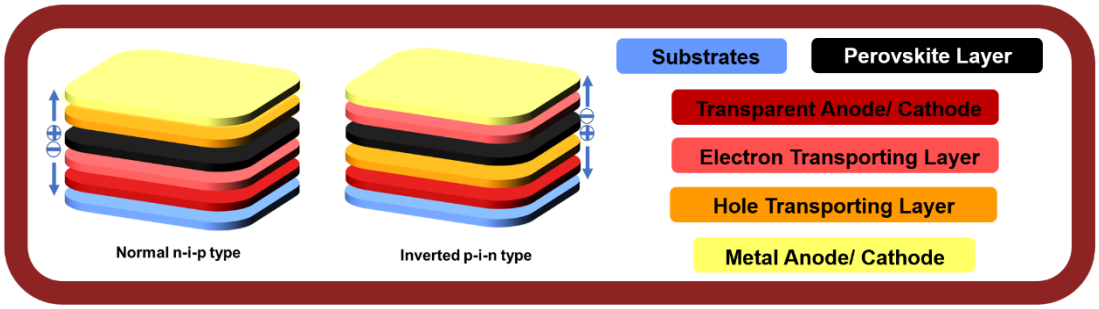

Figure 2.1. The device structure of perovskite solar cells.

Perovskite solar cell structures can be broadly classified into three types. The first type is the traditional mesoscopic n-i-p structure, which employs mesoscopic semiconductor metal oxide, such as TiO_x and SnO_x,[20] as the electron-transporting layer. This approach was pivotal in achieving significant early-stage enhancements in efficiency and remains widely utilized owing to its convenient fabrication. The second type is the planar n-i-p type (normal type), which evolved from the original mesoscopic metal oxide approach due to improvements in depositing metal oxide layers with lower roughness. This device structure is currently the most popular for achieving the highest efficiency in perovskite solar cells. The third type is the planar p-i-n type (inverted type), which relies on well-developed hole-transporting layers, such as PTAA, PEDOT: PSS, and NiO_x.[21-22] The inverted structure is critical for fabricating flexible devices and developing large-area technologies.[23] In addition to the traditional three types, research is also ongoing regarding the transporting-layer-free type in normal or inverted structures. The progress in this area is impressive, largely due to the tunable energy levels of perovskites.[24] The typical structures are illustrated in **Figure 2.1**.

Every layer in perovskites solar cells play a paramount role in high performance devices. Each layer within perovskite solar cells plays a crucial role in achieving high-performance devices. The selection of suitable transporting layers for each perovskite system is critical, and contact interfaces have been identified as being responsible for the majority of nonradiative recombination. Therefore, research efforts have focused on tuning the properties of transporting layers and interfaces, which have contributed significantly to achieving record efficiencies. For instance, the high hole-transporting efficiency of Spiro-OMeTAD has prompted researchers to investigate structure redesign and new doping strategies, both of which have proven effective in enhancing device performance.[25] In addition to improving the quality of typical transporting layers, there are also works focused on designing entirely new transporting layers to offer additional strength and further enhance overall device performance. 2-PACz, for

example, is a promising hole-transporting layer that can potentially replace PTAA, and its performance has been demonstrated in numerous outstanding works.[26]

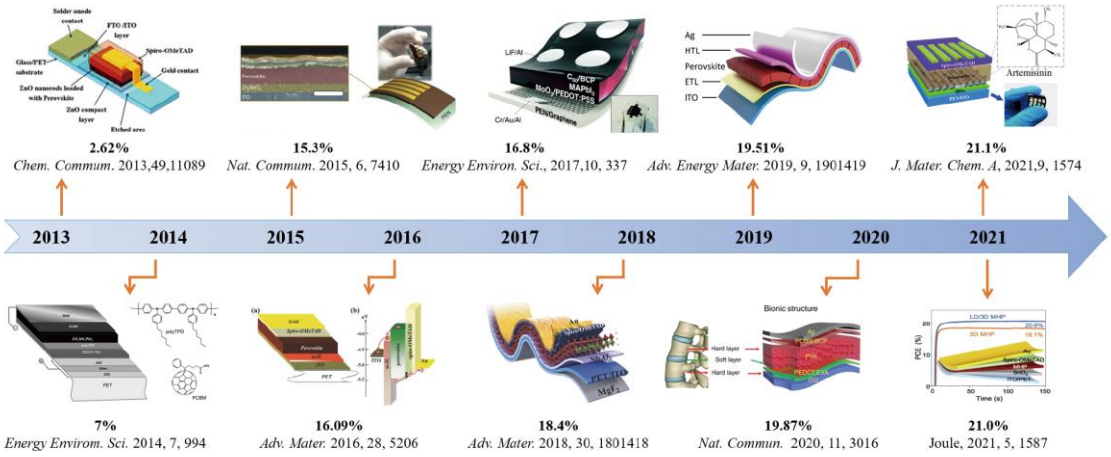

Figure 2.2. Progress in efficiency of flexible perovskite solar cells.[27]

In addition to the layers aforementioned, significant attention has been directed towards the electrodes in perovskite solar cells. ITO (indium tin oxide) is the most commonly used bottom electrode and has been successfully commercialized and implemented in various electronic products. However, ITO is an intrinsically brittle metal oxide that delivers poor flexibility in flexible devices (**Figure 2.2**).[27] This limitation has prompted researchers to explore alternatives to ITO. For instance, silver (Ag) nanowires or nanomeshes exhibit superior conductivity compared to ITO and can be fabricated into various shapes, exhibiting outstanding flexibility.[28] Additionally, many organic mixtures, such as PEDOT:PSS, demonstrate excellent conductivity by designing the structures, and organic materials are renowned for their softness.[29] Consequently, flexible perovskite solar cells represent a promising application with significant potential for commercialization.

2.3 Working Mechanism of Perovskite Solar Cells

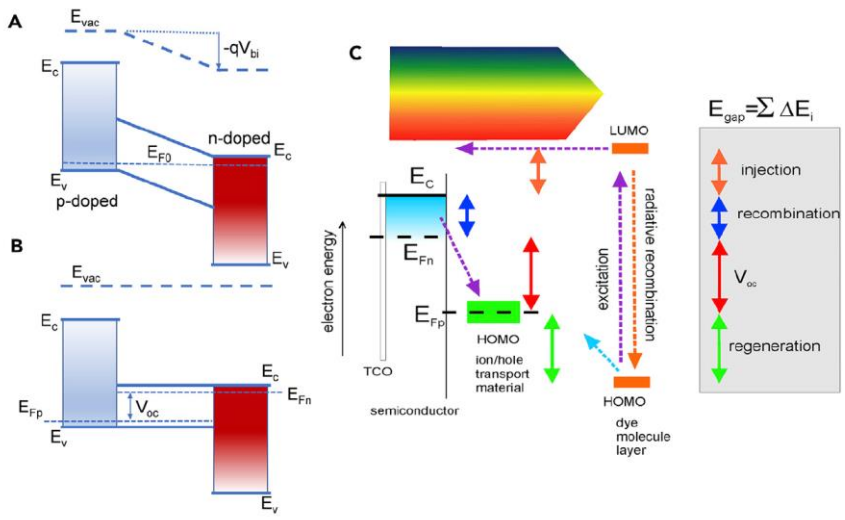

Figure 2.3. Working mechanism of perovskite solar cells.[30]

Perovskite solar cells function more like solid-state p-n junction solar cells (**Figure 2.3**), with the perovskite layer serving as an intrinsic semiconductor sandwiched between two selective contacts. The two transporting layers, hole- and electron-transporting layers (HTLs and ETLs), serve as p and n contacts, respectively. The core mechanism of PSCs is based on the photovoltaic effect. When the perovskite absorbs light, the photo-generated carriers, holes and electrons, must arrive at the contacts to be extracted. Due to the relatively thin film and high dielectric characteristics of perovskite, the carriers in perovskites exhibit high efficiency in charge transport with less potential for nonradiative recombination as compared to other materials. During carrier transport, equilibrium is established, generating a built-in potential that facilitates the separation of holes and electrons. After the holes and electrons are collected by the transporting layers, electrons flow through the external circuit to reach the p-type layer to combine with the holes, thus transforming solar energy into electricity that can be utilized.[30]

2.4 Issues Inside Lead Based Perovskite Solar Cells

Before delving into the progress made in perovskite solar cells, it is crucial to highlight the potential issues that could impede their advancement. While lead-based perovskites

exhibit excellent light harvesting capabilities, there are concerns associated with their ionic nature. Although this characteristic enables efficient carrier transport, it also renders the perovskite phase extremely unstable owing to issues such as ion migration and degradation. Therefore, researchers must strive to strike a balance between achieving high performance and ensuring stability and longevity of the perovskite-based solar cells.

2.4.1 Defects in Lead Based Perovskites

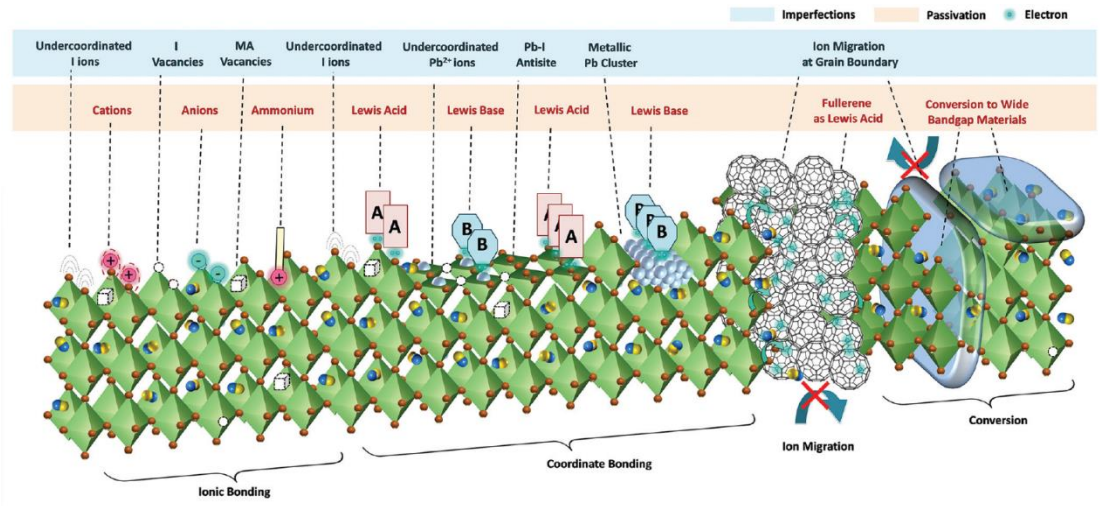

Figure 2.4. Imperfections in perovskites solar cells.[31]

Perovskites are typically fabricated using solution-based methods, such as spin-coating, to form polycrystalline thin films. Polycrystalline thin films exhibit a higher density of grain boundaries and defects compared to their single-crystal counterparts **(Figure 2.4)**. Defects, including point defects and grain-boundary defects, are responsible for nonradiative recombination and energy losses. Moreover, defects are also the primary targets for oxygen and moisture attack, which can lead to perovskite degradation from the defects.[31] Therefore, reducing defect density can help enhance the long-term stability of perovskite-based solar cells. The defect situation in lead halide perovskites is illustrated in **Figure 2.4**.

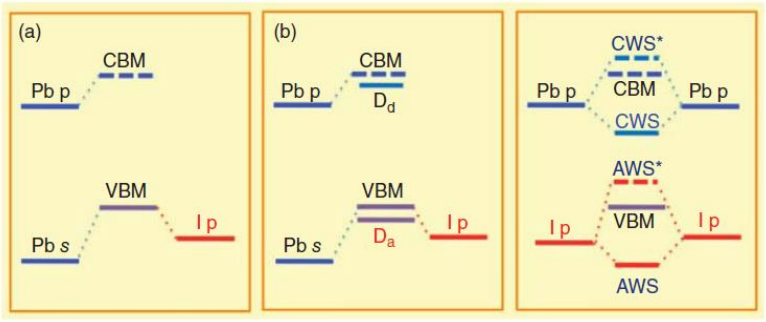

Figure 2.5. (a)The formation of CBM and VBM in perovskites. (b) donor-like and acceptor-like defects from cation and anion vacancies. (c) defects from cation-cation and anion-anion wrong bonds.[32]

Defects are not entirely detrimental to perovskites, as the absorbers must contain a certain amount of shallow-level point defects to generate free carriers with desirable concentrations while avoiding an excess of deep-level defects that may cause detrimental non-radiative recombination. Lead halide perovskites exhibit unique defect properties characterized by high tolerance for defect formation. This means that defects in lead halide perovskites tend to create shallow levels due to their low formation energy. Conversely, defects with high formation energy tend to create deep levels that are harder to control and reduce. And defects with energy levels deep in the bandgap act as Shockley–Reed–Hall non-radiative recombination centers, which are mainly responsible for short minority carrier lifetime and, therefore, low open-circuit voltage (V_{OC}) of the solar cells. This distinct property is attributed to the antibonding coupling between Pb lone-pair s and I p orbitals, which results in high ionicity and the high electronic dimensionality. (**Figure 2.5**)

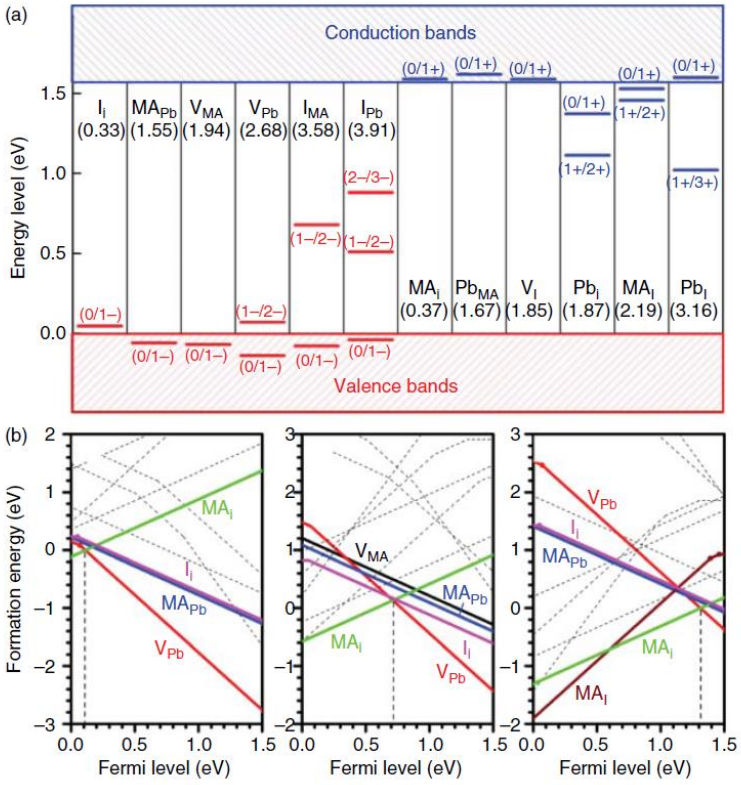

Figure 2.6. (a) Various transition energy levels of points defects in $MAPbI_3$.[33] (b) The formation energy of different point defects in $MAPbI_3$ under I-rich/Pb-poor (left), moderate (middle), and I-poor/Pb-rich (right) chemical conditions.[34]

For various defects in different compositions, the types are different but similar. With thorough investigation by DFT (Density Function Theory) calculation, the formation energy and positions in energy levels of various defects in different compositions are studied. As showed in **Figure 2.6 a**, many defects in the bulk perovskite such as $MAPbI_3$ are shallow defects with low formation energy. For example, the I interstitial (I_i), MA-on-Pb antisite (MA_{Pb}), MA vacancy (V_{MA}), V_{Pb}, MA_i, Pb_{MA}, V_i and MA_i are all shallow defects. On the contrary, deep defects such as I_{MA}, I_{Pb}, Pb_i and Pb_I have much higher formation energy (**Figure 2.6 b**).[33-34] Besides, differs from traditional p-type thin-film solar cell absorbers, perovskites exhibit tunable p or n type depending on the chemical potentials, which are affected by things like solution states and growth conditions. This also suggests that Pb based perovskites have high tolerance to the defects.

In addition to bulk perovskites, grain boundaries and interfaces play even more significant roles in determining the defect density of perovskites. Many studies have demonstrated that defect passivators added to the perovskite precursor solutions are located precisely at the grain boundaries after forming the thin films. These additives typically decrease the formation energy by providing extra interactive forces, such as forming hydrogen bonds to fix the defects.[35] Furthermore, ion migration (especially halide atom migration) is another critical factor that affects defect density. Previous studies have reported that halide atoms in perovskites tend to aggregate during continuous illumination or long-term storage due to the ionic nature of perovskites. Ion migration can lead to a non-uniform perovskite phase and create new defects, such as vacancies and interstitial atoms. Therefore, preventing ion migration is a paramount issue for maintaining low defect density and long-term stability.[36] Recently, interfaces have also attracted significant attention, and interface engineering has become an effective and efficient strategy for enhancing solar cells in every aspect.[37-38] This is because carriers must pass through the interfaces between perovskite and charge-transporting layers and be collected. Therefore, defects at interfaces have a significant impact on charge transport efficiency, nonradiative recombination, and subsequent device performance.

A significant body of research has focused on defect passivation because achieving low defect density is a crucial prerequisite for attaining both high efficiency and long-term stability in perovskite-based devices. In addition to the additive and interface engineering methods mentioned earlier, composition and strain engineering have also been shown to be effective strategies for reducing defects. In summary, controlling defects in perovskites is essential for leveraging their potential in solar energy harvesting.

2.4.2 Composition and Structures of Lead Based Perovskites

Composition plays a critical role in determining the structure of perovskites. However, the crystallization conditions also influence the formation of the structure. The conventional three-dimensional (3D) cubic lattice structure is highly efficient for light harvesting due to its high charge splitting and transporting capabilities. However, the poor stability of the 3D structure hinders its commercial viability. Therefore, low-dimensional perovskites have garnered significant attention due to their superior stability in comparison to their 3D counterparts, and their PCE is also increasing rapidly. Moreover, the composition and resulting structures also determine the Shockley-Queisser limit, which refers to the bandgap and the subsequent efficiency. Thus, the composition and structure determine the fundamental chemical and physical properties of perovskites, and different compositions may be more suitable for different applications of perovskites.

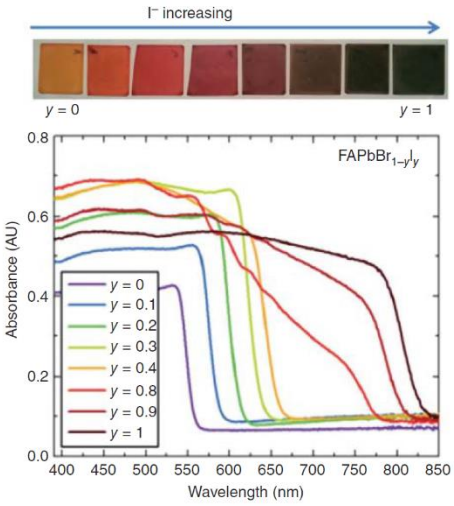

Figure 2.7 The absorption spectra of $FAPbBr_{1-y}I_y$ by tuning the ration of Br^- and I^- [39]

For conventional three-dimensional (3D) perovskites, the range of available compositions is relatively limited compared to low-dimensional counterparts. This is due to the necessity of maintaining the cubic lattice structure, which requires the ions'

radii to match the Goldschmidt tolerance factor ($t = \frac{r_A + r_x}{\sqrt{2}(r_B + r_x)}$) for ABX_3. Consequently, only a limited range of ions can fit into this structure. The metal ions B are typically lead (Pb) and tin (Sn), while X comprises halide ions I^-, Br^-, and Cl^- (F^- has an unsuitable ion radius). The A-site cations can be broadly classified into organic and inorganic types. Organic-inorganic hybrid perovskites based on organic amine salts, such as MA^+ (methylammonium) and FA^+ (formamidinium), exhibit the highest efficiency to date due to their suitable narrow bandgap. Inorganic alkali metals, such as cesium (Cs^+) and rubidium (Rb^+), are widely studied compositions. For instance, Cs^- based pure inorganic perovskites exhibit a wide bandgap and high open-circuit voltage, making them suitable for fabricating tandem solar cells. Although the bandgap depends largely on the halide ion ratio (a high I^- ratio results in a narrow bandgap, while high Br^- leads to a wide bandgap, as shown in **Figure 2.7**),[39] A-site cations can also slightly tune the bandgap. Furthermore, A-site cations strongly influence the stability of perovskites. For example, PSCs based on MA exhibit poor thermal stability due to the organic molecule MA's easy evaporation. In contrast, FA has a slightly higher evaporation temperature and thus higher thermal stability.[40] Pure inorganic perovskites undoubtedly exhibit the highest thermal stability, but their moisture stability is poor. Therefore, composition engineering seeks to harness the benefits while avoiding the drawbacks by tuning various compositions.

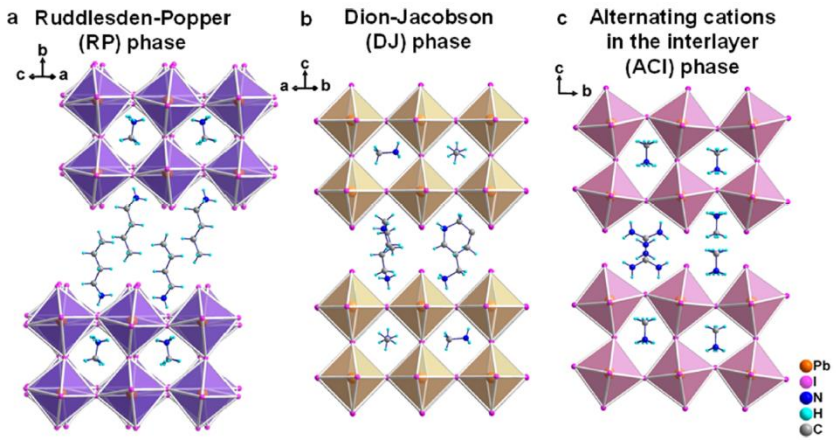

Figure 2.8 Structures of Ruddlesden−Popper phase (a), Dion-Jacobson phase (b) and Alternating cations in the interlayer phase (c) 2D perovskites.[18]

For low-dimensional perovskites, the composition and structures become various due to the diversity of organic molecules. The structures of low-dimensional perovskites could be understood by splitting the 3D structure into smaller parts. For example, the 2D (two dimensional) perovskites are formed by inserting layers of large organic spacers into the 3D cubic structure, The inserting can be along the ⟨100⟩-, ⟨110⟩-, and ⟨111⟩-planes of the 3D structure, giving rise to ⟨100⟩-, ⟨110⟩-, and ⟨111⟩-oriented 2D perovskites.[18] Moreover, the number of the layers (n) that inserted into 3D structures also determine the structures, perovskite properties and therefore performance of devices. As compared to 3D perovskites, the A sites cations are no longer limited by the size problem in 2D perovskites, which enable all kinds of organic molecules show their potentials. Based on different types of organic spacers, the structures of 2D perovskites could be further classified into Ruddlesden-Popper (RP) phase, Dion-Jacobson (DJ) phase and Alternating cations in the interlayer (ACI) phase (**Figure 2.8**). The organic spacers have great impact to the perovskite properties: (1) They can change the distortion of perovskite lattice by tilting the angle of M-X-M bonds; (2) The exciton binding energy (E_b) can be changed by the dielectric constant of the organic spacers; (3) Organic molecules have noticeable hydrophobic effect and thereby providing better water-resistant ability for perovskite devices.[18] Similarly, the zero-dimensional (0D) perovskites, also named quantum dots perovskites, are formed by separating the 3D structure into further smaller part but still retaining the photophysical properties of individual metal halide octahedra. During the separating process, the organic spacers take more responsibilities for the change in properties of perovskites. The small size of 0D perovskites trap the excitons inside the individual octahedra, results in strong Stokes shifted broadband emissions and high exciton binding energy. Therefore, they are unsuitable for behaving as light-absorbing materials because the greatly suppressed split and transportation of carriers. Besides, 0D perovskites have superior stability owing to the tightly surrounded hydrophobic organic molecules. Thanks to these special properties, although it may hard for 0D perovskites to achieve high-performance solar cells, they show great potentials in light emitting devices and are promising to be commercialized.[41]

The challenge in understanding the composition and structures of perovskites lies in the fact that our knowledge is currently insufficient to enable perovskites to realize their full potential in light harvesting devices. For example, it has been discovered that slight adjustments in the composition can effectively suppress the phase transformation of α-$FAPbI_3$, which is an active light absorber but is unstable and readily transforms into the inactive δ phase at room temperature. Additionally, the compositions significantly influence the properties of the precursor and subsequent crystallization process, which typically determines the quality of perovskite thin films. For instance, double and triple cation systems have been shown to be more repeatable and stable in the fabrication process. Similarly, we have limited knowledge of the properties and potential of various low-dimensional perovskites due to their diversity. This diversity requires exploration, and there is a lack of principles and guidelines to aid researchers in designing perovskites with ideal and desirable functions.

2.4.3 Hysteresis in Perovskite Solar Cells

Hysteresis refers to the phenomenon of mismatch between the forward-scanned and reverse-scanned photocurrent density at given bias voltage in *J-V* tests (**Figure 2.9**).[42] This phenomenon generally results in a decrease in average conversion efficiency as the declined characteristics in reverse scan. The reason is uncertain for now but is believed to be strongly associated with the defects in perovskites, the carrier accumulation around interfaces, the ferroelectric behaviors and the ion migrations.

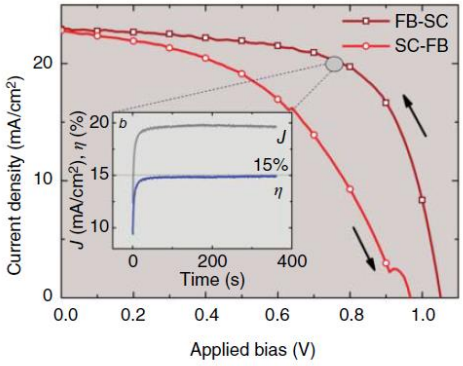

Figure 2.9. The hysteresis phenomenon in the *J-V* curves of perovskite solar cells.[42]

The hysteresis phenomenon is a quite common issue in early stage when using mesoscopic TiO_2 as electron transporting layer. And researchers have adopted many successful strategies, such as additive and interfaces engineering, to eliminate the hysteresis now. One of proposed reason is the ferroelectric effect caused polarization.[43] In organic-inorganic halides perovskites, the non-centrosymmetric lead halide octahedral structure and long-range ordering of dipoles of organic cation by electric field will lead to the generation of ferroelectric effect. The ferroelectric effect caused polarization may decrease the built-in potential and following V_{oc}. However, when researchers used pure PbI_2 (non-ferroelectric material) as light absorbing layer, the hysteresis phenomenon still exists, which suggests that the polarization is not the exclusive reason. Researchers found that the ion migration at perovskite interfaces and grain boundary maybe another competing origin for the hysteresis phenomenon. The activation energy for halides atoms is low as compared to other ions (I^-: 200~230 meV, Pb^{2+}: 810~1620 meV, Cs^+ and MA^+: 590~1120 meV).[44] Therefore, it is great potential for iodide to migrate. Because ion migration is slower than electronic response, therefore, the performance change caused by ion migration will show up in hysteresis. Besides, the ion migration also implies an unstable perovskite phase and working conditions. Because the composition will change as the ion migration is undergoing, and ununiform perovskite phase will cause differentiated bandgap, which compromise the light harvesting ability of original perovskite. In another words, ion migration is unwanted for long-term working stability. Therefore, it is necessary to suppress ion migration as well as hysteresis.

2.4.4 Stability of Perovskite Solar Cells

The instability of perovskites and their devices has been identified as the main obstacle to their mass commercialization.[45] Their instability is such that they are believed to be more stable in outer space, where the primary source of decomposition, moisture, is

absent. In contrast to silicon solar cells, which are both chemically and physically inert to most working conditions, the intrinsic nature of lead-based halide perovskites is unstable. The working lifetimes of silicon solar cells can easily exceed ten years. However, lead-based halide perovskites face stability issues from multiple perspectives (**Figure 2.10**). As previously mentioned, there are problems such as an unstable active perovskite phase and ion migration. Other stability issues include light-soaking stability and self-decomposition. Moreover, the decomposition of perovskites can result in the leakage of lead, a highly toxic heavy metal that poses a threat to all living organisms. Given that the efficiency of perovskite solar cells is approaching its theoretical limit, and their working lifetimes lag behind those of other solar cells, researchers have shifted their focus to addressing the stability issues of perovskite solar cells.

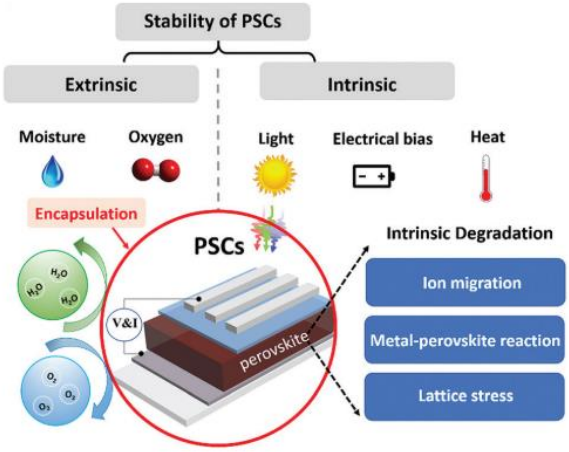

Figure 2.10. The potential reasons for the instability of perovskite solar cells.[46]

Phase stability is an issue we have mentioned before: the $FAPbI_3$ has different phase under different temperatures.[45] The formation of pure α-$FAPbI_3$ generally needs annealing temperature over 150 °C, and it will transform to inactive δ-phase in room temperature if without suppressing strategy. This situation is common in lots of perovskite system. Another typical example is the pure inorganic perovskite $CsPbI_3$, the cubic black α phase is formed at a temperature above 300 °C. This is because Cs^+ is too small to sustain the PbI_6 polyhedra in ideal cubic structure at room temperature and therefore $CsPbI_3$ will degrade to the orthorhombic δ-$CsPbI_3$ when cooling.[47] Hence,

how to sustain the photo-active phase of perovskite is the most basic stability issue to make solar cells. One of the effective and efficient strategy is composition engineering. Still take $FAPbI_3$ system as example, although this perovskite composition is very attracting due to the relatively high thermal stability and redshifted bandgap, stabilizing the pure $FAPbI_3$ in room temperature is remaining a tough question. The main reason for the phase transformation is the small-radius A site cations cannot sustain the PbI_6 polyhedra in ideal cubic structure. Researchers found that small amount doping of multiple cations could effectively suppress the formation of δ-phase because of entropic stabilization effects and tolerance factor tuning.[48] However, such stabilization is traded off with the slightly blue-shifted bandgap (that is the upper efficiency limitation) and potential severe ion migrations. In this respect, additive engineering gives out some solutions. For instance, various additives, such as methylammonium thiocyanate (MASCN)[49], formamidine formate (FAHCOO)[50] and isopropylammonium chloride (IPACl)[51] have been introduced into $FAPbI_3$ perovskites with promising effects. And we will thoroughly introduce these works in the following chapter.

Moisture is a very interesting thing for perovskite: it is proved that suitable amount of water is conducive to form high-quality perovskites thin films; but in the investigation of mechanism for degradation, water is also the one to blame for. The sensitivity is strongly associated with the composition, which is similar to the phase stability mentioned above. For example, water can catalyze the decomposition of $MAPbI_3$ into PbI_2, CH_3NH_3, and HI.[52] Study shows that perovskite phase could combine with water to form hydrous perovskite phase. In this hydrous phase, the kinetic barrier energy for I^- to migrate is largely reduced, which implies the increased migration potential of halide atoms. Consequently, the formation of vacancy point defects, especially I vacancy defects, leads to increased nonradiative recombination.[52] More severely, these new vacancy defects are usually in the deep energy level, which are tough to eliminate once formed. Such deep-level defects will become the primary targets for water to attack and combine, resulting into the snowballing effect and more severe degradation. Considering this situation, the humidity is undoubtedly the one that should be kept away

from perovskite. For tackling this issue, various methods were put forward. For instance, by adopting all kinds of hydrophobic chemicals, especially organic molecules with long alkyls chains or fluorine atoms and organic polymers, the water-resistant ability are prominently elevated. Besides, interfaces engineering is also another effective wat to protect perovskite layer, since the interface is the place that water has the first chance to contact perovskite.[37] For example, the in-situ surface modification by 2D perovskite draw vast pools of attention recently.[53] Because such modification not only tuning the energy level alignment by constructing heterojunction, but also prevent the 3D perovskite from water by using a more water-resistant 2D perovskite as protecting layer.

Although as light-harvesting materials, perovskite is also sensitive to continues intensive illumination. The ionic nature of perovskite provides advantages like highly efficient charge splitting and transportation, it also yields some issues, such as the unfixed ions and cations in the lattice. Light could provide the energy to generate photogenerated carriers, it can also provide the energy to dissociate the perovskite. For example, the blue to UV (ultraviolet) part of the light can provide the energy to break the bonds in organic molecules. This decomposition can happen faster with the help of oxygen even without UV light and these compromises are irreversible. More importantly, we mentioned the activation energy for I^- and other halide atoms are very low.[11] Therefore, the intensive light can also provide the energy for ions in perovskite to migrate and aggregate. The issues brought by ion migrations have been partially illustrate before, the results are fatal because of the severely compromised device performance. When exposed to intensive illumination, ions in perovskite begin to rearrange, resulting into ununiform perovskite phase (I-rich domains and Br-rich domains), which is even severe for multiple cations compositions. As we have mentioned, the ratio of I/Br is utilized to adjust the bandgap of perovskites. Therefore, the I-rich domain will have lower bandgap and carriers will generate lower voltage, which gives deviation of PCE.[11] Fortunately, this process is found to be reversible when light is shadowed, but the detrimental effect still exists during the operation of devices. Therefore, the segregation of halides still needed to be avoided.

2.4.5 Large-area Fabrication of Perovskites Solar Cells

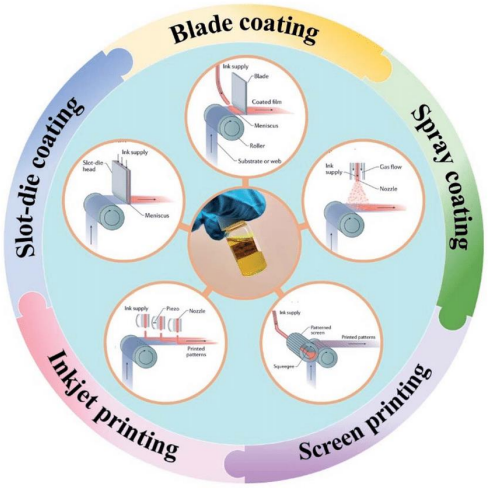

Figure 2.11. Hot methods of large-area fabrication.[54]

The stability is the issue is considered because of the economic benefits; high operational stability definitely decreases the costs for long-term using of solar cells. Another issue for increasing the benefits is mass production methods for fabrication the solar cells. This problem is paramount because the majority of the fabrication methods is spin-coating, which is generally suitable to small-area fabrication and would waste the majority of solution.[12] Therefore, many other fabrication methods were studied, such as blade-coating, slot-die coating and screen-printing. Although the crystallization process of perovskite is always tough to control precisely, the efficiency (over 23%) of small area devices fabricated by some new methods have been approaching the spin coating method. But the efficiency of large area devices is still behind the highest efficiency now. The reasons not only lie with the perovskite layer, but also with the increased areas of other layers. For example, large area will cause phase nonuniformity and following decreased J_{sc} and V_{oc}. Besides, the resistance of transparent electrodes will inevitably increase as the area increases.[12] Therefore, the performance of large-area PSCs still needs improvements. The technology for producing small-area PSCs have begun to be mature and highly reproducible, but methods for the large-area fabrication seems still lack certain principles and instructions. And this step is especially important for the commercialization of perovskite solar cells.

2.5 Additive Engineering for Improving the Performance of Perovskite Solar Cells

Significant progress has been made in the field of perovskite solar cells, with notable improvements in various characteristics that are crucial for commercialization. In addition to high efficiency, researchers have addressed key issues through dedicated efforts, resulting in the development of comprehensive instructional systems that guide further exploration. Compositional engineering, for instance, offers a straightforward yet effective approach to adjust the bandgap and stabilize the perovskite phase;[55] interfaces engineering can greatly passivate the defects at interfaces and facilitate the charge transportation by adjusting energy level alignment;[38] while solvents engineering can help better crystallization[56]. Additive engineering, a critical strategy for improving perovskite solar cells, entails the incorporation of various chemicals into the perovskite structure via the addition of precursors/antisolvents or post-treatment, leading to superior performance. Researchers have identified a plethora of additives that exhibit significant enhancing effects on perovskite solar cells, including defect passivation, increased crystallinity, perovskite phase stabilization, energy level alignment tuning, strain relief, and ion migration suppression. Moreover, many additives exhibit synergistic effects, contributing to the high-performance perovskite solar cells that are currently fabricated. Therefore, a concise but systematic introduction to additive engineering is warranted.

In order to comprehensively understand the role of additives and account for their vast diversity, a concise classification is necessary to provide specific guidance. Various types of additives can be categorized based on their respective positions within the perovskite structure. Certain cations and ions possessing suitable or sufficiently small radii can integrate into the perovskite lattice, such as K^+, Cd^{2+} and SCN^-. And the majority of other additives stay at grain boundaries/ top or bottom surface. For example, organic molecules are generally large-size and have function groups, such as −OH (hydroxy), $-NH_2$ (amino) and −SH (sulfhydryl). These functional groups provide

additional electron pairs to coordinate with unbonded atoms at the surface of the perovskite, thereby reducing defect density. Such molecules can be considered Lewis bases for their ability to donate electrons. In addition to these established additives, new types have been discovered in recent years, including low-dimensional perovskites, fullerene derivatives, and ionic liquids.

2.5.1 Metal cations

The periodic table of elements is dominated by a vast array of metals, with the position of each metal providing valuable guidance for researchers seeking to select suitable doping additives. Accordingly, it is a wise strategy to review the progress of research by following the chemical groups within the periodic table, which can offer valuable insights for the selection of appropriate additives.

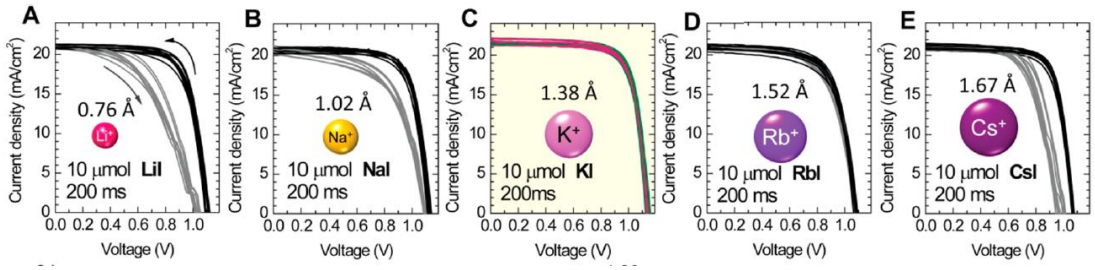

Figure 2.12 (a, b, c, d, e) The ion radius of alkali metals and their impacts to the perovskite solar cells.[57]

For metal cations that used in perovskite, alkali metals are the most widely studied, for their potential of replacing A sites cations. Cs^+ (167 pm) and Rb^+ (152 pm) have suitable ion radius to fit into the perovskite lattice, K^+ (138 pm), Na^+ (102 pm) and Li^+ (76 pm) are regarded as too small to stabilize the perovskite lattice but serve as interstitial ions or staying at grain boundaries instead (**Figure 2.12**). [57] Cs^+ and Rb^+ have been used to stabilize FA-based perovskite to form the multi-cations system for a long time, the hybridized perovskite systems still hold many record efficiencies now.[40, 48] Because FA^+ is larger than ideal A site cation, the tolerance factor of $FAPbI_3$ increase as

compared to $MAPbI_3$, leading to structure distortion from ideal cubic one. By introducing small amount of Cs^+ or Rb^+ that have smaller ionic radius, the distortion can be released to some extent. And the shrank lattice strengthens the interactions among the perovskites and refrains ion migrations. The result shows that both thermal and photo stability are improved owing to a more stable perovskite phase. Besides, researchers also found that Rb^+ could increase the conductivity and grain size and reduce capacitive current and nonradiative recombination of perovskite. The investigation of Cs^+ and Rb^+ have been very mature and widely adopted in many works and reviews owing to their contribution to the performance of PSCs, but for K^+, debates still exist. For example, Cao and coworkers demonstrated that small amount of K^+ ions that incorporated into Cs/MA/FA based perovskites tend to occupy the interstitial sites, thereby suppressing phase segregation and mitigating hysteresis by increasing the diffusion barriers energy for all diffusion paths.[57-58] On the contrast, Zheng et al. showed that the effect of K^+ ions is activated by light illumination, which help to form immobile KBr/KI complexes on the surface and grain boundaries, instead of entering into the lattice. The mobile halide ions defects are reduced by forming such complexes, this further suppress the ion migration. [59-61] Moreover, such complexes are also beneficial to hole extraction efficiency by reducing the interface trapping defect density.[59] Although the exact location of K^+ is still in debate, its conducive effects, such as suppressing ion migrations and hysteresis, are certain. Similarly, Na^+ and Li^+ can also enter perovskite lattice as interstitial atoms. The beneficial effects, such as facilitate the transformation from PbI_2 to perovskite, enlarge grain size and strengthen interfaces interactions, had been repeatedly validated.[62-63]

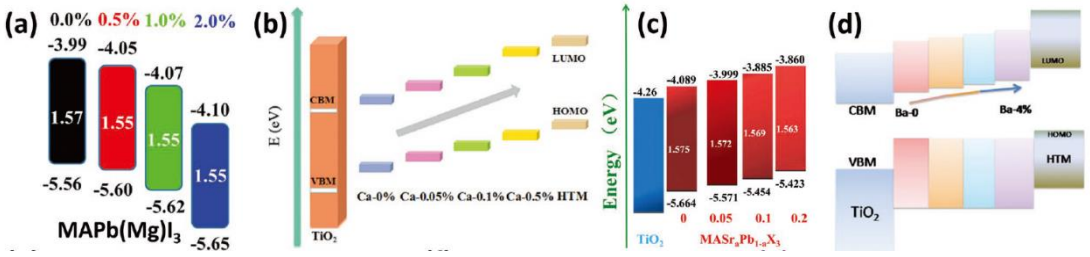

Figure 2.13 (a, b, c, d) The impact of alkaline metals to the energy alignment levels of perovskites.[64-66]

Adjacent to the alkali elements in the periodic table are the alkaline earth metals, which possess similar outermost electron configurations, allowing for the potential formation of perovskite structures. However, pure perovskites based on Ca, Ba, and Sr exhibit bandgaps exceeding 3 eV according to computational analyses, while those based on Mg exhibit unstable lattice structures due to tolerance factors exceeding 1 (1.07). Nevertheless, some promising doping effects have been reported. For example, research shows that Ca^{2+} can work as hard Lewis acid to reduce the size of colloids in perovskite precursor and thereby enlarging the grain size. Besides, Ca^{2+} can form oxide compounds (CaO and $CaCO_3$) at the surface of perovskites, providing passivating and protecting effects.[65] Similarly, Sr^{2+} can also form oxide compounds (SrO, $SrCO_3$ and $Sr(C_2H_3O_2)_2$) at surface and function as n-type materials to facilitate electrons extraction and elevate the fill factor over 85%.[66] The similar electronic configuration enables the potential for Mg/Ca/Sr/Ba enter perovskite lattice, but the change to bandgap and energy level is negligible (**Figure 2.13**).

The d-block and ds-block of the periodic table contain numerous metal elements with +1 or +2 valence states, many of which possess properties that are similar but distinct from those of the alkali and alkaline earth metals. For example, the group containing Cu, Ag, and Au has been investigated for potential use in perovskite solar cells. Cu(I) compounds, such as CuI and CuSCN, were early utilized as hole transporting layer (HTL) in other solar cells. Because Cu(I) additives were found to be interstitial doping in lattice and also have negligible impact to the crystallization process or morphology, therefore, researchers use Cu(I) additives in perovskite mainly for tuning their hole transporting ability or facilitating the HTL-free devices.[67] For Cu (II) additives, the introduction into perovskite precursor can form $CuBr_2$-DMSO-PbI_2 intermediate and therefore larger grain size and smoother surface.[68] Ag(I) have similar ion radius with Pb^{2+} and thus able to replace Pb^{2+} in perovskite lattice, but the coordination ability (4

atoms) is much less than Pb^{2+}(12) in perovskites[69]. Therefore, there are Ag/Bi bi-metal perovskite solar cells for replacing the toxic Pb, but the efficiency is still very low. Researchers have found that both Ag+ and Cu+ serve as p-type dopants in perovskite when added as additives, leading to a downshift of the Fermi level towards the valence band edge. Ionic gold (Au) possesses two valence states (+1 and +3), both of which are unstable and easily revert back to gold. The use of Au in perovskites is limited due to its primary use as an electrode in conventional structures and its contribution to the fast degradation of perovskite. Nevertheless, some studies have reported the beneficial effects of Au nanoparticles on perovskite solar cells.[70]

Apart from the typical ds-region metal Cu/Ag/Au, d region also contains many widely studied metals. For instance, Mn^{2+} showed multiple conducive effects to the Cs^{+}-based perovskites. Mn^{2+} can enter perovskite lattice of $CsPbX_3$, which enable perovskites to form electronic states in the mid-gap region and generate unique charge transfer dynamics.[71] Besides, excessive Mn^{2+} that stay at grain boundaries can deliver defect passivation effect and enhanced hole extraction efficiency.[72] Apart from Mn^{2+}, Co^{2+} was also reported to capable of entering perovskite lattice, but results in negative effects by promoting a transformation from cubic phase to tetragonal phase and decreasing grain size.[73] But for the effects of various fabrication methods, the functions of Co^{2+} is remain in debating.[74] Fe^{2+} is considered as in the same situation with Co^{2+}, the detrimental effects by doping Fe^{2+} are well known in many semiconductors. The degraded performance is demonstrated even when Fe^{2+} is less than 1ppm. Therefore, studies show that Fe^{2+} can also deteriorate perovskite performance when incorporation concentration low to 10 ppm.[75] Although there are also reports claimed that 2% doping pf $FeCl_2$ can elongate the carrier lifetimes, the easily oxidation issue of Fe^{2+} remain unsolved.[76]

The investigation of metal additives is paramount, not only for the purpose of elevating lead-based PSCs, but also for the potentials of substituting Pb^{2+} due to the deadly toxicity of Pb^{2+} and scientists' growing interests in lead-free perovskite solar cells.

Besides, recent studies in interfaces engineering pull many researchers' interests back to metal ion doping. Because they found that by post treating perovskite thin films with very low concentration of metal ions, the beneficial doping gains can be huge.

2.5.2 Ammonium Salts

The highest efficiency of PSCs was achieved on organic-inorganic hybrid perovskites. In the hybrid perovskites, MA^+ and FA^+ are the most widely studied A sites cations. The ammonium salts composed by MA^+/ FA^+, such as MACl (methylammonium Chloride) and MABr (methylammonium bromide), were found to be multi-functional when introduced as extra additives. Besides, the inorganic part such as pseudohalides, including SCN^- (thiocyanate), PF_6^- (hexafluorophosphate) and BF_4^- (hexafluorophosphate), were also reported to have various conducive effects to perovskites. More importantly, the diversity of organic ammonium salts enables researchers to obtain much more opportunities to adjust the effects by synthesizing ammonium salts with various structures. And the versatile functions of some typical ammonium salts will be introduced in this section.

MACl is a prevalent additive now in lots of high-performance PSCs due to its huge impact to the crystallization process. High concentration of MACl that usually more than 30% was utilized to help mediate the perovskite phase transformation.[77-79] The grain size can be increased to several times larger than the control sample, such huge improvements in perovskites thin films quality was attributed to the prominently reduced formation energy of light-active cubic perovskite phase, which starts to facilitate the phase transformation even without annealing.[77] More importantly, the introduced MACl will be removed during the annealing process due to the low evaporation temperature of MA^+, thus causing neglected impact to the bandgap of perovskites. Apart from MACl, there are also many other ammonium salts with similar functions, such as FACl[80] and FABr[81].

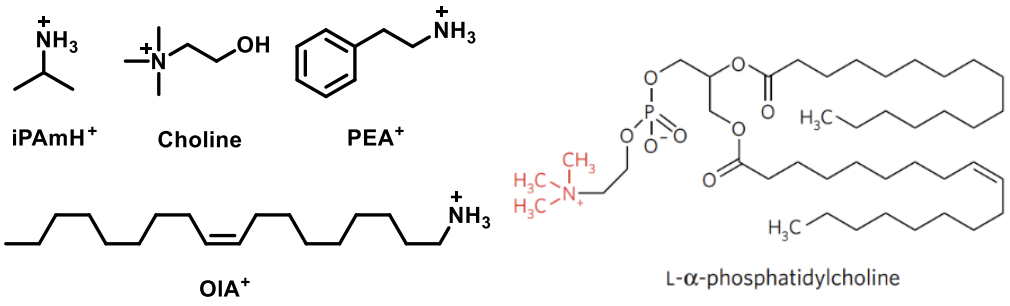

Figure 2.14. The structures of various ammonium salts.

The ammonium salts that could be incorporated into perovskite lattice is restricted by the cation size, which makes the choices of ammonium salts very limited. But one important part in ammonium salts is amino groups, which provides the interactional sites with Pb^{2+} and affects the crystallization process. Therefore, large size ammonium salts can also have great impact to the quality of perovskite thin films, especially at surface and grain boundaries. For example, Seok and coworkers incorporated isopropylammonium chloride (iPAmHCl) to stabilize the α-$FAPbI_3$ phase and delivered certified efficiency over 23.9%.[51] Characterization shows that isopropylammonium cations ($iPAmH^+$, **Figure 2.14**) formed at around grain boundaries by a side chemical reaction between IPA and MACl, which contributes to the reduced defect density and stable light-active phase. Besides, another example is quaternary ammonium halides (QAHs) with a structure of $NR_4^+X^-$, Huang et al. reported a universal passivation effect by introducing quaternary ammonium halides such as L-α-phosphatidylcholine and choline chloride (**Figure 2.14**).[82] Although no extra function groups are introduced except from the original amines, the function of various ammonium halides can still be distinct. This is because the structures of alkyl chains or aromatic rings can also have great impact to things like hydrophobic ability, diploe moment and formation of intermolecular interactions (hydrogen bonds, π -π interactions, etc.). These easily neglected factors may affect the formation energy, moisture resistant ability and energy level alignments.

Another classical example is phenethyl ammonium iodide (PEAI, **Figure 2.14**), which contains an aromatic ring as compared to alkyl chains amines. The aromatic ring makes

PEAI impossible to be incorporated into the 3D perovskite lattice, but also endows PEAI with special functions. PEAI is widely used both in the grain boundaries passivation as well as surface modification by direct adding to precursors or posttreatment. The passivating effect have been widely confirmed in many works, but the passivating mechanism is still under debate. For example, You and coworkers demonstrated that perovskite thin films post treated by PEAI dose not forms 2D perovskites around surface and grain boundaries.[83] It is single PEA^+ molecule instead of PEA_2PbI_4 that enhances the device performance by passivating iodine vacancies. However, many other works claims that PEA^+ molecule tends to form PEA_2PbI_4 when added to the perovskite thin film, and the 2D perovskites can tune the energy alignment with charge transporting layer as well as passivating defects around surface and grain boundaries.[84-85] It is now believed that the passivating mechanism is strongly associated with the perovskite compositions and fabrication methods. But it is definitely necessary to figure out the potential affecting factors to the different passivation mechanism, which may provide additional instructions to design new passivating agents. For instance, researchers utilized fluoridated or brominated PEAI to achieve enhanced passivating effects or provide addition functions, such as moisture-resistant ability, to elevate the performance of PSCs.[86-88]

We have mentioned the potential of forming 2D perovskites when adding ammonium salts directly to 3D perovskites, many researchers took advantage of this trait to modify the perovskite surface with 2D perovskites by posttreatment with various ammonium salts. Such surface modification enables researchers to fabricate inverted PSCs with efficiency over 24%. The structure of ammonium salts shows great impact to the formation of 2D perovskites. In the introduction section, we mentioned that the bandgap of 2D perovskites depends on the n value, which refers to the number of octahedron perovskite layers. Large n value suggests an approaching to pure 3D perovskites and narrow bandgaps, and the control of exact n value of 2D perovskites remains a tough issue. By construction heterojunction on the 3D perovskite surface with 2D perovskites, the energy level alignment can be well adjusted towards charge transporting layer,

thereby facilitating the charge extraction efficiency. For example, Sargent et al. demonstrated preferential growth of n≥3 2D perovskites on perovskites with inverted structure, avoiding the formation of small n 2D perovskites that have unfavorable wide bandgap.[89] Such preferential growth was realized through the design of ammonium salts, they found that PEA tends to form 2D perovskite with n = 2, but 3F-PEA is more inclined to form 2D perovskite with n = 3, which is more favorable to construct a suitable heterojunction. The differential growth reason lies with the extra fluorine atom, which cause steric hindrance and larger strain, therefore slower intercalation. Besides, the theoretical calculation shows lower formation energy 2D perovskite with n = 3 when used 3F-PEA as spacers.[89] The steric hindrance effect was also observed with oleylammonium-iodide (OLAI, **Figure 2.14**), which has 18 C atoms in alkyl chains, Randi and coworkers utilized OLAI to precisely control the 2D perovskite with n = 2. The 2D perovskite with long alkyl chain provide extremely water-resistant ability to the entire device, which retained more than 95% of initial efficiency after 1000 hours stored in damp-heat conditions.[53]

The investigation in ammonium salts have enabled researchers to be well guided when choosing them, but the progress is far from enough. Not only because the great improvements brought by ammonium salts for PSCs, but also for the potential of exploring for new types of perovskites, which is remarkably paramount for low-dimensional perovskites since organic spacers are the main compositions.

2.5.3 Organic Molecules

The development of synthetical of organic chemistry have push forward many materials-related areas. The diverse functional groups in organic molecules provide many instructional strategies to elevate the performance of PSCs. For example, ammonium salts are organic molecules that contain acidated amines. Apart from amine group, there are many other functional groups that could interact with perovskites, such as −COOH, −C=O and −OH. These function groups can play multiple roles in the

formation of perovskites, these roles are reviewed to be critically important to the performance of PSCs. Besides, thanks to the diversities of organic molecules, researchers have explored vast pools of organic additives that possess prominently positive effects to the PSCs.

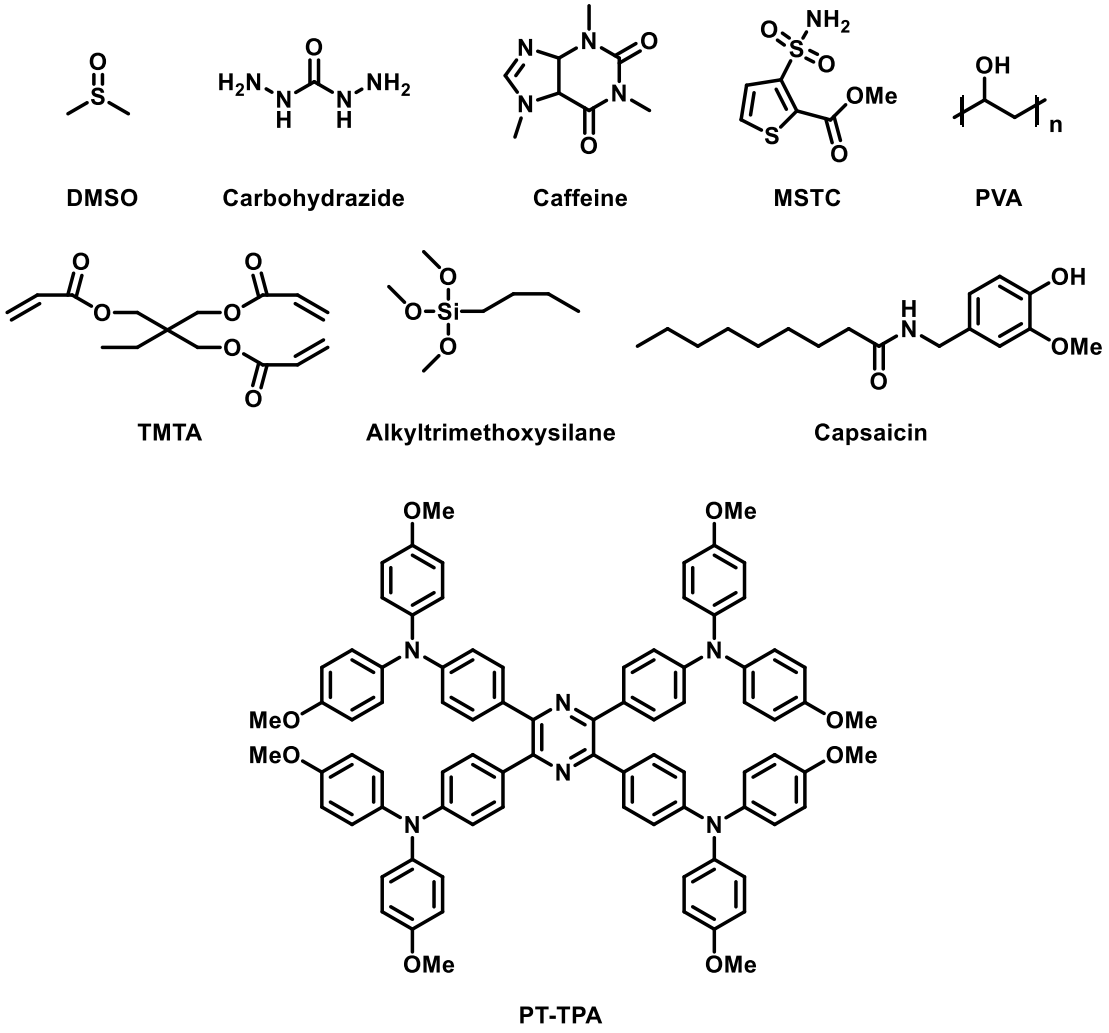

Figure 2.15. The structures of various organic molecules added into perovskites.

The raw materials of perovskites need organic solvents for dissolving and recrystallizing into thin films. The dissolving and recrystallization process are all involved the formation of intermediate with solvents, such intermediate determines the solubility as well as the crystallization speed. For example, the N, N-dimethylsulfoxide (DMSO, **Figure 2.15**) and N-methyl-2-pyrrolidone (NMP) are −C=O / −S=O based organic solvents, DMSO have become the most common solvents as N, N-

dimethylformamide (DMF). The −S=O group can interact with Pb^{2+} to form perovskite-DMSO intermediate, which slow down the phase transformation of intermediate towards perovskite phase and thereby enlarging the grain size. Besides, different ratio of DMSO generate different perovskite-DMSO intermediates, which have various formation energy towards the light-active phase.[56, 90-91] The drawback of DMSO was also recently reported, Huang's work demonstrated the high evaporation temperature of DMSO will cause numerous pinholes in the bottom surface of perovskites because the late evaporation, which severely compromised the device performance. Therefore, they substituted DMSO with carbohydrazide (**Figure 2.15**), a solid organic additive that has −C=O group, to avoid of late evaporation induced pinholes. The −C=O group can function as −S=O group in DMSO to interact with Pb^{2+} and form intermediate but avoids the potential issues. The impact of −C=O group to perovskite crystallization was also observed in caffeine, which contains two −C=O groups.[92] Apart from playing roles in crystallization process, the −C=O group can also passivate perovskite grain boundaries due to the coordinating ability of −C=O group, where the oxygen atoms provide electron lone pairs to unbonded Pb^{2+}.[93]

The coordinating ability of oxygen in −C=O group is attributed to the electron lone pairs, such chemicals are also called Lewis base. Many functional groups can serve as Lewis base to interact with perovskites, such as the −S=O group, $-NH_2$ and −SH (sulfhydryl group)[94]. Their ability to donor extra electrons, also called basicity, can be tuned by attaching different atoms on near chains. Apart from the Lewis base type additives, hydrogen bond in organic molecules is another common force to interact with perovskites. For instance, functional groups like −COOH, −COH and −OH can provide vast pools of hydrogen bonds. Han et al. introducing poly(vinyl alcohol) (PVA, **Figure 2.15**) into $FASnI_3$ to provide nucleation sites and direct the crystal orientation for better thin film quality. The strong $O-H\cdots I^-$ hydrogen bonds can also fix the easily migrate I atoms and thereby suppressing ion migrations and enhancing long-term stability. [95]

Both coordination bonds and hydrogen bonds are affecting the perovskites by forming direct forces. The majority of the organic molecules show their potentials in this way, but there are many organic molecules affect the perovskite with an indirect way. For example, strain management is another hot topic in recent years. The strain in perovskite comes from the distorted lattice, which is caused by multiple potential reasons such as fabrication method and are common problems in many perovskite systems. Reducing strain can enhance PCE as well as device stability. Li and coworkers used trimethylolpropane triacrylate (TMTA, **Figure 2.15**) to post treat perovskite thin films and regulate the surface strain by recrystallization.[96] The partial dissolve of perovskite thin film enables the TMTA to take part in the recrystallization process, therefore releasing the surface strain. Similarly, Loo and coworkers utilized alkyltrimethoxysilane (**Figure 2.15**) to construct a strain-release layer at the interface between perovskite and TiO_2.[97] The strain-release layer can reduce the lattice distortion of above perovskites, resulting into enhanced light-active perovskite phase. Apart from the strain-releasing function, organic molecules can also tune the p/n type of perovskite thin films. Huang and coworkers designed a organic molecule PT-TPA (**Figure 2.15**)(4,4′,4″,4‴-(pyrazine-2,3,5,6-tetrayl) tetrakis (N,Nbis(4-methoxyphenyl) aniline) with donor-acceptor structure, which induces intermolecular charge transfer and p-type doping effects.[98] By modifying the perovskite surface with PT-TPA, a band bending effect forms and facilitate the charge extraction efficiency. Another typical p/n transformation used a nature organic molecule, capsaicin. Bao et al. introduced capsaicin directly into $MAPbI_3$ and fount that capsaicin (**Figure 2.15**) mainly locates around top side of perovskite thin films and cause a direct transformation from p to n type perovskites. Capsaicin also contains −C=O group that could passivate the defects in perovskites.[99] Therefore, the synergistic effects of introducing capsaicin helped to achieve the highest records efficiency on $MAPbI_3$ based PSCs.

In summary, the diverse and multitasking organic additives have help researchers to reap and accumulate lots of experience in designing new types of additives. Although organic additives have been widely investigated, and their mechanism can be partially

classified by the functional groups in the organic molecules, the mechanism of many new functions are still unclear. For example, the reason of p/n type transformation by doping capsaicin was not given in the study, which is critically significant to design new additives to achieve enhanced effects. Moreover, the functions of various organic additives are separately effective, is it possible to achieve multiple effects with one organic additive? The synergistic effects between each additive are also paramount to harvest PSCs with higher efficiency and stability.

2.5.4 Low-dimensional Perovskites

In the introduction section, we provided a basic overview of low-dimensional perovskites, including 2D PSCs and quantum dot LEDs, which have garnered significant attention due to their high stability, quantum confinement, and diverse properties. Although these traits can be both advantageous and disadvantageous depending on the desired application, researchers have found that incorporating low-dimensional perovskites as additives in 3D PSCs can maintain the efficient light-harvesting ability of 3D perovskites while overcoming the poor charge transportation in low-dimensional perovskites, resulting in significant improvements in 3D PSC device performance. This effect is evident from the examples discussed in the previous chapter, which illustrate the construction of heterojunctions on 3D perovskites through surface treatments of ammonium salts.

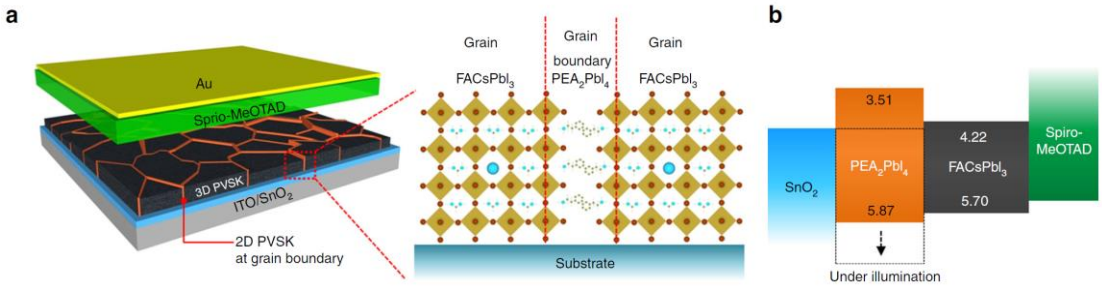

Figure 2.16. Schemes of perovskites device with low dimensional perovskites.[100]

The initial purpose of introducing low-dimensional perovskites into 3D perovskites is to stabilize the unstable perovskite phase such as $FAPbI_3$ and $CsPbI_3$. Yang and coworkers incorporated PEA_2PbI_4 into $FAPbI_3$ to obtain pure phase $FAPbI_3$. And 2D perovskites stay at and passivate grain boundaries and surfaces, which greatly reduces the defect density and elongates carrier lifetimes.[100] An interesting phenomenon is that the effect of adding 2D perovskites or their counterpart ammonium salts is different, this is due to the intermediate in the precursor solution result in different formation states during the crystallization process, but this phenomenon is still in debate.[84, 101-102] Different from constructing heterojunction on the surface with 2D perovskites, the direct addition is a widely adopted passivation method that suitable for perovskites with various compositions, which includes narrow/wide bandgap perovskites and tandem PSCs.[84, 103] Apart from the most widely used PEA_2PbI_4, Zhang and coworkers utilized $EDAPbI_4$ (EDA:ethylenediamine), a 2D perovskite composed of diamine to stabilize $CsPbI_3$.[104] In recent years, this area had grown into a brand-new area, which studies the performance of 2D/3D mixed perovskites, which also called quasi 2D perovskites.

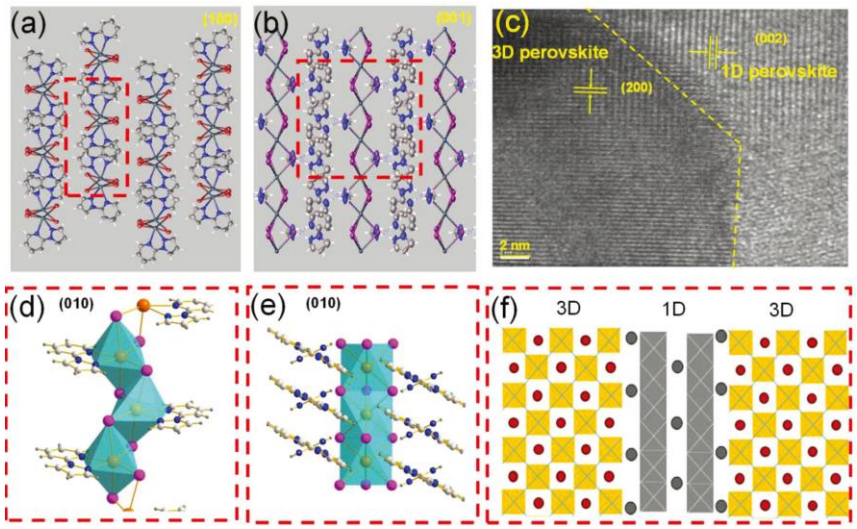

Figure 2.17. The structures of 1D perovskites PbI_2-FAI-PZPY in 3D perovskites. [105]

Except from the mixed 2D/3D perovskites, researchers also incorporated 1D perovskite to boost the performance of 3D perovskite. Mai et al. added 2-(1H-pyrazol-1-yl)pyridine (PZPY) into 3D perovskites to form 1D perovskites and construct 1D-3D

heterojunction structure (**Figure 2.17**).[105] Apart from passivating the defects in 3D perovskites, the 1D perovskites possess flexible liner alignment, which provides the entire device thermodynamic self-repairing ability as well as higher thermal stability. Similarly, Fan and coworkers used bipyridine (BPy) to construct 1D perovskites with lattice that matching the lattice of 3D perovskites. The hybrid perovskites delivered an enhanced device efficiency and stability.[106] The surface modification by 2D perovskites is a very popular method in the hybrid 2D/3D perovskites, there are also works reported similar role of 1D perovskites, but the progress is far lag behind the utilization of 2D perovskites. For example, Chen and coworkers used a polymer cross-lined by propargylammonium (PAI) that contain amine groups to construct the 1D perovskites on top of 3D perovskites. The formed 1D perovskites can effectively passivate grain boundaries, restrain ion migrations and enhance operational stability.[107]

The utilization of 0D perovskites was also demonstrated to promote the performance of PSCs based on 3D perovskites. For example, Zhu and coworkers in situ synthesize various 0D perovskites on $CsPbI_3$ by tuning the stoichiometry of the precursors between CsI and PbI_2. A suitable 0D perovskite Cs_4PbI_6 was chosen to stabilize the black phase of $CsPbI_3$, which helped to deliver the record efficiency of all-inorganic PSCs at that time.[108] The similar stabilizing effect of 0D perovskites was also supported by Yao's work, which used $Cs_4Pb(IBr)_6$ also to stabilize the all-inorganic perovskite $CsPbI_{3-x}Br_x$.[109] The works mentioned above are the studies in all-inorganic perovskites, which is easier to fabricate 0D perovskites via in situ methods. Recently, Wu and coworkers utilized 1,4-bis(amino-methyl)benzene dihydroiodide (p-$PBAI_2$) and 1,3-bis(aminomethyl)benzene dihydroiodide (m-$PBAI_2$) to construct 0D perovskites as capping layer for PSCs with efficiency over 24%, which demonstrates the potential of 0D perovskites.[110] However, the works relating to 0D perovskites used in 3D perovskites are far less as compared to the works in 2D and 1D perovskites. The potential reason may be ascribed to the severe quantum confinement effects caused compromised charge transporting efficiency, which needs judiciously choose the types of 0D perovskites.

To summarize, various types of low-dimensional perovskites are effective additives for enhancing the performance of 3D perovskites in PSCs. Due to their wide bandgap and quantum confinement, low-dimensional perovskites are typically doped in low concentrations or applied as surface medication layers to passivate the surface and grain boundaries of 3D perovskites. Moreover, the easily adjustable bandgap of low-dimensional perovskites enables the construction of heterojunctions with 3D perovskites, facilitating charge transportation and extraction. The exceptional stability of low-dimensional perovskites also contributes to the creation of more stable 3D perovskites, thereby enhancing the long-term stability of PSCs.

2.5.5 Ionic Liquids

Ionic liquids have gained increasing attention in the materials science field due to their unique chemical and physical properties, despite their initial use as solvents in green synthesis. Typically composed of asymmetric organic cations and organic or inorganic ions with easily tunable structures, the diverse range of ionic liquids enables researchers to design materials with ideal functions. The numerous hydrogen bonds and hydrophobic forces present in ionic liquids can affect the properties of both the liquids themselves and the crystallization process of perovskites. Moreover, the ionic nature of ionic liquids has significant impacts on defects passivation, charge transportation, and energy alignment. In this regard, we will provide a brief summary of typical works demonstrating the potential of ionic liquids in perovskite solar cells.

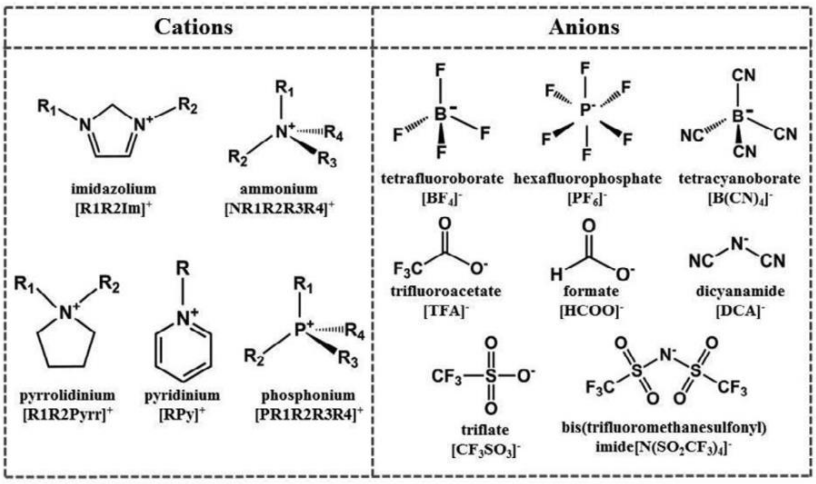

Figure 2.18. Structures of some common parts used in ionic liquids.

Ionic liquids have great impact to the nucleation process, they are inclined to form nano sized aggregates and facilitate the nucleation of perovskites to form large grain size. For instance, Taima and coworkers utilized 1-hexyl-3-methylimidazolium chloride (HMImCl) to effectively enhance the crystallinity of perovskites by forming uniform spherical nanoparticles in the precursor solution.[111] Like the widely used solvent additive DMSO, many ionic liquids are solvents themselves. Taking advantage of the organic parts in ionic liquids, they can coordinate with perovskite composition by forming coordinate bonds or hydrogen bonds. These interactions play vital roles in the dissolving of perovskites precursors and formation of intermediates. For example, Seo et al. used methylammonium formate (MAFa) to tune the crystallization process by using the $HCOO^-$ to interact with Pb^{2+}, which can slow down the crystallization speed and enlarge grain size.[112] Such coordination ability enables the ionic liquids to serve as the exclusive solvents in large area fabrication methods, such as screen printing. Another hot ionic liquid is methylammonium acetate (MAAc), which will evaporate during annealing process and cause neglected impact to perovskite composition. Huang and coworkers reported that MAAc could insert into PbI_2 interlayer space to form $MAPbI_{3-x}Ac_x$ intermediate phase, which may reduce perovskite formation energy and annealing temperature.[113] Another paramount for the widely studied ionic liquids is their improvements in perovskite stability. For example, Henry and coworkers

incorporated 1-butyl-3-methylimidazolium tetrafluoroborate ($BMIMBF_4$) into the perovskite precursors, which could hugely increase the thermal stability and light-soaking stability.[114] The components in ionic liquids interact with the perovskites to immobilize the ions at grain boundaries and surfaces and thereby restrain the ion migrations and degradation, which is vital to retain the stability of overall devices. In another Henry's work, they introduced another ionic liquid 1-butyl-1-methylpiperidinium tetrafluoroborate ($[BMP]^+[BF_4]^-$) to improve the performance of PSCs.[115] Standing from the degradation mechanism, they proposed the plausible reasons for the improved stability brought by the ionic liquids, which is attributed to the suppressed formation of Frenkel defects.

Apart from direct doping strategy, ionic liquids are also used to modify the perovskite surface. The strong dipolar polarization of ionic liquids endows them special physical properties. For example, 1-butyl-3-methylimidazolium tetrafluoroborate ($BMImBF_4$) was incorporated to modify the electron transporting layer TiO_2, which promotes a smoother TiO_2 surface, reduced work function and higher carriers transporting efficiency.[116] Similar works were also carried out to use ionic liquids to modify the charge transportation layer, such as SnO_2, ZnO, NiO_x and PEDOT: PSS.[117] Owing to the ionic nature, some ionic liquids are good conductivity and serve as charge transporting layer. Therefore, ionic liquids are used to modify the surface of perovskites in HTL-free PSCs. For instance, 1-butyl-2,3-dimethylimidazolium chloride (BMMImCl) was adopted to passivate the defects on the surface of perovskite in carbon-based HTL-free $CsPbBr_3$ PSCs.[118] The ionic liquid layer can tune the energy level of perovskite surface towards the energy level of carbon electrode, which enables the valence band of perovskites move close to the work function of carbon electrode. Besides, the organic parts in ionic liquids can be installed with function groups to interact with the perovskites. Therefore, ionic liquids that used to modify the perovskite surface can also passivate the defects at surfaces and grain boundaries.

2.5.6 Conclusions and Prospects

The rapid progress of perovskite solar cells is closely tied to the use of various additives. In this regard, we have provided a brief overview of some of the most widely used additives, including metal cations, ammonium salts, organic molecules, low-dimensional perovskites, and ionic liquids. However, this list is far from comprehensive, given that additive engineering is the most common strategy for enhancing the performance of PSCs from every aspect, and researchers have employed a wide range of additives to achieve many record efficiencies. In light of these advances, it is important to address potential problems and consider future prospects for the commercialization of PSCs.

The extensive research on additives for perovskite solar cells is driven by their significant and diverse effects. The development of additive strategies has led to the formation of systematic principles that provide instructive guidance to researchers. Many additives, such as MACl and PEAI, have become commonplace in various perovskite compositions due to their well-established mechanisms and beneficial effects. However, the search for new additives, including novel types such as hot ionic liquids, and those that can be employed in perovskites is far from complete, and the diversity of additives will continue to expand with the development of synthesis chemistry. Additionally, the relationship among various additives when added to the same perovskite system is a critical issue, as a single additive may not resolve all issues. It is common to add multiple additives to improve PSC performance from various aspects. The synergistic effects among these additives are not always straightforward, as the introduction of one additive may enhance, complement, or even compromise the effects of another. This aspect is less investigated than the exploration of new additives, making further study of additives necessary. In this regard, we will illustrate a new additive and a synergistic effect between two additives that enhance PSC efficiency to over 23%.

Chapter 3 KBF_4 Additive for Alleviating Microstrain, Improving Crystallinity and Passivating Defects in Inverted Perovskite Solar Cells

In this part, we introduce a small amount of KBF_4 as an additive to elevate the quality of triple-cation mixed perovskite thin films. We find that KBF_4 can enhance the crystallinity and alleviate microstrain of the perovskite thin films. Moreover, KBF_4 can passivate defects in perovskite grains, leading to much longer carrier lifetimes. Consequently, the resultant devices show improved fill factor, enhanced device efficiency and better device stability. Under optimum fabrication conditions, triple-cation mixed perovskite solar cells with an inverted structure show power conversion efficiency over 23% as well as excellent stability under different conditions.

3.1 Introduction

The skyrocketing power conversion efficiency (PCE) of organic-inorganic halide perovskite solar cells (PSCs) has enabled them to be the most promising next-generation photovoltaic technology. The merits, such as tunable semiconducting properties, relatively easy processing methods and inexpensive raw materials endow PSCs great potentials for commercialization.[119-120] Numerous efforts have been devoted to enhancing the device performance, including compositional engineering[55], interface engineering[121] and additive engineering[14, 31]. For various perovskite compositions, formamidine (FA)-based PSCs have delivered many record efficiencies owing to their high short circuit current density (J_{sc}) brought by the broad light absorption spectra.[122] However, FA-based perovskite has an unstable black α-phase and can easily undergo a phase transition from black α-phase to photo-inactivated-phase below 150 °C. Multiple strategies had been put forward to tackle the unstable black α-phase. For instance, various additives, such as methylammonium thiocyanate (MASCN)[123], formamidine formate (FAHCOO)[124] and isopropylammonium chloride

(IPACl)[125] have been introduced into FA-based perovskites with promising effects.

For compositional engineering, one of the strategy is to add a small amount of other A site cations such as MA^+ (methylammonium) and Cs^+ (cesium) to stabilize the black α-phase by entropic stabilization effect without compromising the high J_{sc}.[126-127] By adopting a triple-cation system, a stable black α-phase could be achieved under a much lower temperature (100 °C).[128] Moreover, the carrier lifetimes and transportation efficiency in a triple-cation system were also reported to be much longer and higher as compared to traditional double or single cation system.[128] Although great efforts have been devoted to further enhancing the performance of triple-cation based PSCs, many issues remain challenging. For example, the incorporation of A site cations with different size will lead to an increase of mircrostrain because of the distortion of the ideal structure.[129] Such mircrostrain may lead to defects and consequently nonradiative recombination, which will severely compromise the device efficiency and stability.[130-131]

The device structure of PSCs could be generally classified into normal n-i-p type and inverted p-i-n type. Although the record efficiency for PSCs has been achieved in the normal type[122], the inverted PSCs are even more popular in practical applications such as tandem solar cells[132], flexible electronics[133] and large-area devices by blade coating[134]. However, the fabrication of inverted PSCs with high efficiency is more challenging.[135] Herein, we develop a convenient approach to improving the performance of inverted PSCs by introducing an inexpensive additive KBF_4. With the addition of KBF_4, the carrier lifetimes are prolonged in the perovskite layer, which can be attributed to the improved crystallinity, released lattice stain and defect passivation by the additive. Consequently, a champion inverted device with a PCE of 23.04% is achieved while control devices without the additive only show the highest efficiency of 21.13%. Moreover, the device stability is increased by the additive. Therefore, this work provides a convenient approach to fabricating high-performance inverted PSCs.

3.2 Experimental Section

Preparation of triple cation mixed Perovskite solution: the triple cation perovskite solution was prepared by mixing two 1.2 M $FAPbI_3$ and $MAPbBr_3$ perovskite solutions in DMF: DMSO (4:1 volume ratio, v: v) in a particular ratio (e.g. 95:5). The 1.2 M $FAPbI_3$ solution was thereby prepared by dissolving FAI (722 mg) and PbI_2 (2130 mg) in 2.8 mL DMF and 0.7 mL DMSO which contains a 10 molar % excess of PbI_2. The 1.2 M $MAPbBr_3$ solution was made by dissolving MABr (470 mg) and $PbBr_2$ (1696 mg) in 2.8 mL DMF and 0.7 mL DMSO which contains a 10 molar % excess of $PbBr_2$. PEA_2PbI_4 solution was prepared by mixing 489mg PEAI and 461mg PbI_2 in 800 µL DMF. Lastly, 40 µL of a 1.5 CsI solution in DMSO (389 mg CsI in 1 mL DMSO) was mixed with 960 µL of the above-described mixture of $FAPbI_3$ and $MAPbBr_3$ resulting in a nominal perovskite stoichiometry of $Cs_{0.05}(FA_{0.95}MA_{0.05})_{0.95}Pb(I_{0.95}Br_{0.05})_3$, respectively. And 0.5 µL of PEA_2PbI_4 solution are added to the mixed perovskite solution to improve the device performance.

Device fabrication: To fabricate a device structure of glass/ ITO/ PTAA/ Perovskite/ PCBM/ BCP/ Ag, ITO glass substrates were ultrasonically cleaned by deionized (DI) water, acetone and isopropanol for 15 min, respectively. Then, the cleaned ITO substrates were dealt with air plasma for 8 mins before use. Then the substrates were transferred to N_2 glovebox. After the substrates were transferred into glovebox, poly(triaryl amine) (PTAA) solution (2 mg mL^{-1}) was spin-coated at 5000 rpm for 30 s and annealed at 100 °C for 10 min. The substrates were cool down to room temperature before use. 1.2 M perovskite precursor solutions were constructed by mixing FAI, PbI_2, MABr, $PbBr_2$ and CsI in DMF: DMSO mixed solvent with a chemical formula of $Cs_{0.05}(FA_{0.95}MA_{0.05})_{0.95}Pb(I_{0.95}Br_{0.05})_3$. 50 µL of the prepared precursor solution was spin-coated at 1000 rpm for 10 s and 5000 rpm for 30 s onto the PTAA-coated ITO substrate, 50 µL CB as anti-solvent was dripped on the film at 10 s before the end of the last procedure and then annealed at 100°C for 30 min. Afterward, PCBM (20 mg mL^{-1}) and BCP (0.5 mg mL^{-1}) were spin-coated on the films at 1500 rpm for 60 s and

4500 rpm for 30 s, respectively. For solution with KBF_4, different molar ratio of KBF_4 was added to the original 1.2 M $FAPbI_3$ solution. Finally, 200 nm silver electrodes were thermally evaporated onto the films at a chamber pressure of 10^{-7} Torr with a deposition rate of 0.5 Å s^{-1}. The active area of rigid PSC is 0.048 cm^2 and flexible PSC is 0.01 cm^2.

Characterization: J-V curves were measured by a Keithley 2400 source meter with a solar simulator under AM 1.5 G one sun illumination (Newport 66902). The scanning rate was 100 mV s^{-1} with a voltage step of 10 mV. The EQE of the PSCs was obtained from an EQE system under DC mode. To reduce the optical reflection loss, an antireflection (AR) layer was added on the glass side during the test of the champion 5 ℃ antisolvent treated devices. SEM images were measured by a field-emission SEM (Tescan MAIA3). XRD patterns were measured using Cu K_α radiation (Rigaku, Smartlab) to analyze the crystallization of perovskite. PL was measured by the FLS 920 (Edinburgh Instruments, Ltd) with excitation at 645 nm.

Statistical Analysis: The data, figure and statistical graph (*J-V* curves, XRD figures, XPS figures, Williamson−Hall plots, PL, UV-vis, SCLC, EQE, stability tests) in the article is pre-processed and drawn by Origin Pro (ver. 2019). The SEM figure is processed by Digital Micrograph (ver. 3.4). The AFM figure is processed by NanoScope Analysis (ver. 1.7).

Computational methods: DFT: All DFT simulations were conducted using Quantum Expresso (ver. 6.5).[136] All the structures were fully relaxed before the DOS and charge density calculations. The relaxation was performed under Perdew, Burke and Ernzerhof (PBE) exchange-correlation functionals[137] with projector augmented wave (PAW) method. The electronic convergence criterion was set to be 1 x 10^{-6} eV. A plane wave basis set of 450 eV cut-off energy was used.

3.3 Results and Discussion

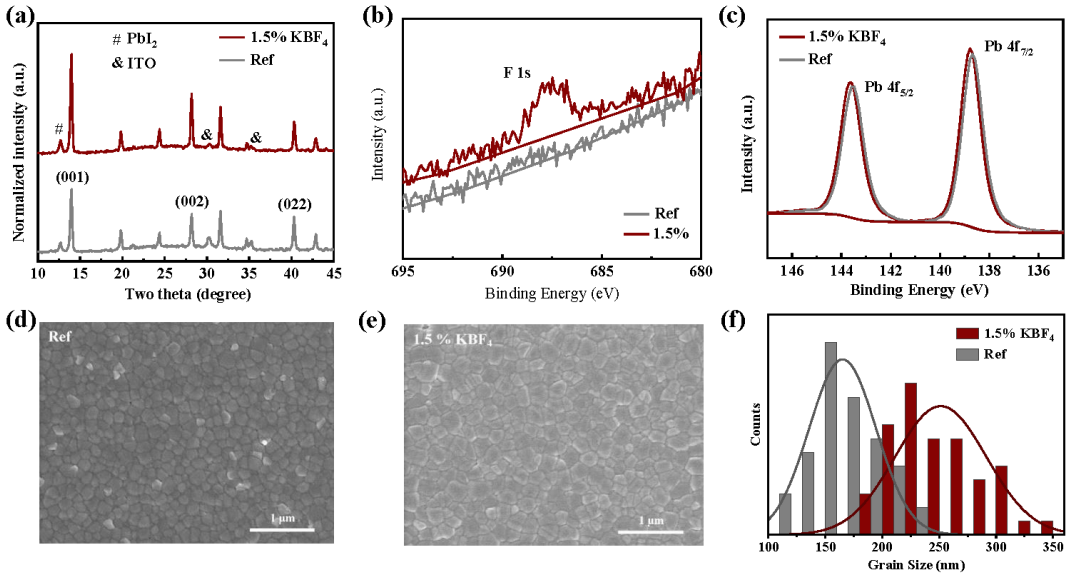

Figure 3.1. (a) The XRD patterns of triple cation mixed perovskite with and without KBF_4. (b, c) XPS spectra of F 1s (b) and Pb 4f (c) for the perovskite films with and without KBF_4. (d, e) The plane-view SEM images of thin films with and without the addition of KBF_4. (f) The distribution of the grain size of perovskite with and without the addition of KBF_4.

A one-step spin-coating method with chlorobenzene antisolvent washing is used to process the KBF_4 mixed $Cs_{0.05}(FA_{0.95}MA_{0.05})_{0.95}Pb(I_{0.95}Br_{0.05})_3$ film in this study as reported earlier. [138-139] KBF_4 is employed with different molar ratios as additive to mix into perovskite precursor solutions. The detailed information for processing is described in the supporting information. Due to the similar ionic radius of BF_4^- (218 pm) and s, BF_4^- may enter into the perovskite lattice to replace I^- ions.[140] Therefore, X-ray diffraction patterns (XRD) and X-ray photoelectron spectroscopy (XPS) were employed to determine the change in perovskite crystal lattice and chemical states. As shown in **Figure 3.1a**, no new peak can be observed in the XRD patterns after the addition of 1.5% KBF_4, indicating that the introduction of KBF_4 does not lead to a new perovskite phase. Besides, the enhanced peak intensity indicates potentially better perovskite texturing or crystallinity. The peaks of unreacted PbI_2 can be attributed to the extra stoichiometric ratio of PbI_2, which is mainly for defects passivation at the

grain boundaries of perovskite.[141-142] Notably, as shown in **Figure 3.2**, some peaks (001, 002, 022) shift to smaller angles for 0.07 degree, indicating an expanded crystal lattice and larger lattice constants induced by the substitution of I^- with BF_4^-. In the XPS spectra shown in **Figure 3.1b**, the characteristic peak of F 1s can be observed at 693.49 eV in a perovskite thin film with 1.5% KBF_4, while it is absent in a control sample without the additive. This result confirms the successful introduction of KBF_4 in the perovskite film. Besides, the characteristic peaks of Pb 4f at 138.77 eV($4f_{7/2}$) and 143.63 eV ($4f_{5/2}$) shift to higher binding energy after the incorporation of KBF_4 due to the high electronegativity of F atoms, suggesting a potential interaction between Pb^{2+} and BF_4^-.The expanded lattice structure is attributed the longer covalent bond between Pb^{2+} and BF_4^-. Although the ionic radius of BF_4^- is slightly smaller than I^-, the interaction between Pb^{2+} and BF_4^- is weaker than that between Pb^{2+} and I^- because the higher polarizability of I^- will facilitate the hybridization with Pb^{2+} and lead to a stronger interaction. Moreover, the spherical electron cloud of I^- is also conducive to hybridization as compared to the tetrahedral one of BF_4^-.[143]

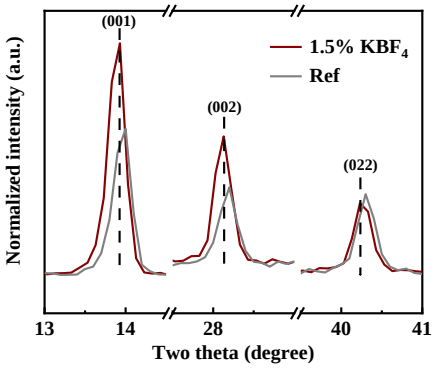

Figure 3.2. A zoom-in XRD patterns of triple cation mixed perovskite with 1.5% and without KBF_4.

To investigate the impact of KBF_4 to the morphology of triple-cation mixed perovskite, the perovskite films were characterized under scanning electron microscopy (SEM). As showed in **Figure 3.1d and 3.1e**, the average grain size of the perovskite obviously increases after the addition of KBF_4, which is clearly presented in the statistical graph

of grain size (**Figure 3.1f**). The enhancement of the crystallinity can be attributed to slower crystallization process due to increased Gibbs energy of perovskite nucleation with the incorporation of pseudo-halide ions into perovskite lattice.[144] The resulting larger grain size can lead to reduced defect density and longer carrier lifetime that will be characterized in the later part. The roughness of the perovskite thin film was then measured by Atomic Force Microscope (AFM), as shown in **Figure 3.3**, the roughness remained almost unchanged when 1.5% KBF_4 was added. However, it increased dramatically from 23.0 to 52.1 nm when 3.0% KBF_4 is applied, indicating a degraded surface morphology.

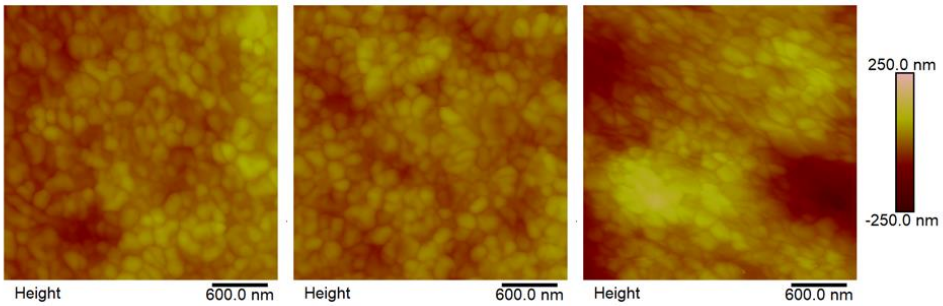

	Ref	1.5%	3.0%
roughness (nm)	22.1	23.0	52.1

Figure 3.3. The AFM figure of the perovskite thin film with different ration of KBF_4.

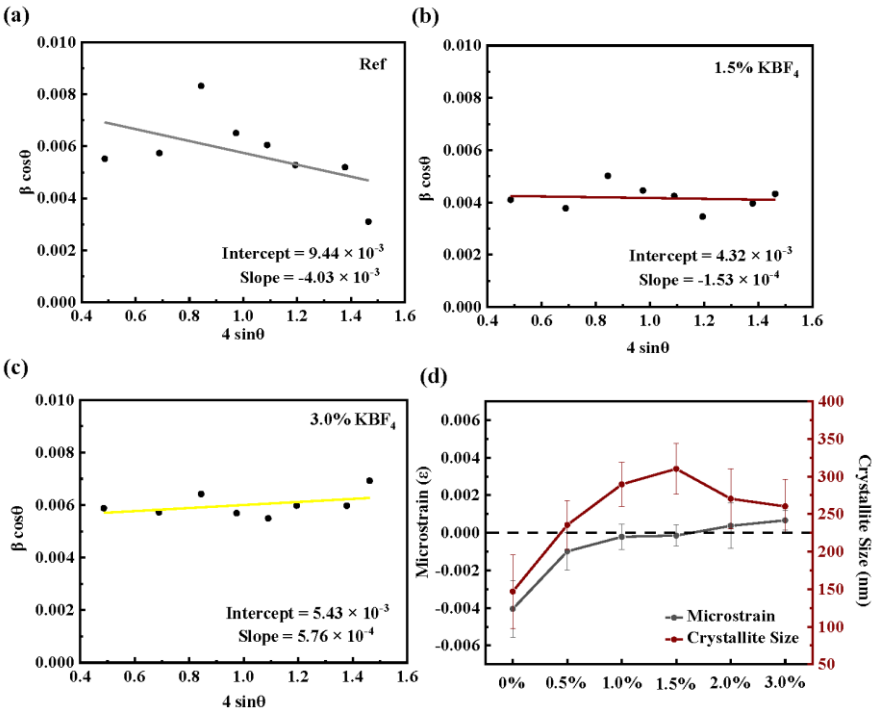

Figure 3.4. (a, b, c) Williamson−Hall plots obtained from XRD patterns of perovskite thin films with different ratios of KBF_4. (d) The trend of microstrain and crystallite size obtained from fitted Williamson−Hall plots.

Next, the mircrostrain in perovskite films were characterized by Williamson-Hall analysis (See supporting information, **Figure 3.4**). Microstrain of a perovskite film is strongly associated with compositional inhomogeneity. In addition, experimental conditions such as annealing temperature could have impact on it.[145] The grain size and the internal strain can be evaluated from the Williamson-Hall analysis of XRD patterns quantitatively by the relationship plot of $\beta hkl \times cos(\theta) = K\lambda\ D + 4\varepsilon \times sin(\theta)$,[129] where β is the full width half maximum (FWHM) of diffraction peaks, h, k, and l are the Miller index, K is the shape factor that is 0.9 for a cubic structure, λ is the wavelength of the incident X-rays and D is crystallite size. **Figure 3.4a-c** show the Williamson-Hall analysis based on the XRD patterns of the perovskites with different KBF_4 addition levels. The grain size and microstrain of the samples are summarized in **Figure 3.4d**. The control sample shows a negative (compressive) strain and small grain size of 150 nm. The lattice strain decreases and grain size increases after the introduction of KBF_4 and reach the lowest strain and the largest grain size whenas 1.5

mol % of KBF_4 is added. However, more addition of KBF_4 leads to negative effect such as increased tensile strain and smaller grain size. Notably, the average grain size is only about 150nm in the control sample without KBF_4 while it is increased to ~300 nm with 1.5 mol% of KBF_4, which is consistent with the observation from SEM images shown in **Figure 3.1f**. Substituting FA^+ with smaller A sites (MA^+ or Cs^+) may distort Pb-I-Pb bonds thereby tilting the PbI_6 octahedron. One of the solutions is to introduce smaller and larger ions together, which is called strain-compensation strategy. In this case, the longer covalent bonds between BF_4^- between Pb^{2+} indicates larger effective radius and thus the introduction of BF_4^- can help balance the distorted lattice structure caused by the incorporation of smaller MA^+ and Cs^+, leading to released strain and decreased defect density.

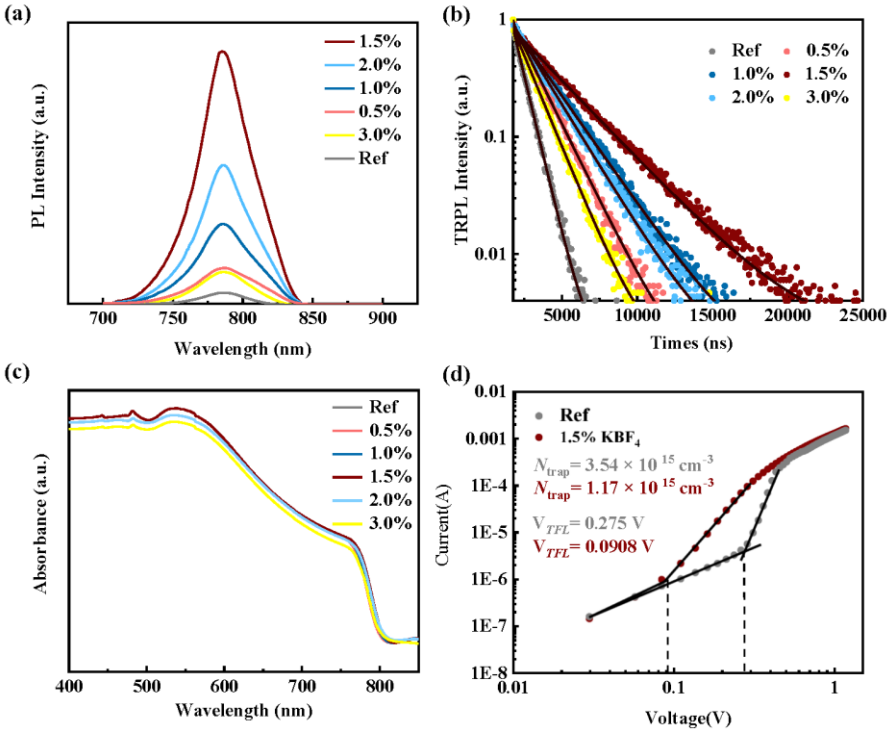

Figure 3.5. (a, b) Steady-state and time-resolved PL of the perovskite thin film with different ratio of KBF_4. (c) UV-vis absorbance and Tauc plot of perovskite thin film with different ratio of KBF_4. (d) The curves of SCLC of the electron-only devices with device structure of ITO/ SnO_2/ Perovskite/ PCBM/ Ag.

Next, the steady-state photoluminescence (PL) tests were performed on perovskite thin

films with different ratios of KBF_4. As shown in **Figure 3.5a**, the PL intensity of perovskite thin film increases after the introduction of KBF_4 and reaches the strongest intensity (790 nm) when 1.5% KBF_4 is applied. However, when extra amount of KBF_4 is added, the peak intensity decreases with the increase of addition level. Then, time-resolved photoluminescence (TRPL) was tested on the samples. The TRPL curves (**Figure 3.5b**) can be fitted with a biexponential decay equation:

$$I_{(t)} = A_1 \exp\left(\frac{-t}{\tau_1}\right) + A_2 \exp\left(\frac{-t}{\tau_2}\right) + I_0 , \quad (1)$$

where τ_1 and τ_2 are the lifetimes of two decay components, A_1 and A_2 are coefficients of the two components and I_0 is a constant. The average lifetime is given by: $\tau_{ave} = \frac{\sum A_i \tau_i^2}{\sum A_i \tau_i}$, where τ_i is decay times and A_i is amplitudes.

As showed in **Table 3.1**, the trend of average lifetime (τ_{ave}) is consistent with the PL intensity. The τ_{ave} reaches the longest time when 1.5% KBF_4 is added, increasing from original 0.799 μs (control sample) to 3.24 μs. The greatly prolonged lifetimes indicate the reduced trap density and suppress nonradiative recombination in perovskite thin films. However, the lifetimes decrease to 2.06 μs and 1.39 μs when the concentration further increases to 2.0% and 3.0%, respectively, which can be attributed to decreased grain size and bigger tensile strain in the films.

Table 3.1. The carrier lifetimes of perovskite thin films with different ratios of KBF_4.

	τ_1 (ns)	A_1	τ_2 (μs)	A_2	τ_{ave} (μs)
Ref	16.1	0.220	0.799	0.840	0.799
0.5%	119	0.0601	1.65	0.882	1.65
1.0%	93.2	0.0275	2.35	0.837	2.35
1.5%	135	0.0384	3.24	0.772	3.24
2.0%	25.5	0.00387	2.06	0.867	2.06
3.0%	3.28	0.0723	1.39	0.837	1.39

The UV-vis light absorption spectra of the triple-cation mixed perovskite are then showed in **Figure 3.4c**. The perovskite thin films with relatively low concentration of KBF_4 show similar light absorption intensity with the control sample. The optical bandgap (E_g) calculated through Tauc plot ($(\alpha h\upsilon)^2 \sim h\upsilon$) are shown in **Figure 3c**, α, h,

and υ were the absorption coefficient, Planck constant, and photofrequency, respectively. The bandgaps of the triple-cation perovskite with different concentrations are calculated to be around 1.54 to 1.55 eV, indicating that KBF_4 leads to negligible impact to the bandgap of perovskite.

To quantitatively assess the defect density of the perovskite films, space charge limited current (SCLC) measurements based on electron-only device (ITO (Indium tin oxide)/ SnO_2 / Perovskite / PCBM/ Ag) were conducted (**Figure 3.4d**). The defect density (N_{trap}) can be calculated from the trap-filling limit voltage (V_{TFL}) by:

$$N_{trap} = \frac{2\,V_{TFL}\,\varepsilon\,\varepsilon_0}{q\,L^2}\ , \qquad (2)$$

where L is the thickness of the perovskite film, q is the elementary charge, ε and ε_0 are the dielectric constants of perovskite and vacuum, respectively.[146-147] The V_{TFL} calculated from the *I-V* curves of SCLC decreases from 0.275 to 0.0908 V. Consequently, the trap density of the perovskite film is reduced from 3.54×10^{15} cm^{-3} to 1.17×10^{15} cm^{-3} when 1.5% KBF_4 is added. This result matches well with the prolonged carrier lifetime measured by TRPL, indicating that the incorporation of KBF_4 could effectively reduce the defects in triple-cation mixed perovskite. This is achieved by releasing the strain in perovskite lattice as we have verified.

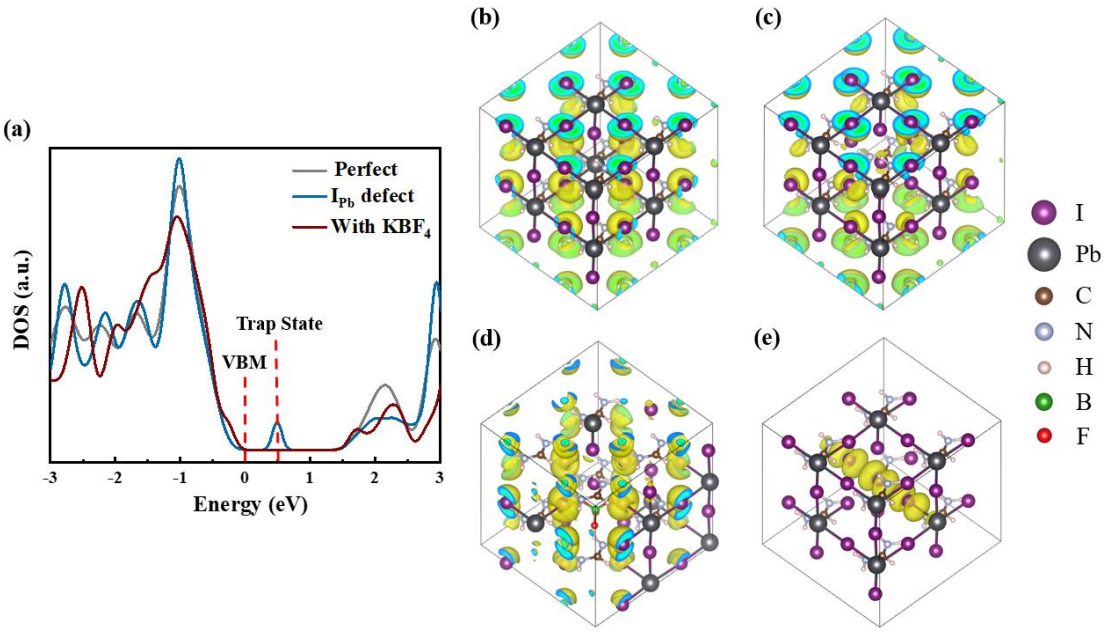

Figure 3.5. DFT calculations for different perovskite supercells. (a) DOS of pristine $FAPbI_3$, $FAPbI_3$ with a I_{Pb} (Pb substituted by I) antisite defect and $FAPbI_3$ with a I_{Pb} antisite defect with BF_4^- substitution of a nearby I^- ion. Simulated charge density distribution of (b) pristine $FAPbI_3$, (c) $FAPbI_3$ with a I_{Pb} (Pb substituted by I) antisite defect and (d) $FAPbI_3$ with a I_{Pb} antisite defect with BF_4^- substitution of a nearby I^- ion at VBM, respectively. (e) Simulated charge density distribution of $FAPbI_3$ with a I_{Pb} (Pb substituted by I) antisite defect at the deep state.

To have a deeper understanding on the defect passivation mechanisms of BF_4^- doped perovskite material, simulation of density-of-state (DOS) and charge density distribution based on density functional theory (DFT) are employed. To simplify the simulation, we calculated the defect passivation effect of replacing I^- with BF_4^- in a $FAPbI_3$ crystal, which is expected to be similar in triple-cation mixed perovskites because the interaction between BF_4^- and Pb^{2+}/ I^- plays a key role. It is well-known that antisite defects related to Pb and I are detrimental for carrier transport since those ions determine the band edge states and such defects tend to form deep traps as Shockley–Read–Hall (SRH) recombination centers.[148-151] To demonstrate the influence of antisite defect on the electronic properties of perovskite and the passivation effect of BF_4^-, the DOS and charge density distribution are simulated for the following structures: 1) 2×2×2 supercells of pristine $FAPbI_3$, 2) 2×2×2 supercells of $FAPbI_3$ with I_{Pb} (Pb substituted by I) antisite defect , 3) 2×2×2 supercells of $FAPbI_3$ with I_{Pb} antisite defect and BF_4^- substitution of a nearby I^- ion. **Figure 3.5a** compares simulated DOS of the three structures. The introduction of antisite defect induces a deep acceptor state near mid-gap, consistent with previous calculation.[152] When BF_4^- ion is introduced near the defect, the deep state is replaced by a swallow state near valence band maximum (VBM), indicating the successful defect passivation of BF_4^-. Such effect can be attributed to the interactions between the electron-rich under-coordinated I^- ions with the electron-deficient fluorine atoms in BF_4^-. To further demonstrate the passivation effect, charge density distributions for different scenarios are visualized (**Figure 3.5b-e**). **Figure 3.5b-d** shows charge density distribution at VBM in the three respective

structures. The charge density is uniformly distributed throughout the cells at this energy level, indicating that the electrons are highly mobile and the swallow state induced by BF_4^- substitution will not cause charge density localization. However, the charge density becomes highly localized near the deep trap state for the defective cell without passivation (**Figure 3.5e**), which implies that such state can act as SRH recombination center. The passivation of such state by BF_4^- ions is therefore beneficial for carrier lifetime. Hence, the simulation gains more insight into the defect passivation effect of BF_4^- ions to perovskite thin film, further justifying the enhanced efficiency and stability of the resultant solar cells.

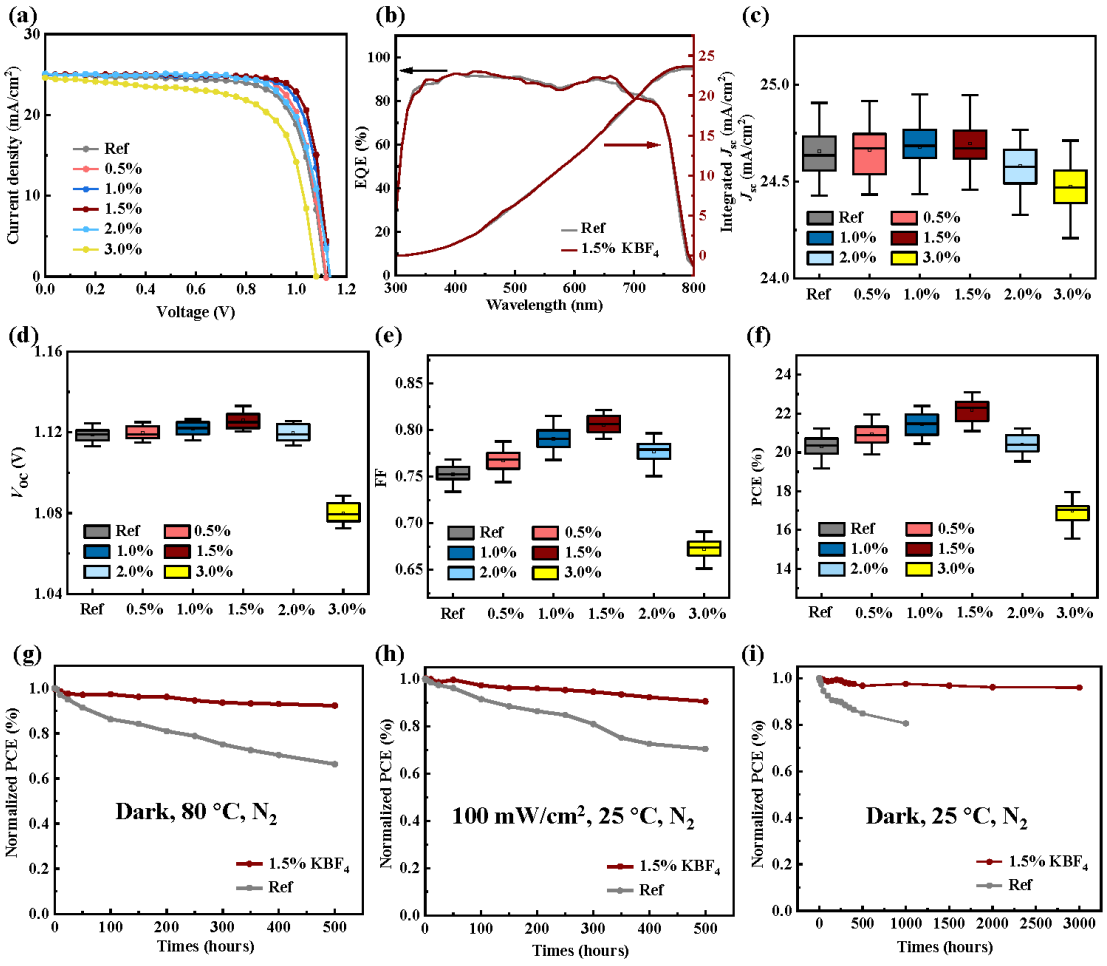

Figure 3.6. (a) *J-V* curves of referential devices and champion devices with different molar ratio of KBF_4. (b) The EQE spectra of the champion device and control device. (c, d, e, f) Comparisons of photovoltaic performance parameters between referential devices and devices with different ratio of KBF_4. (The statistical analysis includes 30

samples in each condition.) (g)Thermal stability test under 80 ℃ heating in N_2 atmosphere without encapsulation. (h) photostability stability test under the continuous illumination (100 mW/cm^2) in N_2 glovebox without encapsulation. (i) Long-time storage stability under dark in N_2 atmosphere without encapsulation.

Next, we fabricated PSCs with the structure of ITO/ PTAA/ $Cs_{0.05}(FA_{0.95}MA_{0.05})_{0.95}Pb(I_{0.95}Br_{0.05})_3$/ PCBM/ BCP/ Ag to investigate the impact of KBF_4 on the performance of PSCs. The control devices without KBF_4 show the maximum PCE of 21.13%, J_{sc} of 24.90 mA cm^{-2}, V_{oc} of 1.12 V and FF of 0.75. Then, the PSC with different ratios of KBF_4 were fabricated. As shown in **Table 3.2**, the device performance increases with the introduction of KBF_4 and shows the best PCE of 23.04 % when 1.5% KBF_4 is introduced. The champion device shows J_{sc} of 24.93 mA cm^{-2}, V_{oc} of 1.13 V and high FF of 0.82 (**Figure 3.6a,** area: 0.048 cm^2). However, the device performance decreases when more KBF_4 is introduced. The J_{sc}, V_{oc} and FF of the devices are decreased to 24.60 mA cm^{-2}, 1.08 eV and 0.67, respectively, when 3.0 % KBF_4 is added. This trend is consistent with the result of PL measurement, which demonstrates that 1.5% KBF_4 delivers the longest carrier lifetime. The external quantum efficiency (EQE) of the devices and integrated J_{SC} are shown in **Figure 3.6b**, which are consistent with the values obtained from the *J-V* curves.

Table 3.2. The parameters of control device, champion device with different ratios of KBF_4. (The statistical analysis includes 30 samples in each condition.)

Sample		J_{sc} (mA cm^{-2})	V_{oc} (V)	FF	PCE (%)
Ref	Champion	24.90	1.120	0.76	21.13
	Average	24.65± 0.25	1.118± 0.003	0.75± 0.01	20.20± 0.92
0.5% KBF_4	Champion	24.88	1.123	0.78	21.78
	Average	24.66± 0.22	1.118± 0.004	0.77± 0.01	20.90± 0.88
1.0% KBF_4	Champion	24.95	1.125	0.80	22.45
	Average	24.67± 0.25	1.121± 0.003	0.79± 0.01	21.43± 0.95
1.5% KBF_4	Champion	24.93	1.130	0.82	23.04
	Average	24.70± 0.23	1.127± 0.003	0.81± 0.01	22.45± 0.62
2.0% KBF_4	Champion	24.85	1.123	0.77	21.58
	Average	24.58± 0.28	1.119± 0.005	0.76± 0.01	20.48± 0.97
3.0% KBF_4	Champion	24.60	1.080	0.67	17.89
	Average	24.46± 0.22	1.080± 0.006	0.66± 0.01	16.93± 0.96

The detailed parameters of the PSCs are demonstrated in **Figure 3.6c-f**. As shown in

the figure, the elevated performance of PSCs is manly attributed to the greatly enhanced FF. The FF in a PSC is associated with the carrier transportation in the bulk of perovskite and interfaces. Low FF is generally caused by severe interfacial non-radiative recombination or low charge extraction efficiency between perovskite and transporting layers.[153-156] Therefore, the introduction of KBF_4 can improve FF by reducing trap density and improving carrier lifetime as evidenced by the result of SCLC and TRPL. Moreover, K^+ ions can modify the interface by forming KBr/KI with uncoordinated halides to passivate the grain boundaries.[59, 157] This KBr/KI solid complex not only prevent halides migration but also enhance electron extraction, which is favorable for device performance.[158]

At the tail of EQE spectra in **Figure 3.6b**, the slope of the exponential EQE defines the Urbach energy (E_u), which is proportional to $\exp((E-E_G)/E_U)$.[159-160] The E_u of the KBF_4-treated device is calculated to be 17.2 meV, which is slightly smaller than the control device of 18.8 meV. Lower Urbach energy generally indicates less defects in the perovskite layer. Thus, the lower E_u of KBF_4-treated device also suggests that KBF_4 can passivate defects in the film. Besides, the bandgaps calculated from EQE spectra were 1.54 eV for KBF_4-treated perovskite and 1.55eV for control device, which matches well to the bandgap obtained from UV-vis absorption spectra.

To investigate the improvement in device stability, we demonstrated the thermal stability (**Figure 3.6g**), photostability (**Figure 3.6h**) and long-term storage stability (**Figure 3.6i**) tests on our devices. The thermal stability test was carried out under 80 ℃ heating in N_2 atmosphere without encapsulation. In this work, the target device maintained over 90% efficiency after heating for 500 hours while the control only kept 70% efficiency at the same condition. Besides, the photostability and long-term storage stability tests were also conducted in N_2 glovebox without encapsulation. It was found that the target device maintained over 89% and 97% efficiency respectively after continuous illumination and storage in inert atmosphere while the control device showed a much poor stability. In triple-cation perovskite, the MA^+ may escape from the

lattice due to its worse thermal stability, thereby leading to migration of uncoordinated halide ions and perovskite degradation. The ion migration is more serious under working conditions.[143] In this case, the introduction of BF_4^- may release the lattice strain and thereby stabilize perovskite lattice. Apart from this, K^+ ions can prevent the ion migrations by forming solid complex KBr/KI with uncoordinated halide ions at grain boundaries, thereby delivering more stable perovskite grain boundaries.[60, 161] Therefore, the combing benefits of BF_4^- and K^+ contribute to the elevated device stability.

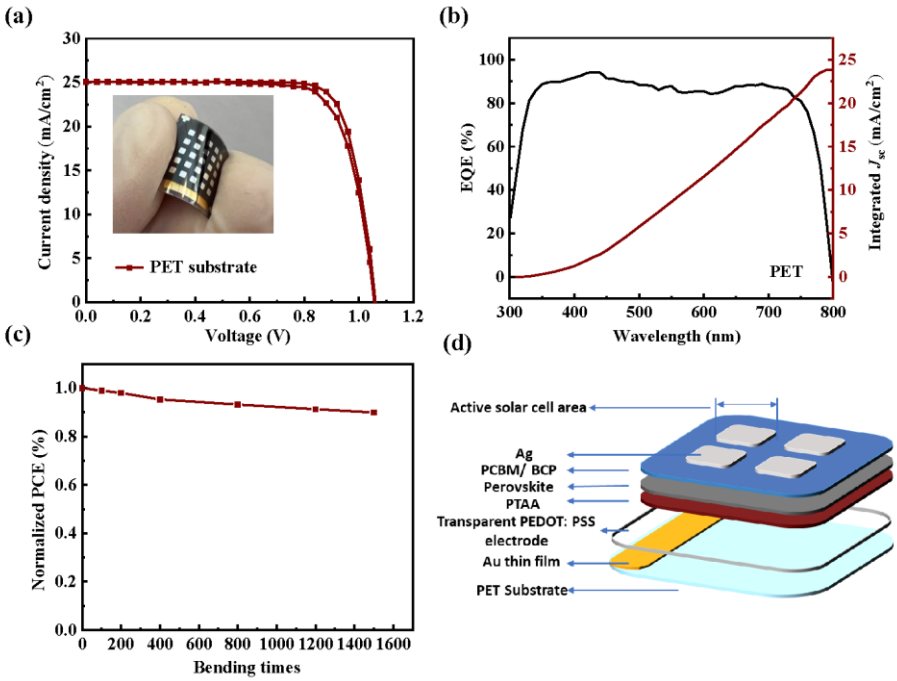

Figure 3.7. (a) The *J-V* curves of flexible PSC with structure of PET/ PEDOT: PSS/ PTAA/ Perovskite/ PCBM/ BCP/ Ag. (b) The EQE spectra of the flexible device. (c) The bending stability of the flexible device. (d) The structure of flexible device.

Considering the good performance of PSC achieved on inverted structure, we carried out our standard fabricating conditions on flexible PET (polyethylene glycol terephthalate) substrate, the structure of the device is composed of PET/ PEDOT:PSS/PTAA/Perovskite/PCBM/BCP/Ag (**Figure 3.7d**). Transparent electrode PEDOT: PSS was prepared according to previous research[162], and an Au film is coated besides the PEDOT:PSS film as a conductor for the convenience of testing. As shown

in **Figure 3.7a**, the flexible PSCs deliver PCE of 21.02 %, J_{sc} of 25.08 mA cm^{-2}, V_{oc} of 1.06 V and FF of 0.79 (area: 0.01 cm^2). The slightly increased J_{sc} is attributed to the higher transparency of PEDOT: PSS film as compared to ITO and matches well with the integrated J_{sc} from EQE (23.83 mA cm^{-2}, **Figure 3.7b**). Moreover, the flexible devices maintain 90 % of the original PCE after bending for more than 1500 times at a bending radius of 8 mm (**Figure 3.7c**).

3.4 Conclusion

In summary, we have demonstrated that a small amount of KBF_4 is an effective additive to boost the performance of triple-cation mixed inverted PSCs. The champion device delivers a PCE of 23.03 %, J_{sc} of 24.93 mA cm^{-2}, V_{oc} of 1.13 V and a high FF of 0.82. We find that KBF_4 can enhance the crystallinity and release microstrain in the perovskite films, which is favorable for the photovoltaic performance. Moreover, the trap density is reduced and nonradiative recombination is suppressed in the perovskite thin film due to defect passivation by BF_4^- in the bandgap. This work provides a convenient strategy to achieve high-performance PSCs with an inverted device structure, which is applicable for the fabrication of flexible, tandem and large-area devices.

Chapter 4 A Convenient Co-Additive Strategy to Boost the Inverted Perovskite Solar Cells.

The utilization of additives has contributed significantly to the performance of perovskite solar cells. Numerous additives had been introduced into the surfaces and bulk of perovskites to improve each aspect of PSCs. In this work, PEA_2PbI_4 and GlyHCl were introduced to enhance perovskite performance via crystallization modulation and facet controlling. The incorporation of these two additives contributed to a significant enhancement in growth of (100) facet, consequently elongation of carriers lifetime and device performance. Tof-SIMS revealed that Gly^+ could also modify the bottom interfaces to enlarge grain size, while PEA_2PbI_4 was uniformly distributed and passivated the bulk of perovskites. The employing of this convenient co-additive strategy resulted in achieving the highest efficiency of 23.8% on inverted PSCs, accompanied by improved device stability.

4.1 Introduction

Over time, the fabrication technologies for perovskite solar cells (PSCs) have evolved significantly, leading to a huge increase in efficiency from 3.8% to over 25.7%. [8-9]. To achieve these advancements, researchers have proposed and implemented numerous strategies, such as additives engineering[14] and surface engineering[163]. For instance, surface engineering has been employed to attain efficiencies exceeding 25% on PSCs with inverted structures recently.[53, 89, 164] Facet engineering draws increasing attention owing to its tight relationship with the performance of perovskites.[165] Researchers tailored the facet orientation via various compositions, ligands and fabrication conditions, which demonstrated a new strategy to enhance the performance of PSCs.[166-167]

Among various facets in perovskites, the (100) facet is considered to be the most coordinated balanced due to its equal distribution of organic cations and halide anions.

This balanced distribution makes the (100) facet the most stable facet during crystal growth, as the fully bonded (100) facet ensures charge neutrality and contributes to a defect-free surface.[166] Furthermore, optoelectronic devices based on the preferred orientation of the (100) facet have demonstrated higher carrier mobility than those based on the (111) facet.[168] Therefore, numerous strategies have been proposed to control the facet orientation towards the preferred (100) orientation, and one effective and efficient method is the use of various ligands. For example, ammonium salts (such as PEAI and OAmI)[100, 169] and pseudohalides anions (such as SCN^- and $HCOO^-$) demonstrate their potential in controlling facet towards (100) dominance.[170]

Glycine (Gly), an essential amino acid for the human body, has been utilized to enhance the performance of perovskite solar cells due to its functional groups, namely the carboxyl and amino groups. Previous studies have employed glycine to pretreat the surfaces of NiO_x/SnO_2 to adjust the energy band and promote charge transfer in PSCs.[171-174] In this study, it was observed that glycine hydrochloride (GlyHCl), the ammonium salt form of glycine, could control the crystal growth with a preferred orientation of (100) facet as well as modify the bottom surface of perovskites. By directly introducing GlyHCl and PEA_2PbI_4 to the precursor solutions, the bulk and bottom surfaces could be effectively passivated by PEA_2PbI_4 and GlyHCl. GlyHCl located at the bottom surface was found to greatly enlarge the grain size and reduce defect densities. The implementation of this co-additive strategy resulted in a notable enhancement in the open-circuit voltage (V_{oc}) and PCE, from 1.04 V to 1.16 V and 19.58% to 23.80%, respectively. Consequently, this study presents a convenient co-additive strategy to manage the crystal orientation and enhance the performance of inverted perovskite solar cells.

4.2 Experimental Section

Preparation of triple cation mixed Perovskite solution: the triple cation perovskite solution was prepared by mixing two 1.2 M $FAPbI_3$ and $MAPbBr_3$ perovskite solutions in DMF: DMSO (4:1 volume ratio, v: v) in a particular ratio (e.g. 95:5). The 1.2 M

$FAPbI_3$ solution was thereby prepared by dissolving FAI (722 mg) and PbI_2 (2130 mg) in 2.8 mL DMF and 0.7 mL DMSO which contains a 10 molar % excess of PbI_2. The 1.2 M $MAPbBr_3$ solution was made by dissolving MABr (470 mg) and $PbBr_2$ (1696 mg) in 2.8 mL DMF and 0.7 mL DMSO which contains a 10 molar % excess of $PbBr_2$. PEA_2PbI_4 solution was prepared by mixing 489mg PEAI and 461mg PbI_2 in 800 µL DMF. Lastly, 40 µL of a 1.5 CsI solution in DMSO (389 mg CsI in 1 mL DMSO) was mixed with 960 µL of the above-described mixture of $FAPbI_3$ and $MAPbBr_3$ resulting in a nominal perovskite stoichiometry of $Cs_{0.05}(FA_{0.95}MA_{0.05})_{0.95}Pb(I_{0.95}Br_{0.05})_3$, respectively. PEA_2PbI_4 solution was prepared by mixing 489mg PEAI and 461mg PbI_2 in 800 µL DMF. And 1.5% of KBF_4 are added to the all the solution.

Device fabrication: To fabricate a device structure of glass/ ITO/ PTAA/ Perovskite/ PCBM/ BCP/ Ag, ITO glass substrates were ultrasonically cleaned by deionized (DI) water, acetone and isopropanol for 15 min, respectively. Then, the cleaned ITO substrates were dealt with air plasma for 8 mins before use. Then the substrates were transferred to N_2 glovebox. After the substrates were transferred into glovebox, poly(triaryl amine) (PTAA) solution (2 mg mL^{-1}) was spin-coated at 5000 rpm for 30 s and annealed at 100 °C for 10 min. The substrates were cool down to room temperature before use. 1.2 M perovskite precursor solutions were constructed by mixing FAI, PbI_2, MABr, $PbBr_2$ and CsI in DMF: DMSO mixed solvent with a chemical formula of $Cs_{0.05}(FA_{0.95}MA_{0.05})_{0.95}Pb(I_{0.95}Br_{0.05})_3$. 50 µL of the prepared precursor solution was spin-coated at 1000 rpm for 10 s and 5000 rpm for 30 s onto the PTAA-coated ITO substrate, 50 µL CB as anti-solvent was dripped on the film at 10 s before the end of the last procedure and then annealed at 100°C for 30 min. Afterward, PCBM (20 mg mL^{-1}) and BCP (0.5 mg mL^{-1}) were spin-coated on the films at 1500 rpm for 60 s and 4500 rpm for 30 s, respectively. For solution with KBF_4, different molar ratio of KBF_4 was added to the original 1.2 M $FAPbI_3$ solution. Finally, 200 nm silver electrodes were thermally evaporated onto the films at a chamber pressure of 10^{-7} Torr with a deposition rate of 0.5 Å s^{-1}. The active area of rigid PSC is 0.048 cm^2 and flexible PSC is 0.01 cm^2.

Characterization: J-V curves were measured by a Keithley 2400 source meter with a solar simulator under AM 1.5 G one sun illumination (Newport 66902). The scanning rate was 100 mV s^{-1} with a voltage step of 10 mV. The EQE of the PSCs was obtained from an EQE system under DC mode. To reduce the optical reflection loss, an antireflection (AR) layer was added on the glass side during the test of the champion 5 ℃ antisolvent treated devices. SEM images were measured by a field-emission SEM (Tescan MAIA3). XRD patterns were measured using Cu K_α radiation (Rigaku, Smartlab) to analyze the crystallization of perovskite. PL was measured by the FLS 920 (Edinburgh Instruments, Ltd) with excitation at 645 nm.

Statistical Analysis: The data, figure and statistical graph (*J-V* curves, XRD figures, XPS figures, Williamson−Hall plots, PL, UV-vis, SCLC, EQE, stability tests) in the article is pre-processed and drawn by Origin Pro (ver. 2019). The SEM figure is processed by Digital Micrograph (ver. 3.4). The AFM figure is processed by NanoScope Analysis (ver. 1.7).

Computational methods: DFT: All DFT simulations were conducted using Quantum Expresso (ver. 6.5).[136] All the structures were fully relaxed before the DOS and charge density calculations. The relaxation was performed under Perdew, Burke and Ernzerhof (PBE) exchange-correlation functionals[137] with projector augmented wave (PAW) method. The electronic convergence criterion was set to be 1 x 10^{-6} eV. A plane wave basis set of 450 eV cut-off energy was used.

4.3 Result and Discussion

The perovskite thin film was fabricated using one-step spin-coating method, with chlorobenzene as antisolvent and composition of $Cs_{0.05}(FA_{0.95}MA_{0.05})_{0.95}Pb(I_{0.95}Br_{0.05})_3$.[1] Different molar ratio of 2D perovskite PEA_2PbI_4 and GlyHCl as additives are directly introduced to the perovskite precursor solutions. The detailed experimental processes are presented in supporting information. As the addition of 2D perovskite PEA_2PbI_4 and ammonium salt GlyHCl may generate

new perovskite phase, the change in perovskite lattice were first examine through X-ray diffraction patterns (XRD). As showed in **Figure 4.1a**, it was observed that no new peaks form in the small angle of XRD patterns after adding two additives, which could be attributed to the undetectably small amount of 2D perovskites by XRD.[100] The XRD patterns were then examined more specifically. The ratio of certain peak in XRD patterns, such as (100) to (011), changes from 1:1 to 1.7:1 when 3.0% GlyHCl is added, indicating the addition of GlyHCl could promote the crystal growth along the preferred orientation plane.

The carboxyl group (-COOH) and amino group ($-NH_3^+$) in GlyHCl have been reported to interact with the PbI_2/perovskites.[175-176] To investigate such interactions, ^1H nuclear magnetic resonance (NMR, **Figure 4.1b**) was conducted. As showed in **Figure 4.1b**, the chemical shifts of ^1H in GlyHCl moved from 8.36 and 3.64 ppm to 8.12 and 3.69 ppm, respectively, indicating the electron density of corresponding hydrogen atom changed. Hydrogen bonds formed between iodine atom in PbI_2 and hydrogen atom in $-NH_3^+$ increase the electron density of H atom, leading to a shift to the high field in the NMR.[177-178] In contrast, lead atoms coordinate with the lone pair electrons in -C=O and increase the electron withdrawing ability of -C=O, causing the decrease of electron density of H atom in the nearby $-CH_2-$ and resulting in peak shifts towards the low field. Given the observed interactions between PbI_2 and GlyHCl, the interactions between perovskites and GlyHCl were investigated through surface X-ray photoelectron spectroscopy (XPS) and Fourier transform infrared spectroscopy (FTIR). The XPS spectra (**Figure 4.1c, d**) showed that the characteristic peaks of Pb 4f (143.57 eV for $4f_{5/2}$ and 138.68 eV for $4f_{7/2}$), I 3d (631.03 eV for $3d_{3/2}$ and 619.55 eV for $3d_{5/2}$) and O 1s (533.11 eV) remain unchanged after the addition of GlyHCl. The unshifted XPS peaks suggest that the chemical environments of electrons of Pb, I and O remained unchanged, indicating no interactions between perovskites and GlyHCl at the perovskite surface. In contrast, the FTIR spectra (**Figure 4.1e**) showed that the peaks of C=O in plane bend and stretch shift to high wavenumber field due to the coordination with Pb^{2+}, from 1224 cm^{-1} and 1733 cm^{-1} to 1254 cm^{-1} and 1750 cm^{-1}, respectively. The

similar shifts were also observed in the peak of N-H bonds, which is consistent with the result of NMR spectra and suggest that the potential interactions between perovskite and GlyHCl.

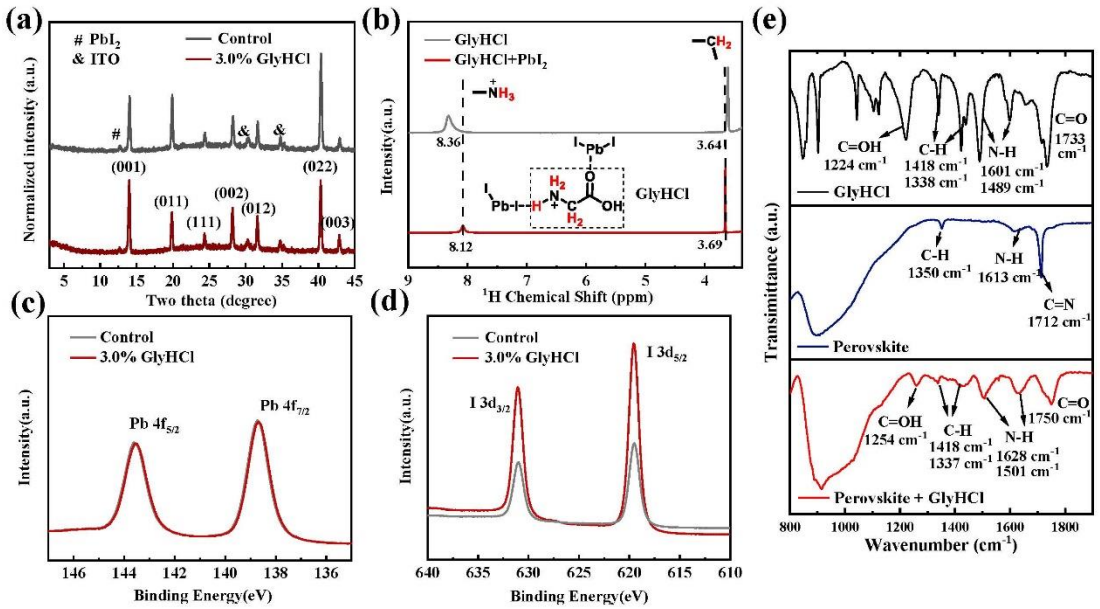

Figure 4.1. (a)The XRD patterns of perovskites with and without 3.0% GlyHCl. (b) The ^{1}H Chemical shift of GlyHCl and GlyHCl+PbI_2. (c, d) XPS spectra of Pb 4f (c) and I 3d (d) for the perovskites with and without 3.0% GlyHCl. (e) The FTIR spectra of GlyHCl and perovskite with/without GlyHCl.

Time of flight secondary ion mass spectrometry (ToF-SIMS, **Figure 4.2a, b**) was then conducted to investigate the distributions of GlyHCl and PEA_2PbI_4 in perovskite thin films. The result showed that the PEA_2PbI_4 was uniformly distributed through the perovskite thin film, while GlyHCl was mainly located at the bottom surface of the perovskite thin film (**Figure 4.2b**). To elucidate the underlying mechanism of GlyHCl accumulation at the bottom surface of the perovskite thin film, the crystallization process was analyzed, as the interaction between PbI_2 and GlyHCl was confirmed via NMR and FTIR. As showed in **Figure 4.2d,** the cross-section SEM image showed that an amorphous phase was observed for the perovskite thin film without annealing. Then, it was observed that there were large voids near the bottom surface of perovskite thin film with 5s annealing (**Figure 4.2e**). However, the voids disappeared and larger perovskite grain size formed after 30 min annealing (**Figure 4.2f**), indicating that the

crystallization follows a downward grain growth. This observation is consistent with the general crystallization process that adopts one-step solution processed method.[179] The annealing process was monitored in **Figure 4.2g**, control sample (left) showed darker yellow as compared to the target sample that contain GlyHCl (right) before annealing. When heating was applied, the perovskite thin film with GlyHCl showed a slightly slower crystallization rate, indicating that GlyHCl could slow down the crystallization process by interact with perovskite intermediate phase. Moreover, NMR analysis was conducted to demonstrate the interactions between GlyHCl and the solvents. As showed in **Figure 4.3**, the peaks of GlyHCl in DMF, DMSO and mixture of DMF/DMSO all exhibited changes, indicating the existence of interactions between GlyHCl and solvents. The interactions between GlyHCl and PbI_2/solvents could have great impact on the formation of intermediate phase and consequently the crystallization process.

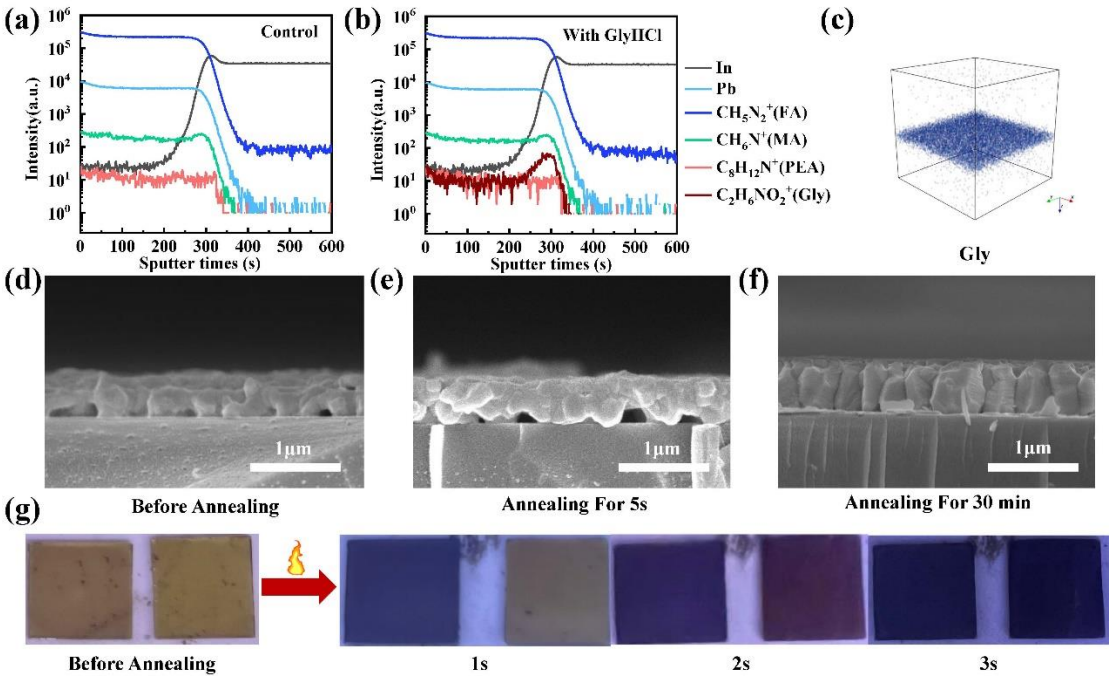

Figure 4.2. (a, b) ToF-SIMS depth profile of perovskite thin films without/with GlyHCl. (c) 3D maps of the distribution of GlyHCl in perovskite thin films. (d, e, f) The cross-section SEM image of the perovskite thin film with 0s (d), 5s (e) and 30min (f) annealing time. (g) The annealing process of perovskites with and without GlyHCl.

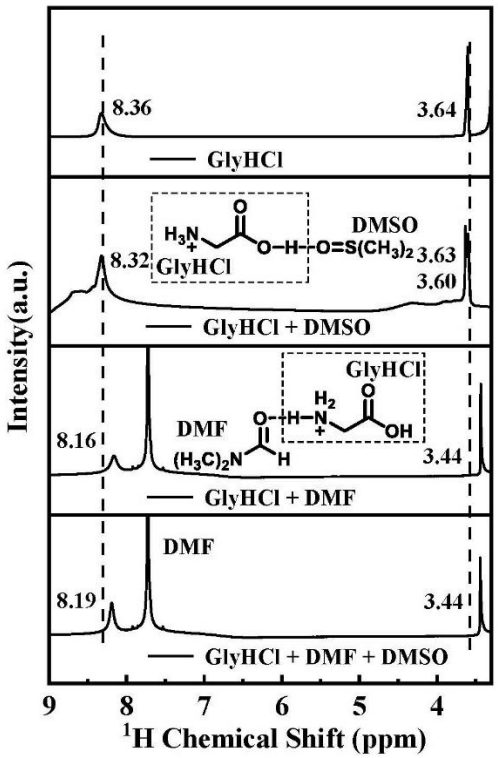

Figure 4.3. The ^{1}H NMR spectra of GlyHCLin DMF, DMSO and mixture of DMF/DMSO.

The interactions between GlyHCl and PbI_2/DMF/DMSO primarily involve hydrogen bonds, where N–H--I and O–H--I are formed between GlyHCl and PbI_2, while O–H--O and N–H--O are formed between GlyHCl and DMF/DMSO. It is noteworthy that the hydrogen bonds between GlyHCl and DMF/DMSO are stronger than those between GlyHCl and PbI_2 due to the higher electronegativity of O as compared to I.[180-181] Hydrogen bonds play a crucial role in the crystallization process of perovskites, as they can mediate the formation of a hydrogen-bond-bridged intermediate that can significantly influence the quality of perovskite thin films.[182] Thus, the crystallization process is depicted in **Figure 4.4a-d** according to the experimental results. As showed in **Figure 4.4a**, the initial solution is a mixture of cations/anion. As the crystallization process follows a downward direction by using one-step solution method, the removal of solvents from the top surface by antisolvent leads to the phase transformation of perovskites (**Figure 4.4b**). During the annealing process, the interactions between Gly and perovskites are gradually replaced by the interactions between Gly and DMF/DMSO, driving the Gly towards the solvents instead of crystalizing with

perovskites (**Figure 4.4c**). As a result, the concentration of GlyHCl in the solvents increases, leading to its final aggregation at the bottom surface of the perovskite thin film (**Figure 4.4d**).

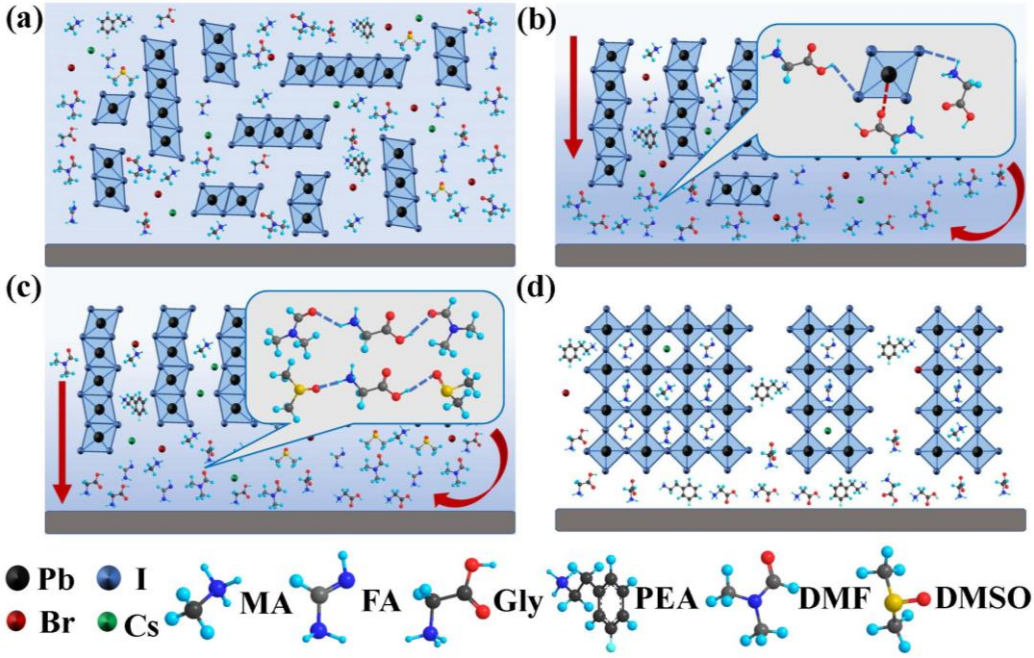

Figure 4.4. **(a-d)** The schematic illustration of crystallization process of perovskite with GlyHCl and PEA_2PbI_4.

Scanning electron microscopy (SEM) and transmission electron microscope (TEM) were used to investigate the change in perovskite morphology and perovskite lattice. The result showed that as the concentration of GlyHCl increases from 0% to 5%, the perovskite grain size progressively increased (**Figure 4.5a-f)**, as demonstrated by the statistical graph of grain size (**Figure 4.5g**). The enhanced crystallinity could be ascribed to the two functional groups in GlyHCl. As previously mentioned, the $-NH_3^+$ group can function as anchor sites for perovskite to grow[183-184], and -COOH group can coordinate with Pb^{2+} to slow down the crystallization process as demonstrated in **Figure 4.5g**[175, 185]. The combinational effect of two function group facilitates the growth of perovskites into large grain size. However, when the concentration of GlyHCl further increase to 5.0% (**Figure 4.5f**), large voids and numerous pinholes began to form at grain boundaries of perovskites. These large voids and pinholes may result in severe carriers recombination and perovskite degradation, which will compromise the device

performance.[186-187]

As small amount of 2D perovskites may be undetectable for XRD, we employed TEM test to determine the existence of 2D perovskites. As showed in **Figure 4.5h and i,** it can be seen that pattern of 2D perovskites lattice is distinct from 3D perovskites lattice, and the interplane spacing of 2D and 3D perovskites are 0.718 nm and 0.320 nm respectively, which are in accord with previous report relating to 2D perovskites PEA_2PbI_4.[84, 100] Additionally, it was observed that 2D perovskites tends to stay at grain boundaries, which may be related to their function of passivating perovskite grain boundaries.[100]

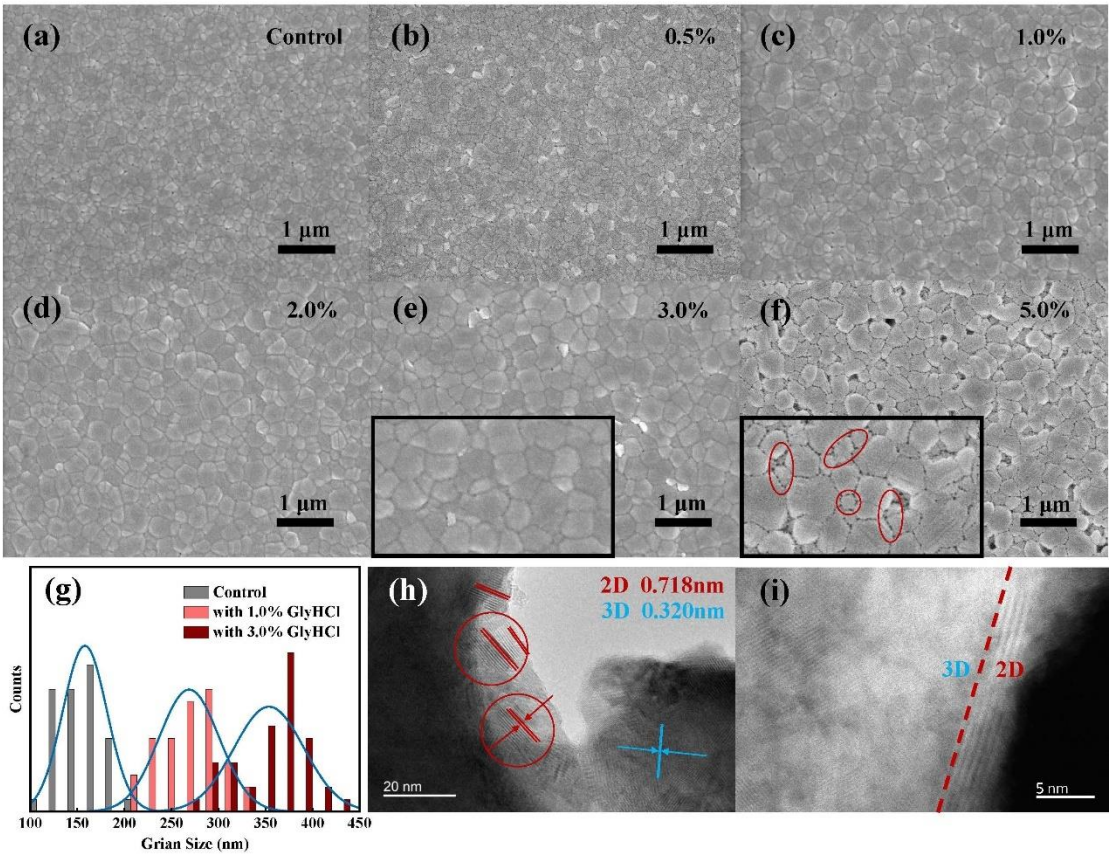

Figure 4.5. (a-f) The plane-view SEM images of perovskite thin films with different ratios of GlyHCl. (g) The distribution of grain size of perovskites without and with with different ratios of GlyHCl. (h, i) The TEM images of perovskite thin films.

To investigate the impact of the addition of GlyHCl and PEA_2PbI_4 to the perovskite thin film quality, the steady-state photoluminescence (PL) tests were conducted on

perovskite thin films with various ratios of GlyHCl and PEA_2PbI_4. As demonstrated in **Figure 4.6a**, the peaks of perovskite are located at 790 nm, and the introduction of various concentrations of GlyHCl does not lead to any shifts to peak positions. But the peak intensity greatly increased as the concentration of GlyHCl increases from 0.5% to 3.0%, and it dropped dramatically when GlyHCl reaches to 5%. This may be attributed to the large cavities and numerous pinholes in the perovskite thin film observed in SEM images, which could cause severe carriers recombination. The combinational effect of GlyHCl and PEA_2PbI_4 can be seen in the **Figure 4.6b**, it demonstrates that the peak intensity increases after introducing PEA_2PbI_4 and become even stronger when adding GlyHCl.

For quantitatively comparing the quality of perovskite thin films, time-resolved photoluminescence (TRPL) was conducted on the thin films. The TRPL curves (**Figure 4.6c**) can be fitted with a biexponential decay equation:

$$I_{(t)} = A_1 \exp\left(\frac{-t}{\tau_1}\right) + A_2 \exp\left(\frac{-t}{\tau_2}\right) + I_0,$$

where τ_1 and τ_2 are the lifetimes of two decay components, A_1 and A_2 are coefficients of the two components and I_0 is a constant. The average lifetime is calculated by equation: $\tau_{ave} = \frac{\sum A_i \tau_i^2}{\sum A_i \tau_i}$, where τ_i is decay times and A_i is amplitude.

Carrier lifetimes were calculated from the decay equation, and the results are presented in **Table 1**. The trend of average carrier lifetimes matched the trend of PL intensity: the τ_{ave} increases gradually from 0.823 μs to 3.51 μs as the concentration of GlyHCl raises from 0% to 3.0%, and τ_{ave} begins to decrease prominently (0.739 μs) when the concentration of GlyHCl further increases to 5.0%. This trend could also be observed in SEM images, the elongated lifetimes are obtained when 3.0% GlyHCl is added, which gave the largest grain size without pinholes and cavities. The elongated lifetimes can be attributed to greatly reduced defect density and suppressed nonradiative recombination by adding GlyHCl. Conversely, the substantially decreased lifetime can be attributed to the large cavities and numerous pinholes, which can induce severe nonradiative recombination and energy losses. The results of PL and TRPL demonstrate

that the quality of perovskite thin films can be greatly improved by adding GlyHCl and PEA_2PbI_4.

To determine the change in the light absorption and band gap of perovskite thin films, UV-vis light absorption spectra were measured (**Figure 4.6d**). The result showed that the introduction of GlyHCl and PEA_2PbI_4 shows negligible impact on the light absorption range and intensity. The optical bandgaps (E_g) were calculated through Tauc plot ($(\alpha h\upsilon)^2 - h\upsilon$), α, h, and υ are the absorption coefficient, Planck constant, and photofrequency, respectively. The bandgaps of perovskite thin films changed from 1.53 eV to 1.55 eV when 0.5% PEA_2PbI_4 and 3.0% of GlyHCl added, the slightly increased bandgap of perovskite thin films could be attributed to the introduction of 2D perovskites, which have a large band gap (2.02 eV).[102]

Table 1. The carrier lifetimes of perovskite thin films with different ratios of GlyHCl with 0.5% PEA_2PbI_4.

	τ_1 (ns)	A_1	τ_2 (μs)	A_2	τ_{ave} (μs)
Control	104	0.220	0.824	0.890	0.823
0.5%	119	0.2601	0.996	0.922	0.996
1.0%	162	0.1276	1.27	0.907	1.27
2.0%	145	0.1394	1.72	0.882	1.71
3.0%	177	0.1288	3.51	0.917	3.51
5.0%	124	0.2723	0.741	0.861	0.739

To quantitatively calculate the holes/electrons defect density of the perovskite films, space charge limited current (SCLC) measurements based on holes-only device (ITO (Indium tin oxide)/ PTAA/ Perovskite/ Au) and electrons-only device (ITO/ SnO_2/ Perovskite/ PCBM/ Ag) were conducted. The defect density (N_{trap}) can be calculated from the trap-filling limit voltage (V_{TFL}) by

$$N_{trap} = \frac{2 V_{TFL} \varepsilon \varepsilon_0}{q L^2},$$

where L is the thickness of the perovskite film, q is the elementary charge, ε and ε_0 are the dielectric constants of perovskite and vacuum, respectively. The V_{TFL} calculated from the *I-V* curves of SCLC are showed in **Figure 4.6e** and **f**. The N_{trap} of holes decreases from 6.93 10^{15} cm^{-3} to 4.36×10^{15} cm^{-3} and N_{trap} of electrons decreases from

2.64 10^{15} cm^{-3} to 1.42×10^{15} cm^{-3} when 3.0% GlyHCl was added. Both holes and electrons trap density were greatly reduced when the GlyHCl was added, which matches well with the prolonged carrier lifetimes measured by TRPL. This suggests that GlyHCl can reduce the defect density, restrain nonradiative recombination and consequently improve the quality of perovskite thin film.

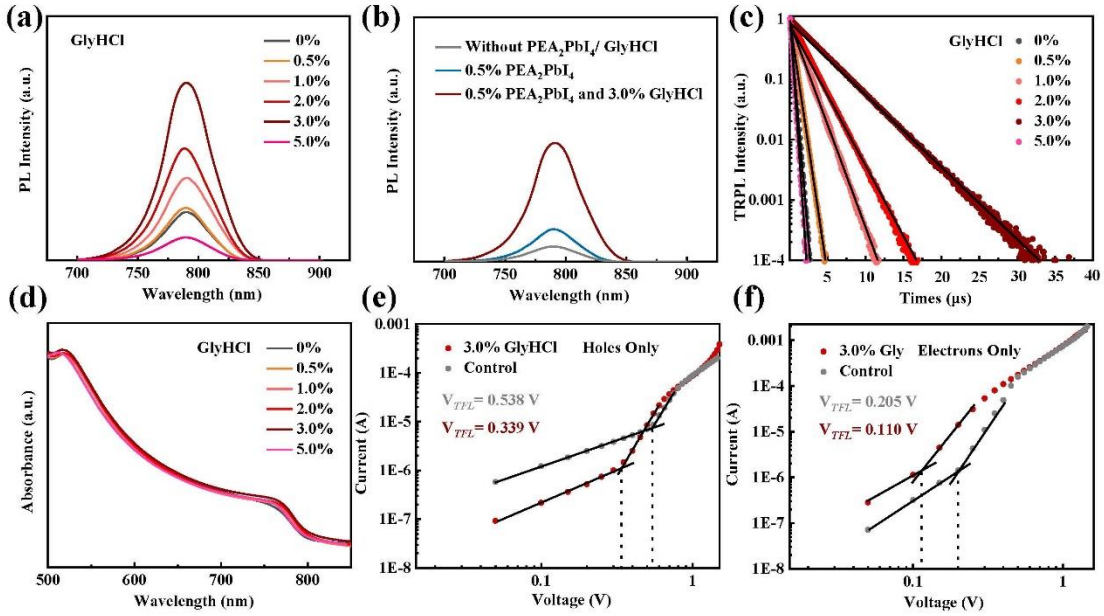

Figure 4.6. (a, b, c) Steady-state and time-resolved PL of the perovskite thin film with different ratio of PEA_2PbI_4 and GlyHCl. (d) UV–vis absorbancet of perovskite thin film with different ratio of GlyHCl. (e) The curves of SCLC of the holes-only devices with a device structure of ITO/ PTAA/ Perovskite/ Au. (f) The curves of SCLC of the electron-only devices with a device structure of ITO/ SnO_2/ Perovskite/ PCBM/ Ag.

To investigate the impact of PEA_2PbI_4 and GlyHCl to the performance of PSCs, PSCs with the structure of ITO/ PTAA/ $Cs_{0.05}(FA_{0.95}MA_{0.05})_{0.95}Pb(I_{0.95}Br_{0.05})_3$/ PCBM/ BCP/ Ag were fabricated. Considering the combinational effects of PEA_2PbI_4 and GlyHCl in improving the quality of perovskite thin film, the optimal concentrations for PEA_2PbI_4 and GlyHCl were thoroughly examined. As showed in **Figure 4.7a**, the V_{oc} and PCE increase from 1.05 eV and 19.58% to 1.12 V and 21.90% respectively when 0.5% PEA_2PbI_4 is added. After the introduction of 3.0% GlyHCl, the champion device shows J_{sc} of 25.55 $mA\cdot cm^{-2}$, further increase in V_{oc} of 1.16 V, FF of 0.8 and PCE of 23.8%. A

more detailed analysis of the relationships between various amounts of PEA_2PbI_4 and GlyHCl are showed in **Figure 4.7b-e** and **Table 2**.

As showed in **Figure 4.7b**, the J_{sc} remains unchanged under low concentration and began to decrease when the concentration excess 0.5%, which decreases from original 25.49 $mA \cdot cm^{-2}$ to 23.89 $mA \cdot cm^{-2}$ as the concentration of PEA_2PbI_4 increased to 1.0%. The compromised J_{sc} can be ascribed to the excessive amount of 2D perovskites, which induce formation of excessive low-dimension perovskites and consequently blueshift of bandgap and poor carriers transportation.[102] And this negative effect is observed when adding excessive amount of GlyHCl (**Figure 4.7b**). Similarly, the combinational enhancements in PSCs come from the elevated V_{oc} and FF by adding suitable amount of PEA_2PbI_4 and GlyHCl. As showed in **Figure 4.7c and d,** both PEA_2PbI_4 and GlyHCl can boost the V_{oc} and FF of PSCs, the V_{oc} can be increased from 1.04 V to 1.11 V by adding single additive PEA_2PbI_4, and it can be further improved to 1.16 V by employing PEA_2PbI_4 and GlyHCl together (**Figure 4.7c**). The enhanced V_{oc} by further introducing GlyHCl could be attributed to the facilitated hole transporting efficiency. The dipole moment in molecule GlyHCl creates an electric filed at the bottom interfaces between hole transporting layer (HTL) and perovskite, and the electric filed will drive holes towards HTL efficiently.[188] However, both V_{oc} and FF begin to decrease when two additives excess the optimal concentrations. The external quantum efficiency (EQE) of the devices and integrated J_{sc} are shown in **Figure 4.7f**, the integrated J_{sc} are calculated to be 24.42 $mA \cdot cm^{-2}$and 24.47 $mA \cdot cm^{-2}$ for control and champion devices respectively, which are consistent with the values obtained from the *J-V* curves.

Table 2. The parameters of control device, champion device with different ratios of GlyHCl under 0.5% PEA_2PbI_4. (The statistical analysis includes 30 samples in each condition.)

Sample		J_{sc} (mA cm^{-2})	V_{oc} (V)	FF	PCE (%)
Control	Champion	25.49	1.120	0.76	21.9
	Average	25.25±	1.110±	0.75±	20. 95± 0.91

		0.25	0.012	0.01	
0.5% GlyHCl	Champion	25.38	1.131	0.77	22.08
	Average	25.26± 0.12	1.125± 0.005	0.75± 0.02	20.90± 0.98
1.0% GlyHCl	Champion	25.52	1.142	0.78	22.75
	Average	25.37± 0.15	1.134± 0.006	0.77± 0.01	21.73± 0.95
2.0% GlyHCl	Champion	25.43	1.150	0.80	23.34
	Average	25.30± 0.13	1.147± 0.003	0.79± 0.01	22.45± 0.91
3.0% GlyHCl	Champion	25.55	1.163	0.80	23.80
	Average	25.40± 0.14	1.150± 0.012	0.79± 0.01	22.98± 0.80
5.0% GlyHCl	Champion	23.80	1.142	0.75	20.60
	Average	23.56± 0.24	1.130± 0.012	0.74± 0.01	16.93± 0.96

At last, the improvements in thermal stability (**Figure 4.7g),** photostability (**Figure 4.7h)** and long-term storage stability (**Figure 4.7i)** of PSCs by employing PEA_2PbI_4 and GlyHCl were investigated. The combinational effect also enhances the stability of PSCs. The control device loss almost 30% of its original PCE after being subjected to thermal condition without encapsulation for 500 hours. And the target device maintained over 96% original PCE with the same condition, which is higher than the PCE of devices with the addition of PEA_2PbI_4 or GlyHCl alone. Similarly, the target device maintained over 93% and 98% efficiency, respectively, after continuous illumination and storage in inert atmosphere, while the control device exhibited much poor stability. The elevated stability cannot be achieved with a single additive, indicating the significance of the combinational effect brought by the co-additive strategy.

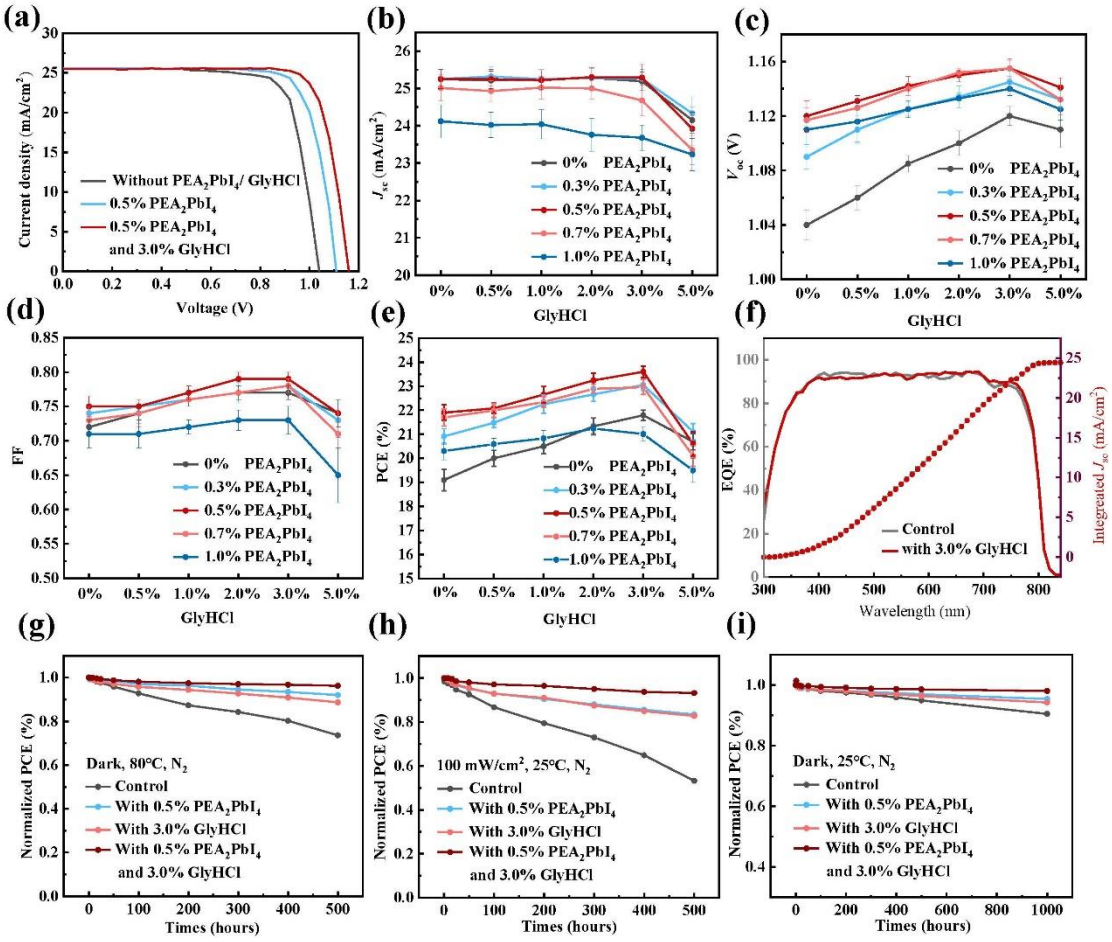

Figure 4.7. (a) *J–V* curves of control devices and champion devices with optimal molar ratio of PEA_2PbI_4 and GlyHCl. Device area: 0.048 cm^2. (b-e) Comparisons of J_{sc}, V_{oc}, FF and PCE between control devices and devices with different ratio of PEA_2PbI_4 and GlyHCl. Thirty samples were measured for each condition. (f) The EQE spectra of the champion device and control device. (g)Thermal stability test under 80 °C heating in N_2 atmosphere without encapsulation. (h) photostability stability test under the continuous illumination (100 mW/cm^2) in N_2 glovebox without encapsulation. (i) Long-time storage stability under dark in N_2 atmosphere without encapsulation.

4.4 Conclusion

In summary, a simple co-additive strategy was employed to boost performance of inverted PSCs. The champion device achieved a PCE of 23.80 %, J_{sc} of 25.55 mA cm^{-2}, V_{oc} of 1.16 V and a high FF of 0.80 with the aid of PEA_2PbI_4 and GlyHCl. From XRD,

NRM, FTIR and Tof-SIMS spectra, it was discovered that GlyHCl strongly interacts with PbI_2/DMF/DMSO to modulate the crystallization process and promote the perovskite to grow along the (100) facet. Moreover, GlyHCl that aggregate at the bottom surface of perovskites could modify the interfaces and facilitate charge transfer. The results of SEM, PL, TRPL and SCLC demonstrate that GlyHCl and PEA_2PbI_4 can enhance the perovskite quality by enlarging grain size, reducing defect density and elongating carrier lifetimes. Overall, the combination effect of PEA_2PbI_4 and GlyHCl provides a convenient co-additive method to boost the performance of inverted PSCs.

Chapter 5 Conclusion and Prospects

5.1 Conclusion

This thesis investigates two novel additives to enhance the performance of inverted perovskite solar cells . The first additive is KBF_4, an inorganic compound that can enter and adjust the perovskite lattice towards a strain-free structure. The release of strain facilitates the production of perovskite thin films with large grain size, reduced defect density, and longer carrier lifetimes. Density functional theory (DFT) calculations support the experimental results and provide a deeper understanding of the passivating mechanism of KBF_4. The improved quality of perovskite thin films enables the construction of solar cells with an efficiency over 23% and a significantly elevated fill factor. Favorable results on rigid substrates motivate the development of flexible PSCs with an efficiency over 21% and a fill factor of 0.79, which is impressive for flexible devices.

The second study focuses on the combinational effect between two additives, PEA_2PbI_4 and GlyHCl. A simple co-additive strategy was employed to boost performance of inverted PSCs. The champion device achieved a PCE of 23.80 %, J_{sc} of 25.55 mA cm^{-2}, V_{oc} of 1.16 V and a high FF of 0.80 with the aid of PEA_2PbI_4 and GlyHCl. From XRD, NRM, FTIR and Tof-SIMS spectra, it was discovered that GlyHCl strongly interacts with PbI_2/DMF/DMSO to modulate the crystallization process and promote the perovskite to grow along the (100) facet. Moreover, GlyHCl that aggregate at the bottom surface of perovskites could modify the interfaces and facilitate charge transfer. The results of SEM, PL, TRPL and SCLC demonstrate that GlyHCl and PEA_2PbI_4 can enhance the perovskite quality by enlarging grain size, reducing defect density and elongating carrier lifetimes. Overall, the combination effect of PEA_2PbI_4 and GlyHCl provides a convenient co-additive method to boost the performance of inverted PSCs.

The target for taking the additive engineering strategy is for improving the performance

of PSCs easily and efficiently. We developed the second work, which using a co-additive strategy, on the basis of the first work. The experimental results showed that, these two strategies work together well and contributed to the best performance of our PSCs. The cooperation of these strategies proves that the potential of additive engineering as well as the importance to explore new additives.

5.2 Prospects

Although the efficiencies of inverted perovskite solar cells demonstrated in this thesis are competitive, there are still limitations to the application of these additives, which represent barriers to the commercialization of PSCs. The first challenge is device stability. Although the efficiency of PSCs has approached that of widely used silicon solar cells, their stability still lags behind. This is not solely the responsibility of additives engineering but rather a challenge shared by all strategies. Moreover, large-area fabrication is another paramount issue. The fabrication process for small-area devices differs significantly from that of large-area devices. For instance, researchers have devoted extensive efforts to using solvents such as DMF and DMSO in small-area devices, as they possess excellent dissolving ability for many additives. However, in large-area fabrication methods, these two solvents are seldom used due to their slow evaporation speeds. This renders many additives exclusive to one solvent system and unsuitable for use in large-area fabrication methods. Apart from solvent problems, many technologies are exclusive to small-area devices, such as the utilization of antisolvent to promote crystallization. Hence, additives engineering should be studied under the large-area fabrication system. Fortunately, accumulated experience provides logical principles for selecting or designing new additives.

Reference

[1] H. Y. Cheng, C. Liu, J. Zhuang, J. Cao, T. Wang, W. Y. Wong, F. Yan, *Adv. Func. Mater.,* **2022**, *32*, 2204880.

[2] A. K. Jena, A. Kulkarni, T. Miyasaka, *Chem. Rev.,* **2019**, *119*, 3036.

[3] J. Y. Kim, J. W. Lee, H. S. Jung, H. Shin, N. G. Park, *Chem. Rev.,* **2020**, *120*, 7867.

[4] N. Papez, R. Dallaev, P. Kaspar, D. Sobola, P. Skarvada, S. Talu, S. Ramazanov, A. Nebojsa, *Mater.,* **2021**, *14*, 461.

[5] N. Mufti, T. Amrillah, A. Taufiq, Sunaryono, Aripriharta, M. Diantoro, Zulhadjri, H. Nur, *Solar Energy,* **2020**, *207*, 1146.

[6] M. Riede, D. Spoltore, K. Leo, *Adv. Energy Mater.,* **2020**, *11*, 2002653.

[7] X. Wu, B. Li, Z. Zhu, C. C. Chueh, A. K. Jen, *Chem. Soc. Rev.,* **2021**, *50*, 13090.

[8] J. J. M. Kim, H. Lu, T.K. Lee, F. T. Eickemeyer, Y. Liu, I.W. Choi, S.J. Choi, Y.H. Jo, H.B. Kim, Sung-In Mo, Y.L. Kim, H,J. Lee, N.G. An, S. Cho, W. R. Tress, S. M. Zakeeruddin, A. Hagfeldt, J.Y. Kim, M. Grätzel, D. S. Kim, *Science,* **2022**, *375*, 302.

[9] Q. Jiang, J. Tong, Y. Xian, R. A. Kerner, S. P. Dunfield, C. Xiao, R. A. Scheidt, D. Kuciauskas, X. Wang, M. P. Hautzinger, R. Tirawat, M. C. Beard, D. P. Fenning, J. J. Berry, B. W. Larson, Y. Yan, K. Zhu, *Nature,* **2022**, *611*, 278.

[10] N.-G. Park, M. Grätzel, T. Miyasaka, K. Zhu, K. Emery, *Nature Energy,* **2016**, *1*, 11.

[11] J. Wei, Q. Wang, J. Huo, F. Gao, Z. Gan, Q. Zhao, H. Li, *Adv. Energy Mater.,* **2020**, *11*, 2002326.

[12] D. Li, D. Zhang, K. S. Lim, Y. Hu, Y. Rong, A. Mei, N. G. Park, H. Han, *Adv. Func. Mater.,* **2020**, *31*, 2008621.

[13] N. J. Jeon, J. H. Noh, W. S. Yang, Y. C. Kim, S. Ryu, J. Seo, S. I. Seok, *Nature,* **2015**, *517*, 476.

[14] S. F. Liu, Y. Guan, Y. Sheng, Y. Hu, Y. Rong, A. Mei, H. W. Han, *Adv. Energy Mater.,* **2019**, *10*, 1902492.

[15] Y. Delannoy, *J. of Crystal Growth* **2012**, *360*, 61.

[16] J. H. Lee, N. G. Park, *Adv. Energy Mater.,* **2019**, *10*, 1903249.

[17] E. Shi, Y. Gao, B. P. Finkenauer, Akriti, A. H. Coffey, L. Dou, *Chem. Soc. Rev.,* **2018**, *47*, 6046.

[18] X. Li, J. M. Hoffman, M. G. Kanatzidis, *Chem. Rev.,* **2021**, *121*, 2230.

[19] Y. L. Zhang, N. G. Park, *ACS Energy Lett.,* **2022**, *7*, 757.

[20] Q. Jiang, X. Zhang, J. You, *Small,* **2018**, *14*, 1801154.

[21] L. Xu, X. Chen, J. Jin, W. Liu, B. Dong, X. Bai, H. Song, P. Reiss, *Nano Energy* **2019**, *63*, 103860.

[22] Y. Qi, M. Almtiri, H. Giri, S. Jha, G. Ma, A. K. Shaik, Q. Zhang, N. Pradhan, X. Gu, N. I. Hammer, D. Patton, C. Scott, Q. Dai, *Adv. Energy Mater.,* **2022**, 2202713.

[23] T. Liu, K. Chen, Q. Hu, R. Zhu, Q. H. Gong, *Adv. Energy Mater.,* **2016**, *6*,

1600457.
[24] Y. Huang, T. Liu, C. Liang, J. Xia, D. Li, H. Zhang, A. Amini, G. Xing, C. Cheng, *Adv. Func. Mater.,* **2020**, *30*, 2000863.
[25] M. Li, Z. K. Wang, Y. G. Yang, Y. Hu, S. L. Feng, J. M. Wang, X. Y. Gao, L. S. Liao, *Adv. Energy Mater.,* **2016**, *6*, 1601156.
[26] M. Chen, G. Kapil, L. Wang, S. Razey Sahamir, A. K. Baranwal, K. Nishimura, Y. Sanehira, Z. Zhang, M. Akmal Kamarudin, Q. Shen, S. Hayase, *Chem. Eng. J.,* **2022**, *436*, 135196.
[27] H. Kong, W. Sun, H. P. Zhou, *J. of Semiconductors,* **2021**, *42*.
[28] M. R. Azani, A. Hassanpour, T. Torres, *Adv. Energy Mater.,* **2020**, *10*, 2002536.
[29] L. Hu, J. Song, X. Yin, Z. Su, Z. Li, *Polymers* **2020**, *12*, 145.
[30] I. Mora-Seró, *Joule* **2018**, *2*, 585.
[31] B. Chen, P. N. Rudd, S. Yang, Y. Yuan, J. Huang, *Chem. Soc. Rev.,* **2019**, *48*, 3842.
[32] W.-J. Yin, T. Shi, Y. Yan, *J. Phys. Chem. C,* **2015**, *119*, 5253.
[33] W. J. Yin, T. Shi, Y. Yan, *Adv. Mater.,* **2014**, *26*, 4653.
[34] S. Grimme, J. Antony, S. Ehrlich, H. Krieg, *J. Chem. Phys.,* **2010**, *132*, 154104.
[35] T. S. Sherkar, C. Momblona, L. Gil-Escrig, J. Avila, M. Sessolo, H. J. Bolink, L. J. A. Koster, *ACS Energy Lett.,* **2017**, *2*, 1214.
[36] A. F. Castro-M., J. Hidalgo, J. P. Correa-B., *Adv. Energy Mater.,* **2019**, *9*, 1901489.
[37] Y. Bai, X. Meng, S. Yang, *Adv. Energy Mater.,* **2018**, *8*, 1701883.
[38] Y. H. Li, H. B. Xie, E. L. Lim, A. Hagfeldt, D. Q. Bi, *Adv. Energy Mater.,* **2021**, *12*, 2102730.
[39] G. E. Eperon, S. D. Stranks, C. Menelaou, M. l. B. Johnston, L. M. Herz, H. J. Snaith, *Energy Environ. Sci.,* **2014**, *7*, 982.
[40] C. Y. Yi, J. S. Luo, S. Meloni, A. Boziki, N. Ashari-Astani, C. Grätzel, S. M. Zakeeruddin, U. Röthlisberger, M. Grätzel, *Energy Environ. Sci.,* **2016**, *9*, 656.
[41] Y. Wei, Z. Cheng, J. Lin, *Chem. Soc. Rev.,* **2019**, *48*, 310.
[42] H. J. Snaith, A. Abate, J. M. Ball, G. E. Eperon, T. Leijtens, N. K. Noel, S. D. Stranks, J. T. Wang, K. Wojciechowski, W. Zhang, *J. Phys. Chem. Lett.,* **2014**, *5*, 1511.
[43] A. K. Jena, H. W. Chen, A. Kogo, Y. Sanehira, M. Ikegami, T. Miyasaka, *ACS Appl. Mater. Inter.,* **2015**, *7*, 9817.
[44] S. Meloni, T. Moehl, W. Tress, M. Franckevicius, M. Saliba, Y. H. Lee, P. Gao, M. K. Nazeeruddin, S. M. Zakeeruddin, U. Rothlisberger, M. Graetzel, *Nat. Commun.,* **2016**, *7*, 10334.
[45] L. Meng, J. You, Y. Yang, *Nat. Commun.,* **2018**, *9*, 5265.
[46] Y. B. Cheng, L. M. Ding, *Energy Environ. Sci.,* **2021**, *14*, 3233.
[47] W. Xiang, S. F. Liu, W. Tress, *Energy Environ. Sci.,* **2021**, *14*, 2090.
[48] T. Bu, X. Liu, Y. Zhou, J. Yi, X. Huang, L. Luo, J. Xiao, Z. Ku, Y. Peng, F. Huang, Y.-B. Cheng, J. Zhong, *Energy Environ. Sci.,* **2017**, *10*, 2509.
[49] H. Lu, Y. Liu, P. Ahlawat, A. Mishra, W. R. Tress, F. T. Eickemeyer, Y. Yang, F.

Fu, Z. Wang, C. E. Avalos, B. I. Carlsen, A. Agarwalla, X. Zhang, X. Li, Y. Zhan, S. M. Zakeeruddin, L. Emsley, U. Rothlisberger, L. Zheng, A. Hagfeldt, M. Gratzel, *Science,* **2020**, *370*, 74.

[50] J. Jeong, Kim, M., Seo, J., Lu, H., Ahlawat, P., Mishra, A., Yang, Y., Hope, M. A., Eickemeyer, F. T., Kim, M., Yoon, Y. J., Choi, I. W., Darwich, B. P., Choi, S. J., Jo, Y. ,Lee, J. H., Walker, B., Zakeeruddin, S. M., Emsley, L., Rothlisberger, U., Hagfeldt, A., Kim, D. S., Gratzel, M., Kim, J. Y., *Nature,* **2021**, *592*, 381.

[51] B. Park, H. W. Kwon, Y. H. Lee, D. Y. Lee, M. G. Kim, G. H. Kim, K.-j. Kim, Y. K. Kim, J. Im, T. J. Shin, S. I. Seok, *Nature Energy,* **2021**, *6*, 419.

[52] Y. H. Kye, C. J. Yu, U. G. Jong, Y. Chen, A. Walsh, *J. Phys. Chem. Lett.,* **2018**, *9*, 2196.

[53] E. U. R. Azmi, A. Seitkhan , F. Aljamaan , M. De Bastiani , E. Aydin , S. De Wolf , A. S. Subbiah , J. Liu ,, M. I. N. G.T. Harrison, M. K. Eswaran, M. Babics, Y. Chen, F. Xu, T. G. Allen, A. ur Rehman, C.L. Wang ,Udo Schwingenschlögl, T. D. A. , *Science,* **2022**, 0.1126/science.abm5784.

[54] C. M. Thi K., L. Atourki, M. Ouafi, S. G. Hashmi, *J. Mater. Chem. A.,* **2021**, *9*, 26650.

[55] S. Tang, Y. Deng, X. Zheng, Y. Bai, Y. Fang, Q. Dong, H. Wei, J. S. Huang, *Adv. Energy Mater.,* **2017**, *7*, 1700302.

[56] N. J. Jeon, J. H. Noh, Y. C. Kim, W. S. Yang, S. Ryu, S. I. Seok, *Nat. Mater.,* **2014**, *13*, 897.

[57] D. Y. Son, S. G. Kim, J. Y. Seo, S. H. Lee, H. Shin, D. Lee, N. G. Park, *J. Am. Chem. Soc.,* **2018**, *140*, 1358.

[58] J. Cao, S. X. Tao, P. A. Bobbert, C. P. Wong, N. Zhao, *Adv. Mater.,* **2018**, *30*, e1707350.

[59] F. Zheng, W. Chen, T. Bu, K. P. Ghiggino, F. Huang, Y. B. Cheng, P. Tapping, T. W. Kee, B. Jia, X. M. Wen, *Adv. Energy Mater.,* **2019**, *9*, 1901016.

[60] M. Abdi-Jalebi, Z. Andaji-Garmaroudi, S. Cacovich, C. Stavrakas, B. Philippe, J. M. Richter, M. Alsari, E. P. Booker, E. M. Hutter, A. J. Pearson, S. Lilliu, T. J. Savenije, H. Rensmo, G. Divitini, C. Ducati, R. H. Friend, S. D. Stranks, *Nature,* **2018**, *555*, 497.

[61] L. Kuai, Y. Wang, Z. Zhang, Y. Yang, Y. Qin, T. Wu, Y. Li, Y. Li, T. Song, X. Gao, L. Wang, B. Sun, *Solar RRL,* **2019**, *3*, 1900053.

[62] S. Bag, M. F. Durstock, *ACS Appl. Mater. Inter.,* **2016**, *8*, 5053.

[63] J. Zhang, R. Chen, Y. Wu, M. Shang, Z. Zeng, Y. Zhang, Y. Zhu, L. Han, *Adv. Energy Mater.,* **2018**, *8*, 1701981.

[64] F. Yang, M. A. Kamarudin, G. Kapil, D. Hirotani, P. Zhang, C. H. Ng, T. Ma, S. Hayase, *ACS Appl. Mater. Inter.,* **2018**, *10*, 24543.

[65] C. Lu, J. Zhang, D. Hou, X. Gan, H. Sun, Z. Zeng, R. Chen, H. Tian, Q. Xiong, Y. Zhang, Y. Li, Y. Zhu, *Appl. Phys. Lett.,* **2018**, *112*.

[66] X. Shai, L. Zuo, P. Sun, P. Liao, W. Huang, E. P. Yao, H. Li, S. F. Liu, Y. Shen, Y. Yang, M. K. Wang, *Nano Energy* **2017**, *36*, 213.

[67] S. Ye, H. Rao, W. Yan, Y. Li, W. Sun, H. Peng, Z. Liu, Z. Bian, Y. Li, C. Huang, *Adv. Mater.,* **2016**, *28*, 9648.

[68] M. Jahandar, J. Heo, C. Song, K. Kong, W. Shin, J. H. Lee, S. Im, S. Moon, *Nano Energy* **2016**, *27*, 330.
[69] S. Shahbazi, C.-M. Tsai, S. Narra, C.-Y. Wang, H.-S. Shiu, S. Afshar, N. Taghavinia, E. W.-G. Diau, *J. Phys. Chem. C,* **2017**, *121*, 3673.
[70] D. Zheng, C. Schwob, Y. Prado, Z. Ouzit, L. Coolen, T. Pauporté, *Nano Energy* **2022**, *94*, 106934.
[71] Q. Wang, X. Zhang, Z. Jin, J. Zhang, Z. Gao, Y. F. Li, S. Z. Liu, *ACS Energy Lett.,* **2017**, *2*, 1479.
[72] D. Bai, J. Zhang, Z. Jin, H. Bian, K. Wang, H. Wang, L. Liang, Q. Wang, S. F. Liu, *ACS Energy Lett.,* **2018**, *3*, 970.
[73] W. Xu, L. Zheng, X. Zhang, Y. Cao, T. Meng, D. Wu, L. Liu, W. Hu, X. Gong, *Adv. Energy Mater.,* **2018**, *8*, 1703178.
[74] M. T. Klug, A. Osherov, A. A. Haghighirad, S. D. Stranks, P. R. Brown, S. Bai, J. T. W. Wang, X. Dang, V. Bulović, H. J. Snaith, A. M. Belcher, *Energy Environ. Sci.,* **2017**, *10*, 236.
[75] J. R. Poindexter, R. L. Z. Hoye, L. Nienhaus, R. C. Kurchin, A. E. Morishige, E. E. Looney, A. Osherov, J. P. Correa-Baena, B. Lai, V. Bulovic, V. Stevanovic, M. G. Bawendi, T. Buonassisi, *ACS Nano.,* **2017**, *11*, 7101.
[76] Q. Cai, H. Li, Y. Jiang, L. Tu, L. Ma, X. Wu, S. Yang, Z. Shi, J. Zang, Y. Chen, *Solar Energy,* **2018**, *159*, 786.
[77] M. Kim, G. H. Kim, T. K. Lee, I. W. Choi, H. W. Choi, Y. Jo, Y. J. Yoon, J. Kim, J. H. Lee, D. Huh, H. Lee, S. Kwak, J. Kim, D. S. Kim, *Joule* **2019**, *3*, 2179.
[78] H. T. Pham, Y. Yin, G. Andersson, K. J. Weber, T. Duong, J. Wong-Leung, *Nano Energy* **2021**, *87*, 106226.
[79] F. Ye, J. Ma, C. Chen, H. Wang, Y. Xu, S. Zhang, T. Wang, C. Tao, G. Fang, *Adv. Mater.,* **2021**, *33*, e2007126.
[80] S. You, X. Xi, X. Zhang, H. Wang, P. Gao, X. Ma, S. Bi, J. Zhang, H. P. Zhou, Z. Wei, *J. Mater. Chem. A.,* **2020**, *8*, 17756.
[81] Y. Li, W. Xu, N. Mussakhanuly, Y. Cho, J. Bing, J. Zheng, S. Tang, Y. Liu, G. Shi, Z. Liu, Q. Zhang, J. R. Durrant, W. Ma, A. W. Y. Ho-Baillie, S. Huang, *Adv. Mater.,* **2022**, *34*, e2106280.
[82] X. Zheng, B. Chen, J. Dai, Y. Fang, Y. Bai, Y. Lin, H. Wei, X. Zeng, J. S. Huang, *Nature Energy,* **2017**, *2*, 17102.
[83] Q. Jiang, Y. Zhao, X. Zhang, X. Yang, Y. Chen, Z. Chu, Q. Ye, X. Li, Z. Yin, J. You, *Nature Photo.,* **2019**, *13*, 460.
[84] D. H. Kim, C. P. Muzzillo, J. Tong, A. F. Palmstrom, B. W. Larson, C. Choi, S. P. Harvey, S. Glynn, J. B. Whitaker, F. Zhang, Z. Li, H. Lu, M. F. A. M. van Hest, J. J. Berry, L. M. Mansfield, Y. Huang, Y. Yan, K. Zhu, *Joule* **2019**, *3*, 1734.
[85] D. S. Lee, J. S. Yun, J. H. Kim, A. M. Soufiani, S. Chen, Y. Cho, X. Deng, J. Seidel, S. Lim, S. Huang, A. W. Y. Ho-Baillie, *ACS Energy Lett.,* **2018**, *3*, 647.
[86] X. Ren, B. Zhang, L. Zhang, J. Wen, B. Che, D. Bai, J. You, T. Chen, S. F. Liu, *ChemSusChem,* **2021**, *14*, 3182.
[87] M. Li, J. Zhou, L. Tan, Y. Liu, S. Wang, C. Jiang, H. Li, X. M. Zhao, X. Gao,

W. Tress, L. Ding, C. Y. Yi, *Energy Environ. Sci.,* **2022**, 10.1002/eem2.12360.
[88] J. Zhou, M. Li, S. Wang, L. Tan, Y. Liu, C. Jiang, X. M. Zhao, L. Ding, C. Yi, *Nano Energy* **2022**, *95*, 107036.
[89] H. Chen, S. Teale, B. Chen, Y. Hou, L. Grater, T. Zhu, K. Bertens, S. M. Park, H. R. Atapattu, Y. Gao, M. Wei, A. K. Johnston, Q. Zhou, K. Xu, D. Yu, C. Han, T. Cui, E. H. Jung, C. Zhou, W. Zhou, A. H. Proppe, S. Hoogland, F. Laquai, T. Filleter, K. R. Graham, Z. Ning, E. H. Sargent, *Nature Photo.,* **2022**, *16*, 352.
[90] Y. Jo, K. S. Oh, M. Kim, K.-H. Kim, H. Lee, C.-W. Lee, D. S. Kim, *Adv. Func. Mater.,* **2016**, *3*, 1500768.
[91] Y. Zhang, M. Chen, Y. Zhou, W. Li, Y. H. Lee, H. Kanda, X. X. Gao, R. Hu, K. G. Brooks, R. Zia, S. Kinge, N. P. Padture, M. K. Nazeeruddin, *Adv. Energy Mater.,* **2020**, *10*, 2001300.
[92] R. Wang, J. Xue, L. Meng, J.-W. Lee, Z. Zhao, P. Sun, L. Cai, T. Huang, Z. Wang, Z. Wang, Y. Duan, J. L. Yang, S. Tan, Y. Yuan, Y. Huang, Y. Yang, *Joule* **2019**, *3*, 1464.
[93] Z. Wu, S. R. Raga, E. J. Juarez-Perez, X. Yao, Y. Jiang, L. K. Ono, Z. Ning, H. Tian, Y. Qi, *Adv. Mater.,* **2018**, *30*, 1703670.
[94] R. Zhou, X. Liu, H. Li, H. Wang, Y. Ouyang, X. Gong, X. Peng, H. Luo, Y. Ni, W. Zou, Y. Lei, *Solar RRL,* **2021**, *6*, 2100731.
[95] X. Meng, J. Lin, X. Liu, X. He, Y. Wang, T. Noda, T. Wu, X. Yang, L. Han, *Adv. Mater.,* **2019**, *31*, e1903721.
[96] H. Zhang, Z. Chen, M. Qin, Z. Ren, K. Liu, J. Huang, D. Shen, Z. Wu, Y. Zhang, J. Hao, C. S. Lee, X. Lu, Z. Zheng, W. Yu, G. Li, *Adv. Mater.,* **2021**, *33*, e2008487.
[97] T. Liu, X. M. Zhao, X. J. Zhong, Q. C. Burlingame, A. Kahn, Y. L. Loo, *ACS Energy Lett.,* **2022**, *7*, 3531.
[98] Q. Jiang, Z. Ni, G. Xu, Y. Lin, P. N. Rudd, R. Xue, Y. Li, Y. Li, Y. Gao, J. Huang, *Adv. Mater.,* **2020**, *32*, e2001581.
[99] S. Xiong, Z. Hou, S. Zou, X. Lu, J. Yang, T. Hao, Z. Zhou, J. Xu, Y. Zeng, W. Xiao, W. Dong, D. Li, X. Wang, Z. Y. Hu, L. Sun, Y. Wu, X. Liu, L. Ding, Z. Sun, M. Fahlman, Q. Bao, *Joule* **2021**, *5*, 467.
[100] J. W. Lee, Z. Dai, T. H. Han, C. Choi, S. Y. Chang, S. J. Lee, N. De Marco, H. Zhao, P. Sun, Y. Huang, Y. Yang, *Nat. Commun.,* **2018**, *9*, 3021.
[101] D. Yao, C. Zhang, S. Zhang, Y. Yang, A. Du, E. Waclawik, X. Yu, G. J. Wilson, H. Wang, *ACS Appl. Mater. Inter.,* **2019**, *11*, 29753.
[102] P. Li, Y. Zhang, C. Liang, G. Xing, X. Liu, F. Li, X. Liu, X. Hu, G. Shao, Y. Song, *Adv. Mater.,* **2018**, *30*, e1805323.
[103] J. Y. Ye, J. Tong, J. Hu, C. Xiao, H. Lu, S. P. Dunfield, D. S. Kim, X. Chen, B. W. Larson, J. Hao, K. Wang, Q. Zhao, Z. Chen, H. Hu, W. You, J. J. Berry, F. Zhang, K. Zhu, *Solar RRL,* **2020**, *4*, 2000082.
[104] M. I. D. T. Zhang, G. Li, F. Xu, N. Guo, M. Grätzel, Y. Zhao, *Sci. Adv.,* **2017**, *3*, e1700841.
[105] J. Fan, Y. Ma, C. Zhang, C. Liu, W. Li, R. E. I. Schropp, Y. H. Mai, *Adv. Energy Mater.,* **2018**, *8*, 1703421.

[106] P. Liu, Y. Xian, W. Yuan, Y. Long, K. Liu, N. Rahman, W. Li, J. Fan, *Adv. Energy Mater.,* **2020**, *10*, 1903654.
[107] N. Yang, C. Zhu, Y. Chen, H. Zai, C. Wang, X. Wang, H. Wang, S. Ma, Z. Gao, X. Wang, J. Hong, Y. Bai, H. P. Zhou, B. B. Cui, Q. Chen, *Energy Environ. Sci.,* **2020**, *13*, 4344.
[108] Z. Li, X. Liu, J. Xu, S. Yang, H. Zhao, H. Huang, S. F. Liu, J. Yao, *J. Mater. Chem. C.,* **2020**, *8*, 6977.
[109] F. Bai, J. Zhang, Y. Yuan, H. Liu, X. Li, C. C. Chueh, H. Yan, Z. Zhu, A. K. Jen, *Adv. Mater.,* **2019**, *31*, e1904735.
[110] Y. Y. J. Chen, H. Dong, J. Li,, X. Zhu, J. Xu, F. Pan, F. Yuan, J. Dai, B. Jiao, X. Hou, Alex K.-Y. Jen, Z. Wu, *Sci. Adv.,* **2022**, *8*, eabk2722
[111] M. Shahiduzzaman, K. Yamamoto, Y. Furumoto, T. Kuwabara, K. Takahashi, T. Taima, *RSC Adv.,* **2015**, *5*, 77495.
[112] J. Y. Seo, T. Matsui, J. Luo, J.-P. Correa-B., F. Giordano, M. Saliba, K. Schenk, A. Ummadisingu, K. Domanski, M. Hadadian, A. Hagfeldt, S. M. Zakeeruddin, U. Steiner, M. Grätzel, A. Abate, *Adv. Energy Mater.,* **2016**, *6*, 1600767.
[113] Y. D. Xia, C. X. Ran, Y. H. Chen, Q. Li, N. Jiang, C. Z. Li, Y. Pan, T. Li, J. Wang, W. Huang, *J. Mater. Chem. A.,* **2017**, *5*, 3193.
[114] S. Bai, P. Da, C. Li, Z. Wang, Z. Yuan, F. Fu, M. Kawecki, X. Liu, N. Sakai, J. T. Wang, S. Huettner, S. Buecheler, M. Fahlman, F. Gao, H. J. Snaith, *Nature,* **2019**, *571*, 245.
[115] N. S. Y.H. Lin, P. Da, J. Wu, Harry C. Sansom, A. J. Ramadan, S. Mahesh, J. Liu, R. D. J. Oliver, J. Lim, L. Aspitarte, K. Sharma, P. K. Madhu, A. B. Morales-Vilches, P. K. Nayak, S. Bai, F. Gao, C.R. M. Grovenor, M. B. Johnston, J. G. Labram, J. R. Durrant, J. M. Ball, B. Wenger, B. Stannowski, H. J. Snaith, *Science,* **2020**, *369*, 96.
[116] S. Song, B. J. Moon, M. T. Hörantner, J. Lim, G. Kang, M. Park, J. Y. Kim, H. J. Snaith, T. Park, *Nano Energy* **2016**, *28*, 269.
[117] X. Deng, L. Xie, S. Wang, C. Li, A. Wang, Y. Yuan, Z. Cao, T. Li, L. Ding, F. Hao, *Chem. Eng. J.,* **2020**, *398*, 125594.
[118] W. Zhang, X. Liu, B. He, Z. Gong, J. Zhu, Y. Ding, H. Chen, Q. Tang, *ACS Appl. Mater. Inter.,* **2020**, *12*, 4540.
[119] Y. Rong, Y. Hu, A. Mei, H. Tan, M. I. Saidaminov, S. I. Seok, M. D. McGehee, E. H. Sargent, H. Han, *Science,* **2018**, *361*, 1214.
[120] N. Li, X. Niu, Q. Chen, H. Zhou, *Chem. Soc. Rev.,* **2020**, *49*, 8235.
[121] D. Luo, X. Li, A. Dumont, H. Yu, Z. H. Lu, *Adv. Mater.,* **2021**, *33*, 2006004.
[122] H. Min, D. Y. Lee, J. Kim, G. Kim, K. S. Lee, J. Kim, M. J. Paik, Y. K. Kim, K. S. Kim, M. G. Kim, T. J. Shin, S. Il Seok, *Nature,* **2021**, *598*, 444.
[123] Y. L. H. Lu, P. Ahlawat, A. Mishra, W. R. Tress, F. T. Eickemeyer, Y. Yang, F. Fu, Z. Wang, C. E. Avalos, B.I. Carlsen, A. Agarwalla, X. Zhang, X. Li, Y. Zhan, S. M. Zakeeruddin, L. Emsley, U. Rothlisberger, L. Zheng, A.Hagfeldt, M. Grätzel, *Science,* **2020**, *370*, 74
[124] A. M. Jaeki J., Minjin K., Jongdeuk S., H. Lu, Y. Yang, M. A. Hope, I. W. C.

Y.J. Yoon, B. Primera Darwich, J. H. Lee, B. Walker, A. Hagfeldt, S. M. Z. , D. S.Kim, M. Grätzel , P. Ahlawat, F. T. E. , S. J. Choi, L. E. , M. K. , Y. Jo, a. J. Y. K. , *Nature,* **2021**, *592*, 381.

[125] H. W. K. B.W. Park, Y. Lee, D.Y. Lee, M.G. Kim , G. Kim , K. Kim, Y. Ki Kim, J. Im , T. J. Shin and S. Il Seok, *Nat. Energy,* **2021**, *6*, 419.

[126] C. Yi, J. Luo, S. Meloni, A. Boziki, N. Ashari-Astani, C. Grätzel, S. M. Zakeeruddin, U. Röthlisberger, M. Grätzel, *Energy Environ. Sci.,* **2016**, *9*, 656.

[127] M. Saliba, T. Matsui, J. Y. Seo, K. Domanski, J. P. Correa-Baena, M. K. Nazeeruddin, S. M. Zakeeruddin, W. Tress, A. Abate, A. Hagfeldt, M. Gratzel, *Energy Environ. Sci.,* **2016**, *9*, 1989.

[128] C. Dong, Z. Wang, L. S. Liao, *Energy Tech.,* **2020**, *8*, 1900804.

[129] H. M. G. Kim, K.S. Lee, D. Y. Lee, S. M.Yoon, S. Il Seok, *Science,* **2020**, *370*, 108.

[130] W. G. L. Zhang, C.J. Tong, X. Chen, T. Cao and M. Chen, *Sci. Rep.,* **2018**, *8*, 7760.

[131] K. A. B. Nicholas R., A. D. Printz, A. Gold-Parker, Y. Ding, M. F. Toney, M. D. McGehee, and R. H. Dauskardt, *Adv. Energy Mater.,* **2018**, *8*, 1802139.

[132] R. Wang, T. Huang, J. Xue, J. Tong, K. Zhu, Y. Yang, *Nat. Photo.,* **2021**, *15*, 411.

[133] G. Tang, F. Yan, *Nano Today,* **2021**, *39*, 101155.

[134] X. Lin, D. Cui, X. Luo, C. Zhang, Q. Han, Y. Wang, L. Han, *Energy Environ. Sci.,* **2020**, *13*, 3823.

[135] Q. i. A. M. Degani, M. Albaladejo-Siguan, Y.J. Hofstetter, C. Cho, F. Paulus, G. Grancini, Y. Vaynzof, *Sci. Adv.,* **2021**, *7*, eabj7930.

[136] P. Giannozzi, S. Baroni, N. Bonini, M. Calandra, R. Car, C. Cavazzoni, D. Ceresoli, G. L. Chiarotti, M. Cococcioni, I. Dabo, A. Dal Corso, S. de Gironcoli, S. Fabris, G. Fratesi, R. Gebauer, U. Gerstmann, C. Gougoussis, A. Kokalj, M. Lazzeri, L. Martin-Samos, N. Marzari, F. Mauri, R. Mazzarello, S. Paolini, A. Pasquarello, L. Paulatto, C. Sbraccia, S. Scandolo, G. Sclauzero, A. P. Seitsonen, A. Smogunov, P. Umari, R. M. Wentzcovitch, *J. Phys. Condens. Matter.,* **2009**, *21*, 395502.

[137] K. B. John P. Perdew, M. Ernzerhof, *Phys. Rev. Lett.,* **1996**, *77*, 3865.

[138] E. G, H. Hempel, S. Caicedo-Dávila, M. Raoufi, F. Peña-Camargo, M. Grischek, R. Gunder, J. Diekmann, P. Caprioglio, K. O. Brinkmann, H. Köbler, S. Albrecht, T. Riedl, A. Abate, D. Abou-Ras, T. Unold, D. Neher, M. Stolterfoht, *ACS Energy Lett.,* **2021**, *6*, 1045.

[139] F. Li, X. Deng, F. Qi, Z. Li, D. Liu, D. Shen, M. Qin, S. Wu, F. Lin, S. H. Jang, J. Zhang, X. Lu, D. Lei, C. S. Lee, Z. Zhu, A. K. Jen, *J. Am. Chem. Soc.,* **2020**, *142*, 20134.

[140] S. Nagane, U. Bansode, O. Game, S. Chhatre, S. Ogale, *Chem. Commun.,* **2014**, *50*, 9741.

[141] D. H. Cao, C. C. Stoumpos, C. D. Malliakas, M. J. Katz, O. K. Farha, J. T. Hupp, M. G. Kanatzidis, *APL Mater.,* **2014**, *2*, 091101.

[142] B. Shi, X. Yao, F. Hou, S. Guo, Y. Li, C. Wei, Y. Ding, Y. Li, Y. Zhao, X. Zhang, *J. Phy. Chem. C.,* **2018**, *122*, 21269.

[143] J. Zhang, S. Wu, T. Liu, Z. Zhu, A. K. Y. Jen, *Adv. Func. Mater.,* **2019**, *29*, 1808833.
[144] M. G. Kim, T. Jeon, H. Park, J. W. Lee, S. Nam, S. G. Kim, *Cryst. Eng. Comm.,* **2016**, *18*, 6090.
[145] H.-S. Kim, N.-G. Park, *NPG Asia Mater.* **2020**, *12*, 12:78.
[146] F. Zhang, S. Ye, H. Zhang, F. Zhou, Y. Hao, H. Cai, J. Song, J. Qu, *Nano Energy,* **2021**, *89*, 106370.
[147] H. Zhang, S. Ye, Y. Hao, P. Zeng, J. Lian, J. Qu, J. Song, F. Zhang, *Chem. Eng. J.,* **2022**, *445*.
[148] M. A. Green, A. Ho-Baillie, H. J. Snaith, *Nat. Photo.,* **2014**, *8*, 506.
[149] Z. Xiao, Z. Song, Y. Yan, *Adv. Mater.,* **2019**, *31*, e1803792.
[150] X. Wang, Y. Qiu, L. Wang, T. Zhang, L. Zhu, T. Shan, Y. Wang, J. Jiang, L. Kong, H. Zhong, H. Yu, F. Liu, F. Gao, F. Wang, C. H. Chen, *Nano Energy* **2021**, *89*.
[151] T. J. Smart, H. Takenaka, T. A. Pham, L. Z. Tan, J. Z. Zhang, T. Ogitsu, Y. Ping, *J. Phys. Chem. Lett.,* **2021**, *12*, 6299.
[152] N. Liu, C. Yam, *Phys. Chem. Chem. Phys.,* **2018**, *20*, 6800.
[153] M. Stolterfoht, C. M. Wolff, Y. Amir, A. Paulke, L. Perdigón-Toro, P. Caprioglio, D. Neher, *Energy Environ. Sci.,* **2017**, *10*, 1530.
[154] Q. Xue, Y. Bai, M. Liu, R. Xia, Z. Hu, Z. Chen, X. Jiang, F. Huang, S. Yang, Y. Matsuo, H. Yip, Y. Cao, *Adv. Energy Mater.,* **2017**, *7*.
[155] X. Zhao, L. Tao, H. Li, W. Huang, P. Sun, J. Liu, S. Liu, Q. Sun, Z. Cui, L. Sun, Y. Shen, Y. Yang, M. Wang, *Nano Lett.,* **2018**, *18*, 2442.
[156] D. Y. Son, J. W. Lee, Y. Choi, I. Jang, S. H. Lee, P. J. Yoo, H. Shin, N. Ahn, M. Choi, D. Kim, N. G. Park, *Nat. Energy,* **2016**, *1*, 16081.
[157] L. Kuai, Y. Wang, Z. Zhang, Y. Yang, Y. Qin, T. Wu, Y. Li, Y. Li, T. Song, X. Gao, L. Wang, B. Q. Sun, *Solar RRL,* **2019**, *3*, 1900053.
[158] T. Bu, J. Li, F. Zheng, W. Chen, X. Wen, Z. Ku, Y. Peng, J. Zhong, Y. B. Cheng, F. Huang, *Nat. Commun.,* **2018**, *9*, 4609.
[159] X. Meng, J. Lin, X. Liu, X. He, Y. Wang, T. Noda, T. Wu, X. Yang, L. Han, *Adv. Mater.,* **2019**, *31*, e1903721.
[160] S. Zhang, S. M. Hosseini, R. Gunder, A. Petsiuk, P. Caprioglio, C. M. Wolff, S. Shoaee, P. Meredith, S. Schorr, T. Unold, P. L. Burn, D. Neher, M. Stolterfoht, *Adv. Mater.,* **2019**, *31*, e1901090.
[161] J. Cao, S. X. Tao, P. A. Bobbert, C. P. Wong, N. Zhao, *Adv. Mater.,* **2018**, *30*, 1707350.
[162] X. Fan, W. Nie, H. Tsai, N. Wang, H. Huang, Y. Cheng, R. Wen, L. Ma, F. Yan, Y. Xia, *Adv. Sci.,* **2019**, *6*, 1900813.
[163] J. Z. Chen, N. G. Park, *ACS Energy Lett.,* **2020**, *5*, 2742.
[164] W. X. Z. X.D. Li, X.M. Guo, C.Y. Lu, J. Wei, J.F. Fang, *Science,* **2022**, *375*, 434.
[165] F. T. E. C. Ma, S. Lee, D. Kang, S. J. Kwon,M. Grätzel, N.-G. Park, *Science,* **2023**, *379*, 173.
[166] C. Q. Ma, M. Grätzel, N. G. Park, *ACS Energy Lett.,* **2022**, *7*, 3120.
[167] A. D. Taylor, Q. Sun, K. P. Goetz, Q. An, T. Schramm, Y. Hofstetter, M. Litterst,

F. Paulus, Y. Vaynzof, *Nat. Commun.,* **2021**, *12*, 1878.
[168] S. Dong, Z. Y. Hu, P. Wei, J. Han, Z. Wang, J. Liu, B. L. Su, D. Zhao, Y. Liu, *Adv. Mater.,* **2022**, *34*, e2204342.
[169] X. Zheng, Y. Hou, C. Bao, J. Yin, F. Yuan, Z. Huang, K. Song, J. Liu, J. Troughton, N. Gasparini, C. Zhou, Y. Lin, D. Xue, B. Chen, A. K. Johnston, N. Wei, M. N. Hedhili, M. Wei, A. Y. Alsalloum, P. Maity, B. Turedi, C. Yang, D. Baran, T. D. Anthopoulos, Y. Han, Z.-H. Lu, O. F. Mohammed, F. Gao, E. H. Sargent, O. M. Bakr, *Nat. Energy,* **2020**, *5*, 131.
[170] S. Li, J. Xia, Z. Wen, H. Gu, J. Guo, C. Liang, H. Pan, X. Wang, S. Chen, *Adv. Sci.,* **2023**, *10.1002/advs.202300056*, 2300056.
[171] C. Fang, Q. Zhao, F. Zhao, F. Huang, Y. Peng, Z. Ku, Y. B. Cheng, Z. Fu, *RSC. Adv.,* **2022**, *12*, 10863.
[172] Y. Lei, H. Li, X. Liu, C. Qiu, H. Wang, X. Gong, Y. Ni, R. Feng, J. Peng, Y. Liu, H. Li, *Org. Electr.,* **2022**, *108*, 106573.
[173] J. Du, L. Feng, X. Guo, X. Huang, Z. Lin, J. Su, Z. Y. Hu, J. Zhang, J. Chang, Y. Hao, *J. Power Sources* **2020**, *455*.
[174] H. Wang, Z. Yang, W. Guo, Y. Ji, Y. Zhou, J. Dang, M. Wang, *J. Alloys Compd.,* **2022**, *890*, 161912.
[175] X. Li, W. Sheng, X. Duan, Z. Lin, J. Yang, L. Tan, Y. Chen, *ACS Appl. Mater. Inter.,* **2022**, *14*, 34161.
[176] Y. Ogomi, A. Morita, S. Tsukamoto, T. Saitho, Q. Shen, T. Toyoda, K. Yoshino, S. S. Pandey, T. Ma, S. Hayase, *J. Phys. Chem. C,* **2014**, *118*, 16651.
[177] X. Li, M. I. Dar, C. Yi, J. Luo, M. Tschumi, S. M. Zakeeruddin, M. K. Nazeeruddin, H. Han, M. Gratzel, *Nat. Chem.,* **2015**, *7*, 703.
[178] T. Yang, L. Gao, J. Lu, C. Ma, Y. Du, P. Wang, Z. Ding, S. Wang, P. Xu, D. Liu, H. Li, X. Chang, J. Fang, W. Tian, Y. Yang, S. F. Liu, K. Zhao, *Nat. Commun.,* **2023**, *14*, 839.
[179] X. X. S. Chen, B. Chen, L. L. Kelly, J. Zhao, Y. Lin, M.F. Toney, J.S. Huang, *Sci. Adv.,* **2021**, *7*, eabb2412.
[180] J. T. Katharina W., Stefan Z., and Barbara K., *J. Phys. Chem. A,* **2010**, *114*, 9529.
[181] K. L. Svane, A. C. Forse, C. P. Grey, G. Kieslich, A. K. Cheetham, A. Walsh, K. T. Butler, *J. Phys. Chem. Lett.,* **2017**, *8*, 6154.
[182] F. Li, X. Deng, Z. Shi, S. Wu, Z. Zeng, D. Wang, Y. Li, F. Qi, Z. Zhang, Z. Yang, S. H. Jang, F. R. Lin, S. Tsang, X. Chen, A. K. Y. Jen, *Nature Photo.,* **2023**, *doi.org/10.1038/s41566-023-01180-6*.
[183] Z. Y. W. Wu, P. N. Rudd, Y. Shao, X. Dai, H. Wei, J. Zhao, Y. Fang, Q. Wang, Y. Liu, Y. Deng, X. Xiao, Y. Feng, J.S, Huang, *Sci. Adv.,* **2015**, *5*, eaav8925.
[184] D. Li, L. He, Z. Pang, F. Wang, L. Fan, X. Liu, M. Wei, L. Yang, *Solar RRL,* **2022**, *6*, 2200297.
[185] S. Fu, X. Li, L. Wan, Y. Wu, W. Zhang, Y. Wang, Q. Bao, J. Fang, *Adv. Energy Mater.,* **2019**, *9*, 1901852.
[186] M. E. Kayesh, T. H. Chowdhury, K. Matsuishi, R. Kaneko, S. Kazaoui, J.-J. Lee, T. Noda, A. Islam, *ACS Energy Lett.,* **2018**, *3*, 1584.
[187] X. D. S. Chen, S. Xu, H. Jiao, L. Zhao, J.S. Huang, *Science,* **2021**, *373*, 902.

[188] F. Ansari, E. Shirzadi, M. Salavati-Niasari, T. LaGrange, K. Nonomura, J. H. Yum, K. Sivula, S. M. Zakeeruddin, M. K. Nazeeruddin, M. Gratzel, P. J. Dyson, A. Hagfeldt, *J. Am. Chem. Soc.,* **2020**, *142*, 11428.